



**CALIFORNIA
ENERGY COMMISSION**



**CALIFORNIA
NATURAL
RESOURCES
AGENCY**

ENERGY RESEARCH AND DEVELOPMENT DIVISION

FINAL PROJECT REPORT

Lower Cost High Performance and High Efficiency Pilot-Ignited Directly Injected HD Natural Gas Engine

April 2025 | CEC-500-2025-016



PREPARED BY:

Sandeep Munshi
Westport Fuel Systems Inc.
Primary Author

Reynaldo Gonzalez
Project Manager
California Energy Commission

Agreement Number: PIR-08-045

Reynaldo Gonzalez
Branch Manager
ENERGY SYSTEMS & TRANSPORTATION BRANCH

Jonah Steinbuck, Ph.D.
Director
ENERGY RESEARCH AND DEVELOPMENT DIVISION

Drew Bohan
Executive Director

DISCLAIMER

This report was prepared as the result of work sponsored by the California Energy Commission (CEC). It does not necessarily represent the views of the CEC, its employees, or the State of California. The CEC, the State of California, its employees, contractors, and subcontractors make no warranty, express or implied, and assume no legal liability for the information in this report; nor does any party represent that the uses of this information will not infringe upon privately owned rights. This report has not been approved or disapproved by the CEC, nor has the California Energy Commission passed upon the accuracy or adequacy of the information in this report.

PREFACE

The California Energy Commission's (CEC) Energy Research and Development Division manages the Gas Research and Development Program, which supports energy-related research, development, and demonstration not adequately provided by competitive and regulated markets. These natural gas research investments spur innovation in energy efficiency, renewable energy and advanced clean generation, energy-related environmental protection, energy transmission and distribution and transportation.

The Energy Research and Development Division conducts this public interest natural gas-related energy research by partnering with RD&D entities, including individuals, businesses, utilities and public and private research institutions. This program promotes greater gas reliability, lower costs and increases safety for Californians and is focused in these areas:

- Buildings End-Use Energy Efficiency
- Industrial, Agriculture and Water Efficiency
- Renewable Energy and Advanced Generation
- Natural Gas Infrastructure Safety and Integrity
- Energy-Related Environmental Research
- Natural Gas-Related Transportation

Lower Cost High Performance and High Efficiency Pilot-Ignited Directly Injected HD Natural Gas Engine is the final report for Agreement Number PIR-08-045, conducted by Westport Fuel Systems Inc. The information from this project contributes to the Energy Research and Development Division's Gas Research and Development Program.

For more information about the Energy Research and Development Division, please visit the CEC's research website (www.energy.ca.gov/research/) or contact the Energy Research and Development Division at ERDD@energy.ca.gov.

ABSTRACT

This project was conducted to investigate improvements to Westport Fuel Systems' natural gas fueled heavy-duty high-pressure direct injection (HPDI) engine product, the Westport HD 15L. The key objectives were to reduce cost, improve efficiency, and increase power while maintaining regulated tailpipe emissions below legislated standards and decreasing sensitivity to variations in fuel quality. The work was conducted by Westport's technology office as part of a larger ongoing HPDI product improvement and cost reduction project at Westport.

Keywords: high-pressure direct injection engine, HPDI engine, exhaust-energy recovery systems, virtual sensor, high efficiency combustion, natural gas, diesel

Please use the following citation for this report:

Munshi, Sandeep. 2025. *Lower Cost High Performance and High Efficiency Pilot-Ignited Directly Injected HD Natural Gas Engine*. California Energy Commission.
Publication Number: CEC-500-2025-016.

TABLE OF CONTENTS

Preface.....	i
Abstract	ii
Executive Summary.....	1
CHAPTER 1: Introduction	2
High-Pressure Direct Injection (HPDI) of Natural Gas	2
Aims and Objectives.....	4
CHAPTER 2: Prototype-A Engine Development and Baseline	5
Base Engine System Installation.....	5
Test Condition Definition	7
Prototype-A Engine Baseline Testing	8
CHAPTER 3: Cost Reduction	10
Overall Cost Reduction Analysis	10
New Fuel Pressure Control Module Design and Development.....	11
Injector Cost Reduction Evaluation.....	12
Prototype (J236) Injector Design and Procurement	13
J236 Injector Components and Performance.....	14
Injector Durability Evaluation.....	17
Cost Reduction Potential from Exhaust Aftertreatment Systems	19
Conclusions	21
CHAPTER 4: Efficiency Enhancement through Engine Hardware Optimization	23
Engine Cycle Modeling and Analysis	23
Effect of Valve Timing	23
Engine Valvetrain Low Friction Coating Study.....	24
Exhaust Energy Recovery	24
Electrical Turbo-Compound Detailed Analysis.....	26
Efficiency Improvement and Energy Recovery Conclusions	28
CHAPTER 5: Virtual Sensor for Combustion Robustness Control	29
Available Virtual Sensing Technologies and Hardware Selection	29
Virtual Sensor Architecture and Controls Integration	31
Design of Virtual-Sensor Based Combustion Control	32
Fuel Composition Compensation with Virtual-Sensor Based Controller	33
Virtual Sensor Combustion Compensation Conclusions	35
CHAPTER 6: Engine Combustion Enhancement	36
CFD Model.....	36
CFD Simulation of Advanced Combustion Strategies.....	37
Piston Bowl Shape	37

Injector Parameters Modeling Analysis	38
Partially-Premixed Combustion.....	39
Experimental Engine Testing of Improved HPDI Combustion Strategies.....	40
Engine Operating Parameter Variations	40
Compression Ratio and Swirl Effects.....	44
Intake Valve Closing Timing.....	45
High Flow Injectors	47
Split Injection/Multiple Injections	48
Experimental Evaluation of Advanced Combustion Modes	50
Partially-premixed Combustion.....	50
Homogeneous Charge Compression Ignition.....	51
Fumigated (Premixed) Combustion	53
Combustion Enhancement Summary	54
CHAPTER 7: Aftertreatment Optimization	56
DOC Performance	56
Metallic DOC/DPF.....	57
Exhaust Thermal Management:.....	58
Joint EATS Optimization in Conjunction with Engine Optimization.....	60
CHAPTER 8: Final Engine Configuration and Calibration.....	61
Final Engine Architecture	61
Fumigation System with Prototype-B Engine	61
High-load Prototype-B Engine Performance	62
Calibration Points for Prototype-B Engine.....	63
Mode-by-mode Optimization with Prototype-B Engine	64
Final Calibration Development.....	67
Performance and Emissions Verification of Prototype-B Engine	67
Verification of Fuel Composition Protection from Virtual Sensor.....	68
Verification of Final Engine Hardware and Calibration	71
Prototype-B Emissions and Fuel Consumption	72
Final Engine Calibration Summary	73
CHAPTER 9: Final Cost Reduction Evaluation	75
Engine Cost Savings.....	75
Fuel Consumption Cost Savings	75
CHAPTER 10: Final Conclusions	78
CHAPTER 11: Technology Transfer and Production Readiness Plans.....	80
Technology Transfer Plan	80
Production Readiness Plan.....	81
Glossary and List of Acronyms	83
References	85

LIST OF FIGURES

Figure 1: KW T408 SARE with a B-double trailer configuration powered by an HPDI engine.....	2
Figure 2: Westport HPDI Fueling System Overview	3
Figure 3: Prototype-A engine and aftertreatment system installed in test cell.....	6
Figure 4: Engine torque curve using baseline engine calibration.....	8
Figure 5: PM and CO emissions from the baseline, as a percent of the contribution to the total engine-out emissions over the full engine test cycle	9
Figure 6: NOx and THC emissions as a percentage of the total engine-out emissions over the full engine test cycle.....	9
Figure 7: Relative cost for HPDI fuel system and major subsystems. Fuel Conditioning Module is the fuel control module used to regulate the gas pressure to the injectors.....	10
Figure 8: Assembled Gas Control Module.....	11
Figure 9: Function cost Pareto diagram, HPDI injector.....	13
Figure 10: J236 upper body, nozzle, and selected components as received.....	15
Figure 11: Photos of J236 injector components and assembly as received from the supplier.....	15
Figure 12: Diesel and natural gas flow rates versus commanded pulse-widths, relative to the maximum flow rate. Flow rates shown for two representative J236 injectors (serial numbers A3207 and A3141).	16
Figure 13: Composite emissions over single-cylinder engine test cycle, comparing two individual prototype injectors relative to reference (standard J36 injector). Results shown are the emissions or performance for the injector divided by the value for the reference injector.....	17
Figure 14: Injector durability test stand used to evaluate prototype injectors.....	18
Figure 15: Before- and after-durability testing flow curves for the J236 prototype injector.....	18
Figure 16: Borescope view of pilot needle seat (inside gas needle) after engine test	19
Figure 17: Needle seating surface after engine test (red marking was added after disassembly to aid alignment inspection).....	19
Figure 18: Relative size and platinum group metal loading for two prototype DOCs.....	21
Figure 19: DPF size comparison for partial-flow DPF.....	21
Figure 20: Schematic of simulated exhaust energy recovery system.....	26

Figure 21: Net system efficiency improvement (including engine and turbo-generator work) as a function of engine brake power with constant fueling at SET mode 8 (B100 – 100 percent load at 1490 RPM).....	27
Figure 22: Sensitivity of individual sensor measurement values to changes in net heat release calculated from cylinder pressure data. Shown are: intake manifold pressure (top-left); calibrated knock sensor output (top-right); exhaust temperature (lower-left); exhaust oxygen concentration (lower right).	30
Figure 23: Schematic of information flow for virtual sensor.....	31
Figure 24: Functional architecture for prototype-A control system.....	32
Figure 25: Virtual sensor control algorithm flow chart. SOC, HR, and CHR stand for start-of-combustion, heat release, and cumulative heat release, respectively.....	33
Figure 26: Demonstration of virtual sensors correction of fueling quantity to maintain target power. Cylinder pressure (left) and HRR (right) for standard (MN87), base fueling with low MN fuel (MN65) and the virtual-sensor corrected fueling (MN65).....	34
Figure 27: Torque at each of the 12 SET modes (excluding idle) for the baseline (MN87), uncorrected (MN54 with baseline injection commands), and corrected (MN54 with the virtual-sensor based injection correction) conditions.....	34
Figure 28: CFD validation results, heat-release rates (left), and emissions (right) for two generic HPDI combustion conditions	36
Figure 29: Acetylene concentration and mixture fraction in combustion chamber with base piston geometry (top) and new piston design (bottom)	37
Figure 30: Change in CFD-based predicted emissions at high load from base piston to new piston design.....	38
Figure 31: Effect of nozzle geometries on predicted PM, unburned fuel, NO _x , and indicated specific fuel consumption (ISFC), compared to baseline. All at SET mode 8 (full load, 1500 RPM), with EGR.....	38
Figure 32: CFD predictions of engine-out PM and CH ₄ for baseline and two partially-premixed combustion strategies (PPC(A)' and 'PPC(B)')	39
Figure 33: Phi-T plots for baseline and two partially-premixed combustion strategies, showing mixture fraction concentration at a fixed timing (10oCA ATDC). Left: baseline; center: PPC(A); right: PPC(B). The plots show the relative concentration of the unburned and burned gases relative to the regions where significant concentrations of NO, acetylene, and unburned hydrocarbons are formed.....	40
Figure 34: Effects of EQR on engine-out PM for all tests conducted using the prototype-A engine and standard fuel quality	41
Figure 35: Effect of injection pressure on PM mass, BSFC, and NO _x emissions at mid-speed, 75 percent load operating condition (B75)	41

Figure 36: Effects of IMT on FSN-NO _x and HC-NO _x trade-offs. Multi-cylinder engine operating at steady state at mode 4 (B75: 1493 RPM, 75 percent load).....	42
Figure 37: Effects of coolant temperature on composite BSFC, PM, NO _x , and HC over the SET cycle.....	42
Figure 38: Combined effects of pilot fueling quantity (pilot Q) and separation delay (timing) on PM-NO _x and BSFC-NO _x tradeoffs, at baseline and reduced pilot quantities and standard and minimum pilot-gas delay.....	43
Figure 39: Composite emissions results; emissions are engine-out.....	44
Figure 40: Image of cylinder head fire deck (viewed from below [inside the combustion chamber]) showing swirl plates installed in intake ports	44
Figure 41: Images of baseline piston (left) and modified piston (right)	45
Figure 42: Full single-cylinder engine cycle composite (engine-out) emission results comparing emissions with base (17:1) compression ratio with 15:1 CR standard intake ports and 15:1 with swirl plates (SP) installed in the intake to increase swirl.....	45
Figure 43: Effect of LIVC on single-cylinder engine emissions over the SCRE 9-mode test cycle. Emissions are composite over the full test range.	46
Figure 44: Heat release rate and cylinder pressure during pumping for standard and LIVC40 cam phasings. SCRE data taken at 1500 RPM, 50 percent load.....	47
Figure 45: Torque at high load with high-flow injectors compared to baseline injector capabilities	48
Figure 46: Relative change in power-specific emissions and fuel consumption at the torque curve for the high-torque calibration versus the baseline torque settings	48
Figure 47: Effects of split gas injection on CH ₄ and BSFC, relative to NO _x , at 1200 RPM, 25 percent load.....	49
Figure 48: Split pilot injection effects on CH ₄ -NO _x and BSFC-NO _x trade-offs. Split pilots 1 and 2 refer to two different pilot separation timings. Results shown for 1200 RPM, 25 percent load.	49
Figure 49: Effects of PPC on PM and NO _x emissions as a function of EGR.....	50
Figure 50: Effects of PPC on BSFC as a function of EGR.....	51
Figure 51: Composite emissions for PPC over 13 mode cycle	51
Figure 52: FSN-NO _x and BSFC-NO _x trade-offs comparing HCDI and HPDI strategies at 1500 RPM, mid-load conditions	52
Figure 53: CH ₄ -NO _x and BSFC-NO _x trade-offs, comparing HCCI and HPDI strategies at 1500 RPM, low-load conditions	52
Figure 54: Fumigation system schematic, including control connections	53
Figure 55: FSN versus torque comparing fumigated combustion to HPDI at 1493 RPM.....	54

Figure 56: Exhaust gas temperature versus torque for fumigated and HPDI combustion	54
Figure 57: Comparison of emissions conversion efficiency across EATS with two prototype DOCs relative to baseline EATS performance (negative value indicates reduced conversion efficiency).....	56
Figure 58: Prototype DOC/DPF system installed on test cell engine	57
Figure 59: Metallic DPF results, including single or double-brick systems for both DOC and DPF	58
Figure 60: Temperature drop between turbocharger outlet and DOC inlet over all 13 SET modes, with and without insulation on the exhaust system.....	58
Figure 61: Changes in DOC and SCR emission conversion efficiencies with the addition of insulation. DOC results refer to reduction in total HC across the DOC, SCR refers to reduction in total NOx across the SCR. For the SCR, DEF injection was equal with and without insulation.	59
Figure 62: PM reduction versus NOx compared to the required SCR efficiency to maintain tailpipe NOx emissions, and regime where extra margin on tailpipe NOx would be available.....	60
Figure 63: FSN as a function of engine torque for prototype-B HPDI and fumigated combustion strategies. FSN normalized by the FSN at 75 percent load for the HPDI with EGR case.....	62
Figure 64: BSFC as a function of engine torque for prototype-B HPDI and fumigated combustion strategies. BSFC normalized by the BSFC at 75 percent load for the HPDI with EGR case.....	62
Figure 65: Heat-release rate and cylinder pressure at peak torque, 1493 RPM, for prototype-A and prototype-B engines. Prototype-B shown for both base (475 hp) and 520 hp ratings.....	63
Figure 66: Engine torque curve and calibration points for 520 hp prototype-B engine. The prototype-A (475 hp) engine torque curve is also shown for comparison.	64
Figure 67: Optimization trade-offs at B100 (1493 RPM, 100 percent load) for calibration of prototype-B engine. All values normalized by the optimum point selected for the final calibration, shown by the red square.....	65
Figure 68: Turbine inlet temperature and peak cylinder pressure versus engine-out NOx for the final calibration at B100 (1493 RPM, 100 percent load) for the prototype-B engine. Turbine inlet temperature and PCP normalized by engine limit. NOx normalized by the optimum point selected for the final calibration, shown by the red square.	65
Figure 69: Optimization trade-offs at C50 (1770 RPM, 50 percent load) for final calibration of prototype-B engine. All values normalized by the optimum point selected for the final calibration, shown by the red square.....	66

Figure 70: Turbine inlet temperature and peak cylinder pressure versus engine-out NO_x for the final calibration at C50 (1770 RPM, 50 percent load) for the prototype-B engine. Turbine inlet temperature and PCP normalized by engine limit. NO_x normalized by the optimum point selected for the final calibration, shown by the red square.67

Figure 71: Mode-by-mode torque for MN90 and MN54 fuels using the virtual sensor69

Figure 72: Pressure trace and heat release rate for reference fuel (MN90), MN54 fuel with base injection timings, and MN54 fuel with corrected injection timings set with the virtual-sensor based controller. Prototype B engine with 520 hp calibration, 75 percent load, 1220 RPM (A75).69

Figure 73: Key engine-out emissions and hardware parameters for reference fuel (MN90), MN54 fuel with base injection timings, and MN54 fuel with corrected injection timings set with the virtual-sensor based controller. Prototype B engine with 520 hp calibration, 75 percent load, 1220 RPM (A75).70

Figure 74: Effect of low-quality (MN54) fuel on composite emissions for the prototype-B 520 hp engine. Emissions are shown relative to the standard (MN90) fuel.71

Figure 75: 13-mode cycle composite engine-out and tailpipe emissions and fuel consumption for prototype-B engine for 520 hp, relative to the prototype-A engine for 475 hp72

Figure 76: Total fuel consumption and diesel contribution at individual modes, for the 520 hp prototype-B engine relative to the 475 hp prototype-A engine. All individual modes except idle shown.73

Figure 77: Discounted savings from prototype-B improved efficiency relative to prototype-A. Base condition values: discount rate (DR) 0.05; natural gas fuel cost: 2.32 \$/gallon diesel equivalent; annual mileage: 80,000; diesel fuel cost: 4.12 \$/gallon.....76

LIST OF TABLES

Table 1: Prototype-A Engine Hardware Specifications5

Table 2: Steady-State Test Points7

Table 3: Exhaust Aftertreatment Component Rankings20

Table 4: DLC Coatings Considered for Valvetrain Friction Reduction24

Table 5: Comparison of energy recovery technologies25

Table 6: Mode-by-mode Efficiency Improvements with Electrical Turbo-Compound27

Table 7: Sensors Evaluated for Virtual Sensor29

Table 8: Mass-based Gaseous Fuel Composition for Virtual Sensor Verification.....68

Table 9: Margin for regulated emissions for prototype-B engine and standard fuels at 520 hp74

Executive Summary

This project was conducted to investigate improvements to Westport Fuel Systems' (Westport) natural gas fueled heavy-duty high-pressure direct injection (HPDI) engine product, the Westport HD 15L. The key objectives were to reduce cost, improve efficiency, and increase power while maintaining regulated tailpipe emissions below legislated standards and decreasing sensitivity to variations in fuel quality. The work was conducted by Westport's technology office as part of a larger ongoing HPDI product improvement and cost reduction project at Westport.

The targeted increase in engine power was demonstrated through the use of higher-flow injectors plus a revised engine calibration. These combined to achieve a 10-percent increase in rated power (to 520 horsepower) while maintaining tailpipe emissions below the U.S. Environmental Protection Agency and California Air Resources Board 2010 levels over a 13-mode steady-state cycle. Efficiency was also slightly increased through the optimized calibration. Further significant efficiency improvements could be achieved through the use of exhaust-energy recovery systems that were evaluated in this project.

A virtual sensor was developed to enable the engine controller to adjust the fueling commands for changes in fuel composition. The final version of the virtual sensor combines the intake manifold pressure sensor with a start-of-combustion sensor based on bearing-cap mounted knock sensors. The information from these two sources is combined and processed by a separate controller that adjusts the natural gas start-of-injection timing and pulse width. The system was demonstrated to maintain engine torque for methane numbers as low as 54.

Cost reduction exercises for the California Energy Commission program were combined with other initiatives at Westport to achieve significant cost reductions on key fuel system components. Evaluation of new aftertreatment systems revealed significant cost savings potentials from reduced precious metal loadings, particularly in the diesel oxidation catalyst. These savings could be combined with engine-out emissions reductions through calibration improvements and modifications to minimize the pollutant reduction requirements of the aftertreatment system.

The project met the key objectives, and further technology development is planned for the enhanced 15L HPDI engine. Further refinement of both the hardware and the engine calibration will be needed to convert the results to a product-ready engine certified over a transient test-cycle. This work will be conducted by the Westport product development team as part of the ongoing product improvement exercises.

CHAPTER 1:

Introduction

The application of natural gas to heavy-duty transportation applications offers the potential for reduced dependence on liquid fossil fuels and lower greenhouse gas (GHG) emissions while substantially reducing fuel costs. Implementing a natural gas combustion system that maintains the performance and efficiency of the diesel engine has been hampered by the stability of the methane molecule, a principal constituent of natural gas, which prevents controllable autoignition combustion. Most current natural gas engines replace the non-premixed autoignition of a diesel engine with a premixed, spark-ignition system for natural gas. Premixing of natural gas dictates a reduction in compression ratio to avoid knock, while the need to maintain a combustible stoichiometry over the full engine map results in the need to throttle at part load; both steps significantly reduce efficiency compared to a diesel engine. To avoid these effects, the natural gas can be injected directly into the cylinder at high pressure and burned in a predominantly non-premixed manner; however, a separate ignition source is required. In Westport's system for high-pressure direct injection (HPDI) of natural gas, this is provided through diesel pilot combustion used to ignite a non-premixed natural gas jet.

The project work focused on improving Westport's existing HPDI of natural gas engine technology, with a focus on the Westport HD 15L HPDI engine. The project used experimental engine testing and computational analysis to provide a more robust, lower cost, higher performance, and higher efficiency combustion system while still meeting California and North American emission regulations.

High-Pressure Direct Injection (HPDI) of Natural Gas

HPDI is a pilot-ignited non-premixed natural gas combustion strategy that uses a two-fuel concentric-needle injector. It is in service in commercial heavy-truck applications in North America and Australia (Figure 1). In-use results show that performance and efficiency are essentially equivalent to the base diesel engine, while approximately 95 percent of the fuel used (on an energy basis) is natural gas. Compared to other natural gas combustion strategies, the fact that HPDI is non-premixed leads to low methane emissions and high natural gas substitution rates while retaining the diesel engine's high efficiency.

Figure 1: KW T408 SARE with a B-double trailer configuration powered by an HPDI engine

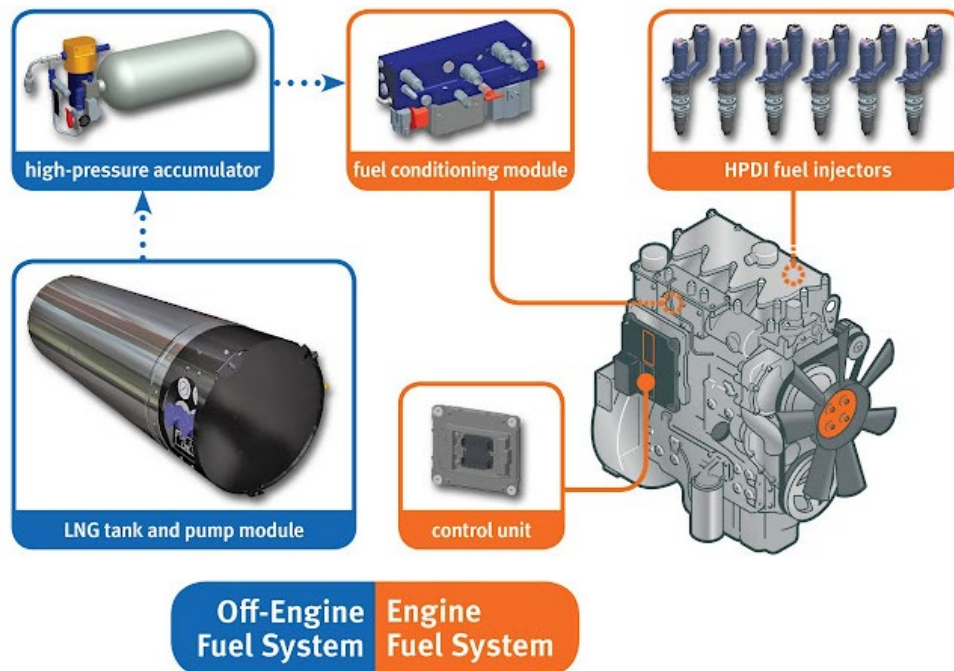


The HPDI combustion process relies on a late-cycle high-pressure injection of natural gas directly into the combustion chamber of the engine. The air exchange and compression process are identical to that of a traditional diesel engine. As the piston approaches top-dead-centre of the compression stroke, a small amount of diesel is injected. This diesel injection is followed by an injection of natural gas through separate nozzle holes within the same injector body. Typically, the gas and diesel holes are aligned so that each gas jet is adjacent to at least one diesel spray. The separate diesel pilot sprays auto-ignite, providing multiple ignition sources that are spatially distributed, ensuring ignition of all the natural gas jets. The natural gas combustion then proceeds in a predominantly non-premixed fashion. As a result, engine knock is avoided and the base diesel engine's compression ratio can be retained. Because the natural gas is not premixed, load control is achieved by simply reducing the fuel flow, as in a conventional diesel; part-load throttling is not required. Compared to an identical diesel engine, an HPDI-equipped engine provides the following benefits:

- Well-to-wheel GHG emissions reduced by over 20 percent
- Equivalent efficiency, power, and torque
- Reduced fueling cost over the life of a typical heavy-duty truck
- Reduced dependence on liquid fossil fuels

A schematic of the HPDI fueling system for a heavy-duty truck is shown in Figure 2. The off-engine fueling system shown in the figure is a liquefied natural gas (LNG) system, complete with storage tanks, compressor pumps, and fuel conditioning for a heavy-duty truck.

Figure 2: Westport HPDI Fueling System Overview



Aims and Objectives

The overall aim of this project was to develop an improved HPDI fueling system to provide improved performance with lower upfront and operating costs while meeting all relevant emission regulations. The specific objectives of the work were:

1. Reduce the HD HPDI engine system component costs (fuel system, in particular injectors and fuel rail pressure control module, and exhaust after treatment) by 20 percent.
2. Reduce HPDI fuel consumption by 5 percent from current levels over a European Steady-state Cycle (ESC) test, which will lead to a 20 percent lower ESC averaged fuel consumption compared to today's spark-ignition engine.
3. Improve HPDI power density by 10 percent (up to 21.5 bar) from the current level, which will lead to an engine power density that is approximately 25 percent higher compared to the average performance of today's spark-ignition engines.
4. Maintain emissions below U.S. Environmental Protection Agency (EPA) 2010 emissions targets (0.2 grams per brake horsepower-hour NO_x, 0.01 grams per brake horsepower-hour PM, 0.14 grams per brake horsepower-hour NMHC) while improving on today's GHG emissions by approximately 20 percent.
5. Improve engine operating robustness to natural gas quality and achieve satisfactory engine operation for a wider range of Wobbe index (45-55 MJ/std.m³ based on lower heating value of NG) and methane number (50-100).

CHAPTER 2:

Prototype-A Engine Development and Baseline

The base engine used in this work was a Westport HD 15L HPDI engine. The engine was a Cummins ISX 15L diesel engine equipped with a Westport HPDI fueling system, including injectors, natural gas fuel supply system, and a separate fueling control computer. The remaining engine hardware (including piston geometry and valve timing) and auxiliary systems (including air handling and exhaust aftertreatment) are the same as on the base ISX platform. The prototype-A engine was developed and installed in the test cell to enable evaluation of improvements to both the base ISX engine hardware and the Westport fueling system that would further optimize the engine system for natural gas combustion.

Base Engine System Installation

A Westport HD 15L HPDI engine equipped with a new production aftertreatment system was integrated in a test cell at Westport. Key engine specifications are provided in Table 1. The test cell was equipped with an eddy-current dynamometer capable of absorbing power up to the levels intended for the project. Automated test-cell control hardware was used to communicate with both the base engine control unit (ECU) and the Westport fueling system controller. The engine installation showing the exhaust aftertreatment is shown in Figure 3.

Table 1: Prototype-A Engine Hardware Specifications

Base Engine	Cummins ISX 15L
Bore/Stroke/Connecting Rod Length	137/169/261 mm
Swept Volume	2.49 L/cylinder
Number of Cylinders	6
Compression Ratio	17:1
Air Handling	VGT, intercooled, cooled EGR
Fuel System	Westport HPDI
Injector	J36
Hole Number/Angle	Diesel: 7/180; Gas 9/180
Fuel Rail Pressure	Up to 30 MPa

Figure 3: Prototype-A engine and aftertreatment system installed in test cell



The engine was fully instrumented for research purposes. This included in-cylinder pressure monitoring using water-cooled Kistler pressure transducers, high-resolution crank-angle measurements using an optical encoder, and intake and exhaust system pressures and temperatures. Base performance information, including diesel and gas flow rates, charge air flow, and engine torque, were also measured. The prototype-A engine system was equipped for emissions measurements with sampling from both before and after the aftertreatment system (referred to as engine-out and tailpipe respectively). Gaseous emissions were measured using a Horiba MEXA7100D-EGR twin bench, equipped with two full sets of analyzers to provide carbon monoxide (CO), methane (CH₄), total hydrocarbon (THC), carbon dioxide (CO₂), nitrogen oxides (NO_x), and oxygen (O₂) concentrations simultaneously from both sampling points. Particulate matter (PM) mass was also measured using gravimetric filters (using a Sierra Instruments BG-2 sampling system), sampled either engine-out or tailpipe. To reduce the time required for testing, gravimetric PM samples were only taken at selected modes; for most of the work, filter smoke number (FSN) was used as a surrogate for PM mass. This was measured for all tests using an AVL smoke meter. The instrumentation output was collected and compiled through dedicated test-cell hardware, which was then passed through standardized data-processing routines. The results were then available to the research team for interpretation and further analysis.

To enable more advanced combustion strategies (to be tested on-engine in Q6 and later), the intake air handling system was modified to provide better control over the intake manifold temperature and pressure. The charge air handling system used both a conventional feed through an air-to-water charge air cooler and a bypass around the cooler. The design implemented here included a throttle valve in the bypass used to control the pressure drop, and hence flow rate, through this bypass. To maintain realistic charge air temperatures, a PID control algorithm was added to the engine control system. This control system adjusts the relative quantity of the flow bypassing the charge cooler to maintain the target intake manifold

temperature (IMT). Improved intake manifold pressure control was also considered to be desirable for some of the combustion strategies; as a result, a throttle valve was added to the intake upstream of the exhaust gas recirculation (EGR) mixer.

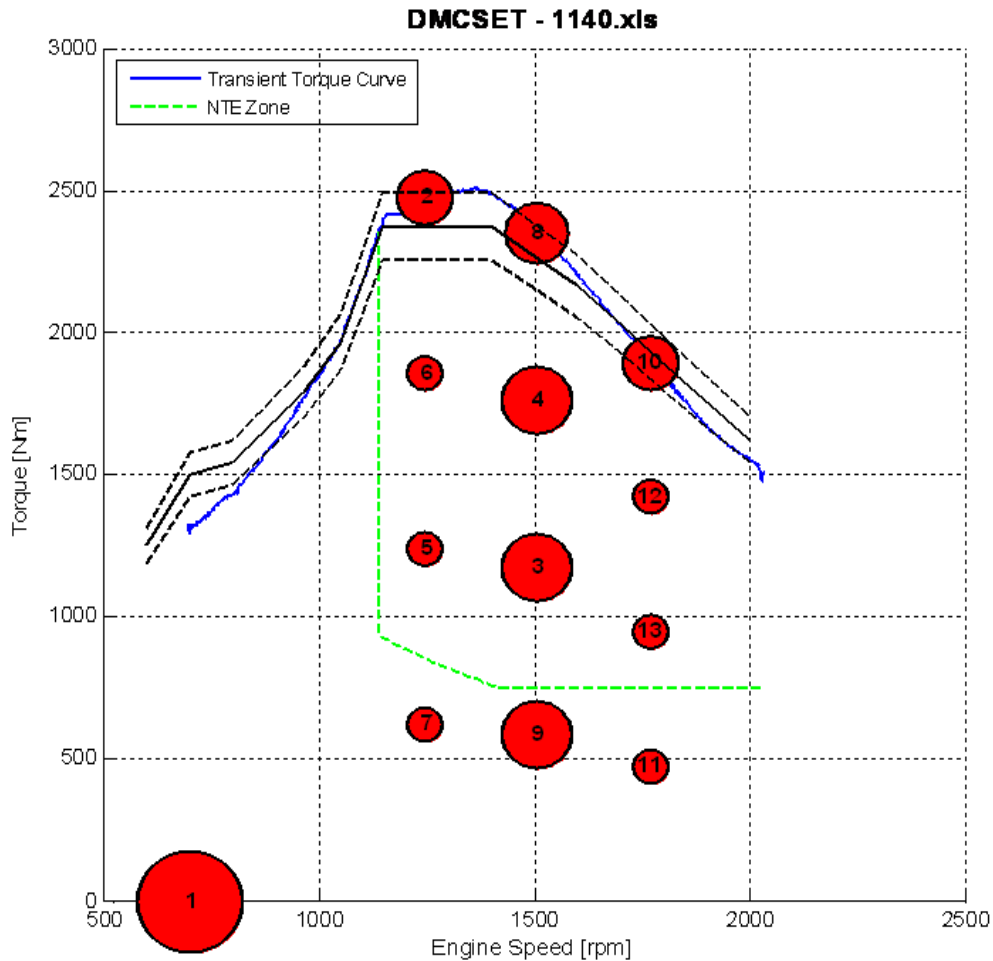
Test Condition Definition

The engine testing conducted in this project focused on the supplemental emissions test (SET) 13-mode steady-state cycle. These points are functionally equivalent to the 13 modes of the ESC and are widely used for heavy-duty engine testing under steady-state conditions. The modes are listed in Table 2, including the engine speed and torque, the mode identifier, and the weighting factor. To generate a composite value for emissions or fuel consumption, the results at each individual mode are recorded, then multiplied by the weighting factor and summed to get an SET-cycle composite value. These are shown schematically in Figure 4.

Table 2: Steady-State Test Points

SET cycle mode	Mode	Speed (RPM)	Torque (N.m)	Weighting Factor
1	Idle	650	0	0.15
2	A100	1220	2300	0.08
3	B50	1493	1100	0.1
4	B75	1493	1650	0.1
5	A50	1220	1150	0.05
6	A75	1220	1725	0.05
7	A25	1220	575	0.05
8	B100	1493	2200	0.09
9	B25	1493	550	0.1
10	C100	1750	1880	0.08
11	C ₂₅	1750	470	0.05
12	C75	1750	1410	0.05
13	C50	1750	940	0.05

Figure 4: Engine torque curve using baseline engine calibration



Prototype-A Engine Baseline Testing

As part of the engine commissioning, the functionality of the prototype-A was verified in the engine test cell. Baseline testing with and without the exhaust aftertreatment system (EATS) was also carried out. The baseline tests were repeated at quarterly intervals throughout the project to identify any changes in engine performance. Further, after any change to base engine hardware (such as injectors or aftertreatment components) the baseline test sequence was replicated.

The baseline engine-out emissions are shown in Figure 5 and Figure 6. These results are presented in the form of percentage contribution of the weighted engine-out emissions at a specific mode to the total engine-out emissions over the composite SET cycle. The results reveal that PM and CO are dominated by high-load operating modes, while NO_x and unburned hydrocarbons are more evenly distributed. All the results presented here are for the baseline calibration for the engine at the beginning of the project.

Figure 5: PM and CO emissions from the baseline, as a percent of the contribution to the total engine-out emissions over the the full engine test cycle

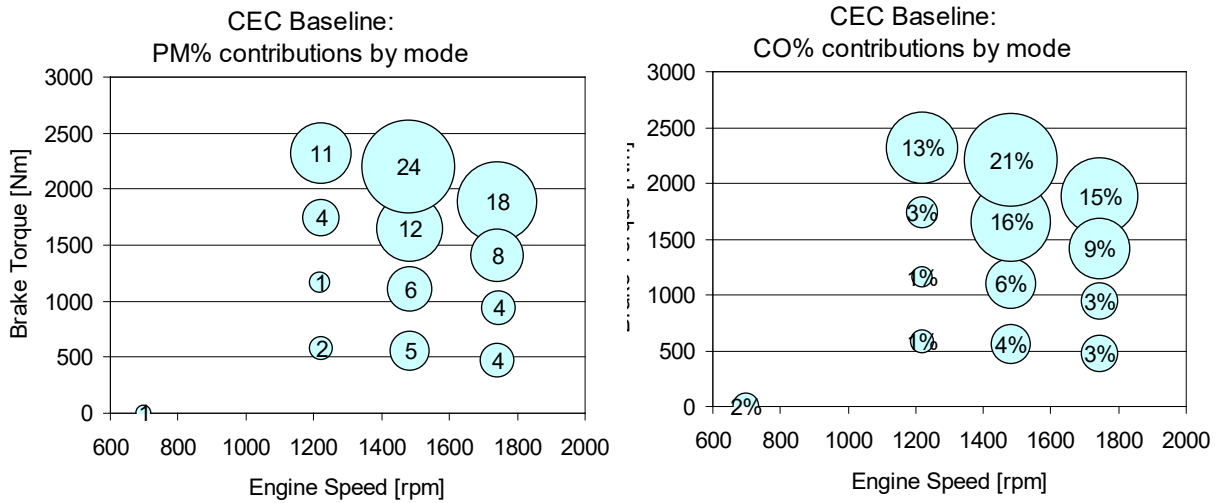
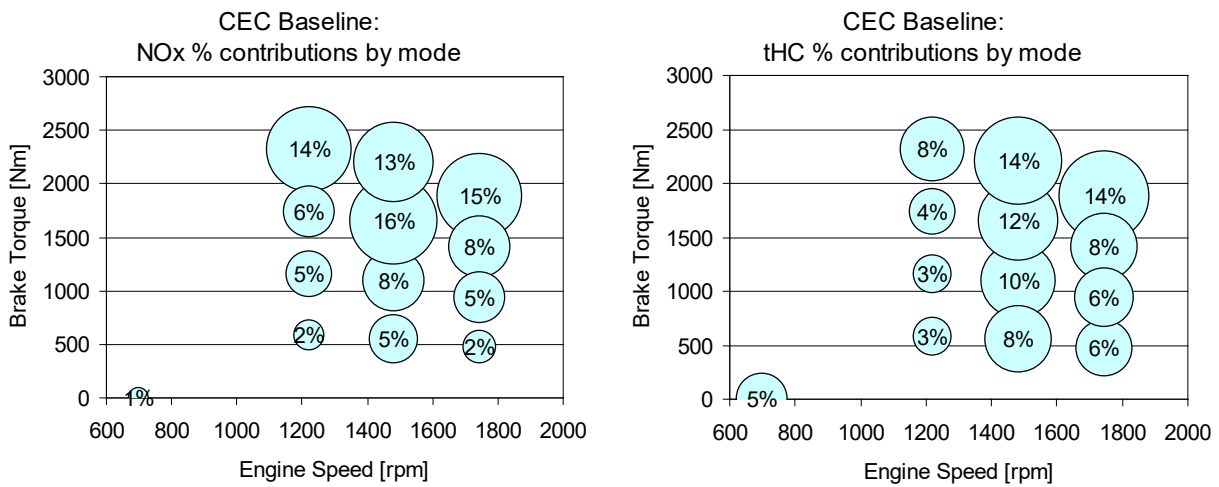


Figure 6: NOx and THC emissions as a percentage of the total engine-out emissions over the full engine test cycle



CHAPTER 3:

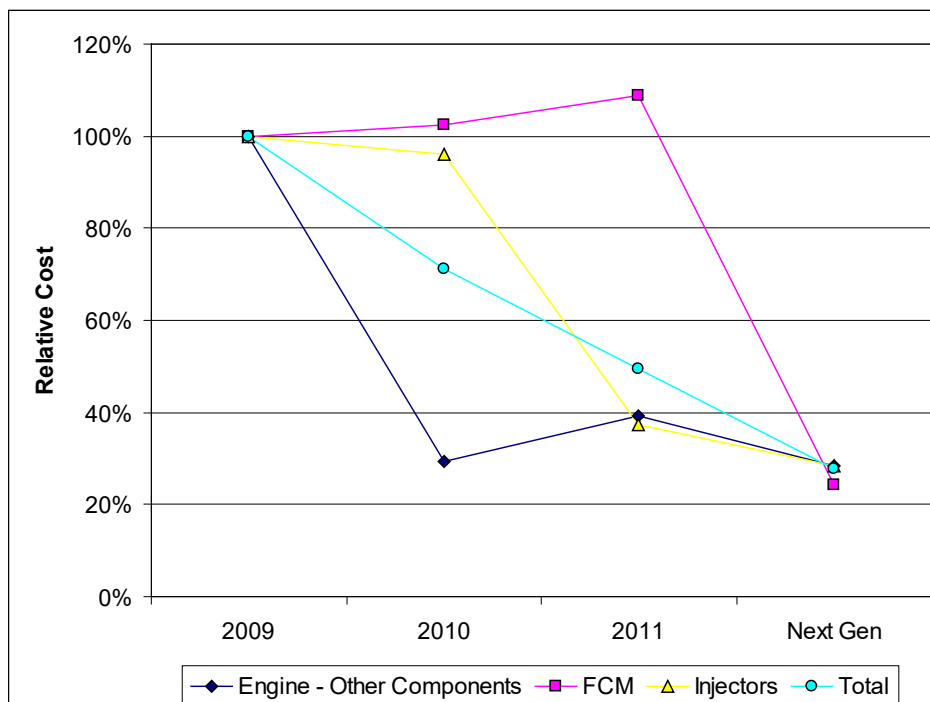
Cost Reduction

One of the key objectives of the work was to reduce the overall cost of the Westport fuel system. This is part of an ongoing process at Westport to reduce system costs and make the HPDI product more attractive in the market. Westport completed preliminary design work on new concepts resulting from a Value Analysis/Value Engineering (VAVE) exercise prior to the start of this project. The main cost reduction targets for the HPDI fueling system were the injectors and the fuel pressure control module. As part of this project, a new injector design was developed that focused on reducing cost while improving functionality for application across platforms. Further cost-reduction exercises were also conducted on the exhaust aftertreatment and the fuel pressure control modules.

Overall Cost Reduction Analysis

The overall, fuel-system wide cost reduction initiative was undertaken to target significant cost savings as a result of design improvements, process improvements, and supplier changes. As shown in Figure 7, this effort was highly successful at reducing the overall system cost, which is down by approximately 50 percent from 2009 to 2011, with a further reduction to approximately 25 percent of the 2009 system cost projected for the next generation of HPDI fuel system.

Figure 7: Relative cost for HPDI fuel system and major subsystems. Fuel Conditioning Module is the fuel control module used to regulate the gas pressure to the injectors

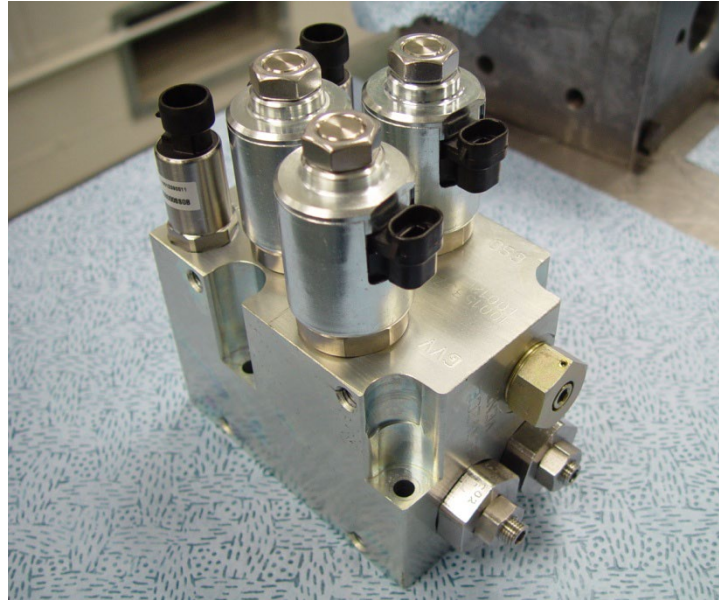


It should be noted that the overall reduction to 25 percent of the 2009 baseline cost is achieved through reductions for each of the major subsystems (as shown in Figure 7) of nearly equal proportion. The major decrease in injector cost between 2010 and 2011 shown in the figure was a result of a change in primary supply for the current J36 injectors (this does not represent the new injector designed in this project). Likewise, the projected reduction in the Fuel Conditioning Module (FCM) cost from 2011 to the next generation fuel system is achieved primarily by working with a new supplier who was able to provide a significantly lower cost for the main pressure regulator. The design improvements to the injector and the fuel pressure control to be undertaken in this work are additive to the cost reductions demonstrated in Figure 7.

New Fuel Pressure Control Module Design and Development

In an attempt to reduce the cost and complexity of the HPDI fuel system, the design and development of a new fuel pressure regulation system, the gas control module (GCM) was undertaken. The GCM, shown in Figure 8, represents a significant design change from the existing FCM. The FCM used a direct pressure control on the diesel and then controlled the gas pressure relative to the diesel. The GCM was designed to control the gas and diesel rail pressures independently. As well, the FCM provided a continuous range from minimum to maximum operating pressure; the new GCM was designed to only operate at two discrete set pressures.

Figure 8: Assembled Gas Control Module



While the GCM functioned as designed, several functionality problems were identified. For one, the HPDI injectors require that the diesel rail pressure exceed the gas rail pressures at all times. While this is automatically controlled in the FCM, the GCM isolates the two fuels and uses pressure sensing to control downstream pressure. As a result, under certain conditions the gas rail pressure could exceed the diesel rail pressure, which may impair the functioning of the injectors. Furthermore, limiting the rail pressure to two discrete values imposed a

significant constraint on the engine calibration, as rail pressure is a key lever for controlling emissions and engine performance. Ultimately, it was determined that the technical challenges of the GCM concept are surmountable. However, it was determined that cost-reduction of the existing FCM could achieve similar cost targets to the GCM while maintaining the full range of performance afforded by continuous pressure control. This effort led to the replacement of the DLSR supplier and the associated cost reduction identified in section 3.1.

Injector Cost Reduction Evaluation

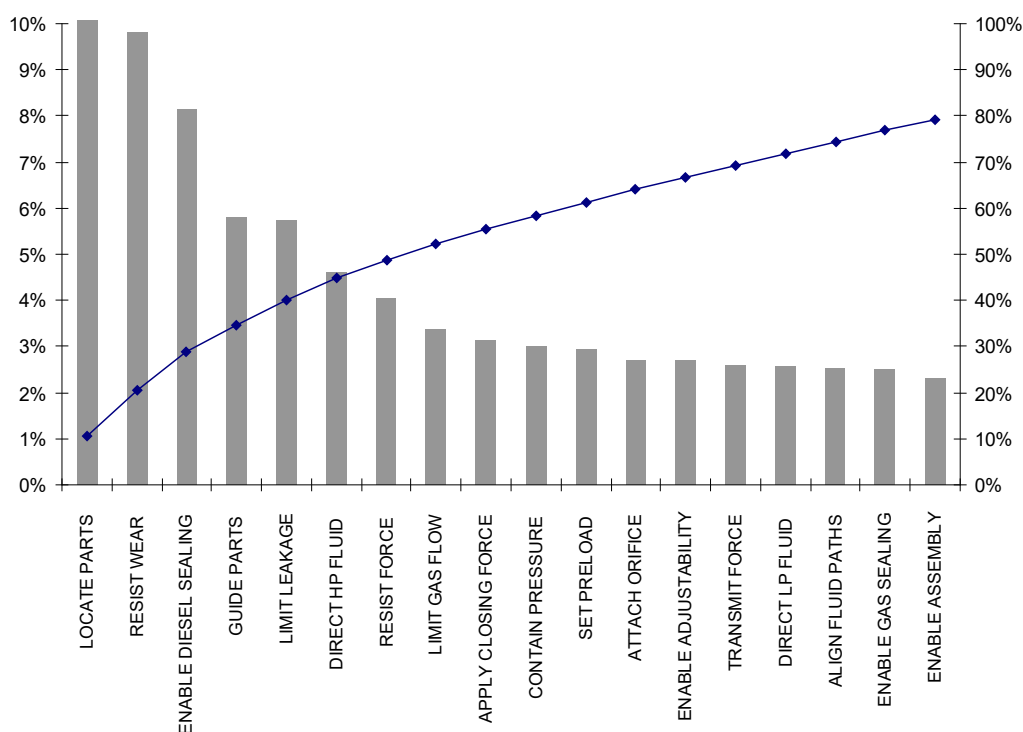
A cost-reduction assessment (VAVE) was conducted for the model J36 Westport HPDI injectors. First, an overall cost breakdown for the existing injector design was carried out, and material costs were found to account for approximately 73 percent of the total. This fraction of overall cost was the primary target for reduction. Next, component costs were analyzed and it was found that about 30 percent of the components accounted for the majority of the overall system cost. The key components identified in this exercise are:

- Valve seat
- Actuator block
- Injector body
- Gas needle and nozzle assembly
- Solenoid stator and armature
- Gas plunger and cap
- Pilot needle and plunger

Given that a large proportion of the system cost is contained in this small number of components, they make ideal targets for design improvements.

For the third stage of the analysis, the overall system was broken down by function, and the component costs associated with fulfilling each function were compiled. The key injector functions and their cumulative cost associated with achieving these functions are shown below in a Pareto diagram (Figure 9). With reference to the figure, it was found that the top eight functions accounted for 50 percent of the cost. The top 18 functions (shown in the figure) accounted for nearly 80 percent of the cost as shown below.

Figure 9: Function cost Pareto diagram, HPDI injector



Finally, brainstorming was carried out on the key functions identified from Figure 9 to generate the master list of cost reduction activities to be screened. The process generated a total of 516 ideas; a three stage screening process was used to reduce this on the basis of chances for success, feasibility, and potential impact to reach a total of 14 ideas to fully detail and summarize. Filtering these ideas to those assessed with a high probability of success (75 percent or greater) ultimately produced eight ideas selected as the top priorities for cost reduction activity on the injector. These ideas are summarized below:

1. One piece body control block
2. Simplified drillings
3. Modular actuators
4. Reconfigure nozzle body sealing surface groove
5. Modify the pilot needle geometry
6. Allow edge breaks
7. Use analysis to verify production requirements
8. Smaller actuators

Collectively, these actions represent a potential savings of approximately 20 percent on the overall cost of the injector.

Prototype (J236) Injector Design and Procurement

The results of the analysis discussed above were applied to the new injector design (model J236) prepared in this project. The J236 focused on a simplified injector design to reduce manufacturing costs while maintaining or improving functionality and reliability. The overall

design concept is to generate a generic nozzle with all the complex components located in a single, self-contained assembly. This would enable removal of the plungers, orifices, springs, and other components from the injector body, while simplifying the manufacturing with fewer drillings and complex flow passages. Specific components were identified for improved manufacturability and/or functionality. For example, the gas nozzle was modified so that there were no drillings for diesel passages and the gas passages were only simple drillings. Similarly, the pilot needle was lengthened to provide a greater tolerance to pilot seat eccentricity and to reduce part number. The pilot sleeve was also redesigned to be simpler, enabling future material upgrades as well as removing concentricity requirements. Functionally, the key difference for the new J236 injectors is that both the diesel and gas needles are actuated by diesel rather than by gas pressure.

The design process identified the following key benefits for the new J236 injectors compared to the standard J36 model injectors used on the current Westport HD 15L engines:

- A 33-percent reduction in number of components (excluding actuators) and reduced complexity for remaining components
- Decoupling of gas and diesel supply pressures to enable more flexibility in fuel rail pressure regulation
- Reduction in moving masses within injector to improve response times and durability

Once the injector design was completed, fabrication of the prototype components was ordered from Christopher Tool and Die. Electrical discharge machining of the nozzle holes for both gas and pilot was provided by a Westport production partner.

J236 Injector Components and Performance

The finished J236 injector parts were received, assembled, and the prototype injector's behavior was characterized on a flow test rig. Photos of the injector components as received and after assembly are shown in Figure 10 and Figure 11. Rig testing for flow rates and leakage was also performed. The results of the flow tests for two representative injectors are shown in Figure 12. The flow results reveal that for these injectors, the gas and pilot flows are consistent over a wide range of pulse widths. However, at low diesel pulse widths, the flow rates start to diverge; this is not surprising given the small quantity of diesel flow and this variability is within the expected range for these injectors.

Figure 10: J236 upper body, nozzle, and selected components as received



Figure 11: Photos of J236 injector components and assembly as received from the supplier

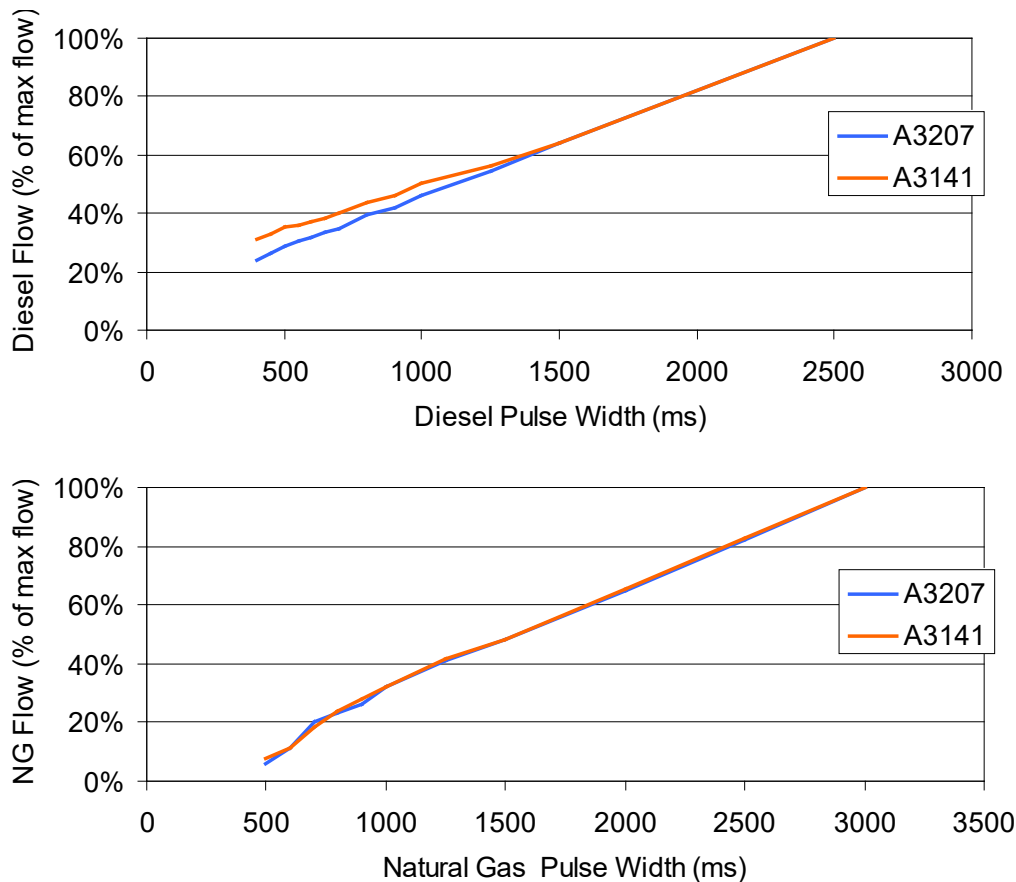


A: Assembled injector (less feed orifices, screens, o-rings, and actuators)



B: Comparison of new fully assembled J236 (right) with stock J36 (left)

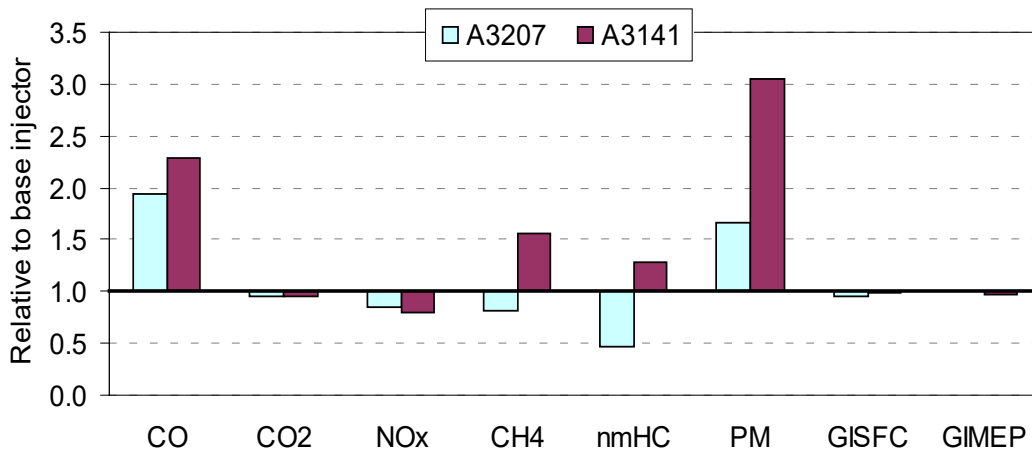
Figure 12: Diesel and natural gas flow rates versus commanded pulse-widths, relative to the maximum flow rate. Flow rates shown for two representative J236 injectors (serial numbers A3207 and A3141).



After receiving and testing the injectors on the test rig, they were installed in a single-cylinder research engine (SCRE) to evaluate performance and emissions. The SCRE was used for the initial testing because it enables detailed observation of the performance of individual injectors. This is considered particularly important for prototype injectors as a way to understand the general behavior of the injectors as well as to evaluate injector-to-injector variability. Summary results are provided in Figure 13, over a six-mode cycle involving 50 percent and 75 percent load at 1200, 1500, and 1800 revolutions per minute (RPM). The results clearly demonstrate that the basic performance of the injectors (in terms of power, gross indicated mean effective pressure, efficiency, and gross indicated specific fuel consumption) are within a few percentage points of the baseline injector. This level of variability is expected with the single-cylinder engine; therefore, these results indicate that the injectors can meet the desired performance. The emissions, also shown in Figure 13, demonstrate greater variability. NO_x emissions were consistently reduced by 10 to 15 percent. Conversely, CO and PM emissions were increased for both injectors, although the magnitude of the increase is variable. This may be attributed to part-to-part variability with the prototype injectors; seeing as both CO and PM are easily removed with existing aftertreatment systems, these changes are not a concern for meeting 2010 emissions standards. Hydrocarbon (HC)

emissions varied as well, with one injector showing reduced HC emissions and another showing increased HC emissions. In both cases, the change in regulated non-methane hydrocarbon (nmHC) emissions is within the range that the exhaust aftertreatment can absorb. As a result, it is reasonable to conclude that the prototype injector design is functional and does not differ substantially from the base injector in terms of its capability to meet 2010 emissions standards.

Figure 13: Composite emissions over single-cylinder engine test cycle, comparing two individual prototype injectors relative to reference (standard J36 injector). Results shown are the emissions or performance for the injector divided by the value for the reference injector.



Injector Durability Evaluation

After the flow and engine testing, the injectors were installed in a test stand to evaluate the durability of the prototype components. Figure 14 shows a photo of the durability test stand during the injector testing. The injector performance before and after the durability tests is shown in the flow curves provided in Figure 15. The results show that the diesel flow dropped marginally at low pulse widths over the duration of the tests; this reduction is within the range of uncertainty and is not considered to be significant. The maximum flow through the gas injector was also slightly reduced, but as this was only observed at substantially longer pulse-widths than used in normal operation, it is not considered to be a significant result. As such, the injectors passed the durability test with no component failures identified during the durability testing. At the end of the evaluation, several injectors were disassembled for evaluation. Selected photos of the disassembled injectors are shown in Figure 16 and Figure 17. It is worth noting that no significant degradation in the injector parts is seen between pre- and post-testing of the prototype injectors.

Figure 14: Injector durability test stand used to evaluate prototype injectors

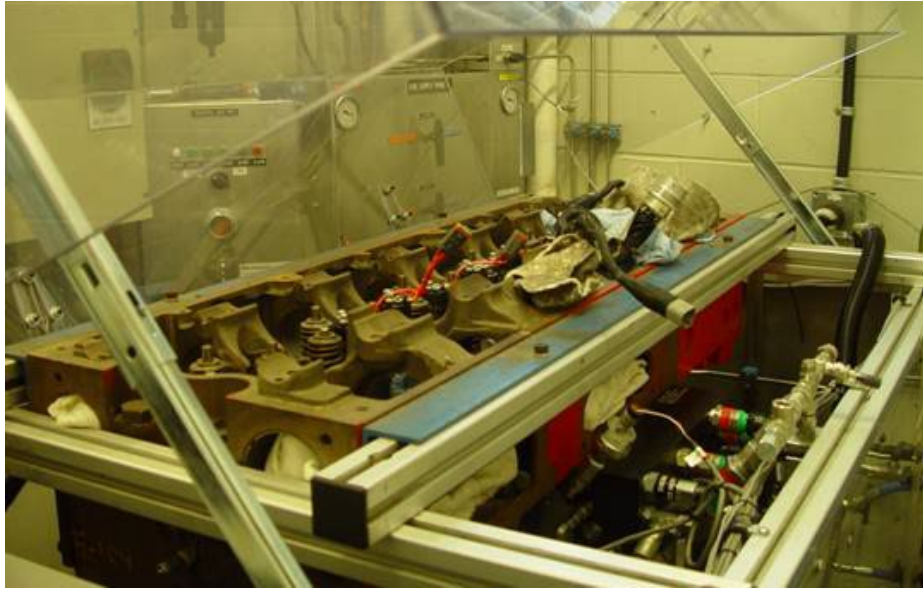


Figure 15: Before- and after-durability testing flow curves for the J236 prototype injector

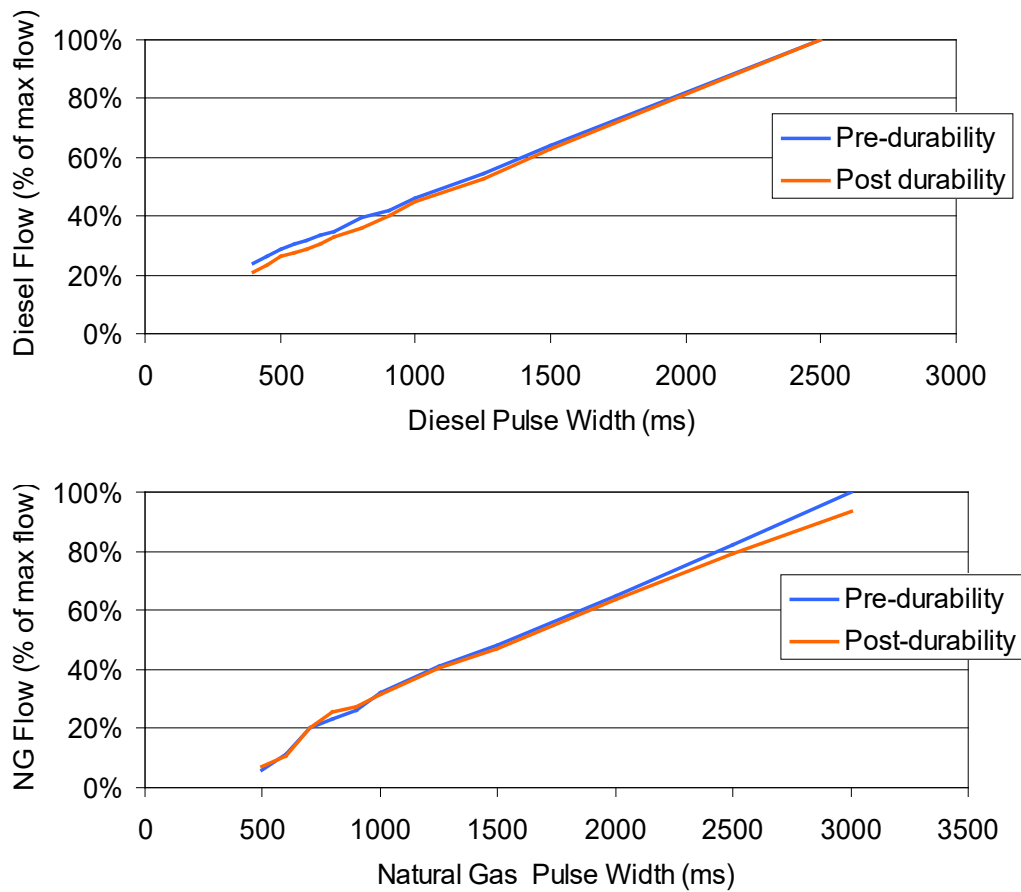
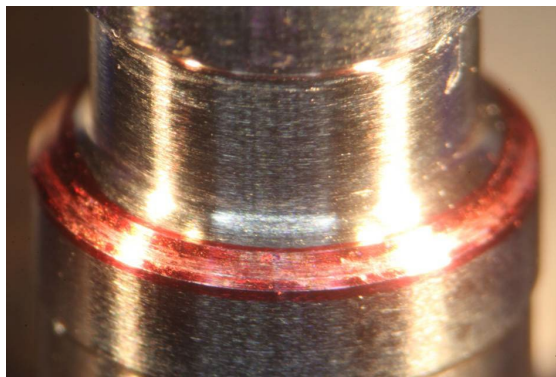


Figure 16: Borescope view of pilot needle seat (inside gas needle) after engine test



Figure 17: Needle seating surface after engine test (red marking was added after disassembly to aid alignment inspection)



Cost Reduction Potential from Exhaust Aftertreatment Systems

Aside from the fuel system, one of the main engine system costs is in the exhaust aftertreatment, especially in a heavy-duty diesel engine. These systems vary with manufacturer but typically include a diesel oxidation catalyst (DOC), diesel particulate filter (DPF), and a selective catalytic reducer (SCR). Each of these components have a specific function: the DOC oxidizes CO and nmHC as well as some of the volatile organic material that could contribute to PM. DPFs are designed to dramatically reduce PM by capturing it in a filter bed. This builds up a 'soot cake' over time, which must be periodically removed through a regeneration process. Finally, the SCR is used to reduce NOx emissions when ammonia is mixed into the exhaust stream and is then passed over a catalyst. These systems, while effective for diesel, are large and complex and require a significant amount of precious metal catalyst, leading to a high cost. As the natural gas HPDI engine is expected to have lower engine-out emissions (especially of PM and NOx) than an equivalent diesel, it should be possible to reduce the size and complexity of the aftertreatment system while still meeting emission standards.

Recent developments in engine EATSs were reviewed, and several cost-saving options available for heavy-duty natural gas engines were identified, and discussions with key manufacturers including Johnson Matthey, Umicore, and Emitec were conducted. Discussions

were also conducted with Amminex regarding their Ammonia Storage and Delivery System. This is a solid-state NOx control system that uses selective catalytic regeneration without the common liquid-urea dosing system.

The effectiveness of various NOx and PM aftertreatment technologies were analyzed based on literature reviews and data obtained from aftertreatment system manufacturers. Combustion regimes responsible for NOx and PM production for HPDI combustion were identified from previous test results. These results helped narrow down strategies to downsize or eliminate NOx and PM aftertreatment systems. The effectiveness of insulating the exhaust system to raise exhaust temperature was also studied. Various aftertreatment options are ranked (shown in Table 3) based on cost, system complexity, efficiency, hardware availability, etc. Based on the ranking, a DOC with reduced precious metal loadings, optimized for emissions from the HPDI combustion process, and a partial flow DPF were selected for further analysis. The solid-state SCR was assessed to not be at a sufficiently high state of development for the current evaluation, but remains of interest in future work.

Table 3: Exhaust Aftertreatment Component Rankings

		Efficiency	System Cost	Operation Cost	Impact on Engine Efficiency	Total Score	Rank	Availability
NOx Control	Solid-SCR	9	3	3	3	102	1	N
	Lean NOx Trap	1	9	9	1	64	4	Y
PM Control	DOC with reduced PGM loading	3	9	9	3	84	2	Y
	Downsized Wall-flow DPF	3	9	1	1	58	5	Y
	Partial-flow DPF	1	9	9	3	66	3	Y
Combined NOx&PM control	2-way SCR/DPF	1	9	3	3	48	6	N

(rankings based on a 1/3/9 scale of worse/equivalent/better than current system; weightings for categories efficiency: 9; system cost: 3; operating cost: 3; impact on efficiency 1)

Based on the engine-out gaseous and PM emissions at ESC 13 modes, the required conversion efficiency for the EATS was identified in order to meet the U.S. EPA 2010 emission standards. These were specified at: >85 percent NOx conversion, >50 percent PM capture, and >15 percent nmHc conversion. The specifications (dimensions, catalyst precious loadings, etc.) for the proposed reduced-cost DOC were then identified in conjunction with the selected suppliers, as shown in Figure 18. Two diesel oxidation catalysts (DOC-B and DOC-C) with reduced precious metal loading (for cost reduction exercise) were procured. One DOC and one partial-flow DPF (both with reduced size; the DPF is shown in Figure 19), on a metallic instead of a conventional ceramic substrate, were ordered and procured from another supplier.¹ The performance of these systems are discussed in this report, and the joint optimization of the engine-out emissions and the aftertreatment system are discussed in detail.

¹ Under the terms of our non-disclosure agreements (NDA) with the catalyst suppliers, we cannot divulge the supplier’s name or the details of the prototype hardware under review.

Figure 18: Relative size and platinum group metal loading for two prototype DOCs

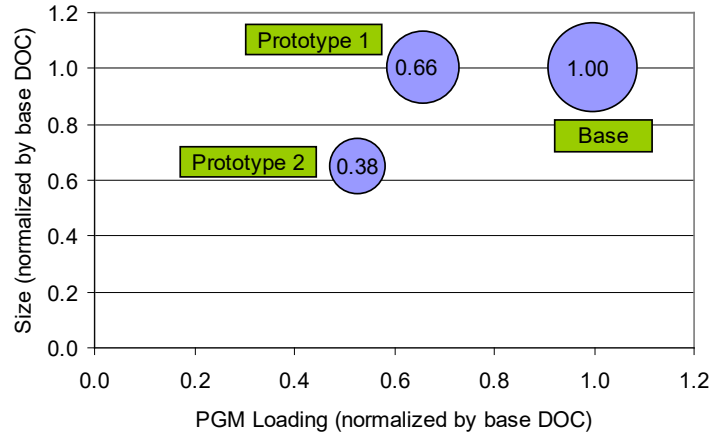
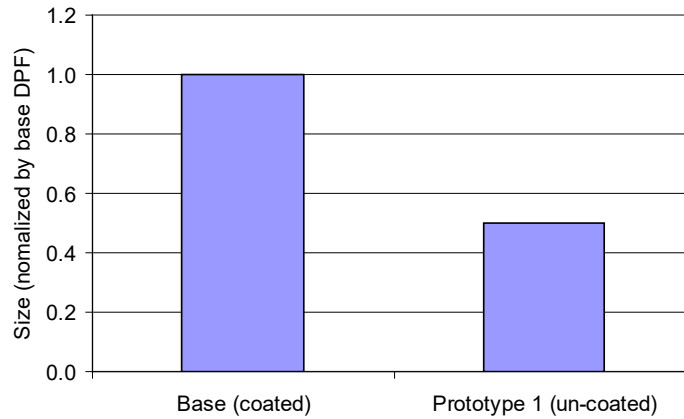


Figure 19: DPF size comparison for partial-flow DPF



Conclusions

Fuel system, aftertreatment, and base engine costs were reviewed as part of ongoing design and cost-reduction exercises at Westport. Significant cost reduction opportunities were identified in key fuel system components and in the aftertreatment system. The results from these studies are:

1. Changing suppliers for the rail pressure control module and for the base injectors achieved 75 percent cost reductions for each of these critical components with no significant change in design or performance.
2. A new, lower cost fuel rail pressure control module was designed. The new design could maintain only two pressures, compared to the continuous range of pressures achieved using the base system. This restriction on flexibility negatively impacted the engine's emissions levels and transient performance, and as such the original design is retained.
3. A new injector was designed with a lower expected manufacturing cost and increased flexibility between engine platforms. Testing revealed that the prototype injectors have

equivalent tailpipe emissions to the base injector with no reliability problems encountered over 300 hours of testing.

4. Analysis of the aftertreatment system reveals that the key areas for cost reduction are reducing the precious metal content in the DOC and reducing the size of the DOC and DPF. Prototype DOCs were identified for further evaluation that reduced precious metal content by as much as 60 percent. A prototype DOC/DPF combination was identified that is half the size of the existing DPF and uses an uncoated DPF substrate, further reducing precious metal loadings.

CHAPTER 4:

Efficiency Enhancement through Engine Hardware Optimization

The Westport HD 15L HPDI engine used as the base for this project is built on a Cummins ISX engine architecture. Aside from the fueling system, the HPDI engine retains the base engine hardware from the diesel, including the air exchange system (turbocharger, aftercooler, EGR system) and valvetrain. Optimization of these systems for the natural gas engine could improve HPDI fuel consumption and performance. Several areas were identified as offering the potential for optimization. The strategies evaluated were: improved air-handling through optimized valve timing; waste energy recovery; and engine friction reduction. These concepts were evaluated using analytical and computational techniques.

Engine Cycle Modeling and Analysis

An existing calibrated GT-Power model for the Westport HD 15L HPDI engine used in previous work at Westport was adapted for this project. The model was set up and run to simulate effect of changing the valve timing and duration on engine performance and efficiency. Numerical predictions have been performed on an HPDI engine with intake valve events allowed to vary without the limitation of the current cam design (variable valve timing). A GT-Power engine model was also used to study engine operation at peak torque (1200 RPM, 100 percent load). Three scenarios were applied to the engine mode that differ from the current peak torque operation condition of the 2010 engines. These were increased boost, reduced intake air temperature, and reduced engine compression ratio. With increased boost, fueling could be increased to keep the air fuel ratio AF constant, and the Break Mean Effective Pressure (BMEP) was increased by about 15 percent. The modeling suggested that a fuel economy penalty of about 4 percent, as start-of-injection (SOI) timing had to be delayed to keep maximum cylinder pressure under the limit. The model predicted that the effect of reduction of intake air temperature on BMEP enhancement is minimal. With reduced compression ratio from 17:1 to 15:1, the model predicted about 8 percent increase of BMEP. The fuel economy in this case had a penalty of about 3 percent due to reduced compression ratio; however this could be offset by a more advantageous phasing of the SOI at peak torque.

Effect of Valve Timing

Effects of intake valve profiles on the engine fuel economy were predicted at ESC B speed under load conditions of 100 percent and 25 percent. Initial results indicated that some improvement in engine efficiency (1- to 3-percent reduction in brake specific fuel consumption [BSFC]) was possible depending upon engine operating condition with both the early and later intake valve closing (IVC) strategies. However, for a turbocharged engine, the varied IVC resulted in changing charge conditions (including equivalence ratio [EQR] and EGR), which would be expected to significantly affect the combustion process and corresponding

performance and emissions. Results of detailed engine tests conducted to evaluate these findings are reported in a later section of this report.

Engine Valvetrain Low Friction Coating Study

Reduction of mechanical friction was identified as one potential route for improving engine efficiency without impacting the combustion process or pollutant emissions. An initial review of the technical literature indicated that the application of low-friction coatings to the valvetrain could reduce frictional losses. This review identified that only diamond-like carbon (DLC) materials were appropriate for this work, as other low-friction coatings did not have the wear resistance to provide benefit over the life of the engine. Even for DLC, its ability to provide friction reduction over the extremely long life of a modern heavy-duty engine has not been widely demonstrated, with most of the benefits having been demonstrated in light-duty automotive applications. The coatings identified from the literature are listed in Table 4.

Table 4: DLC Coatings Considered for Valvetrain Friction Reduction

DLC Coating	Best Lubricating Oil Match
Hydrogenated DLC a-C:H	Poly-Alpha-Olefin (PAO)
Metal-dope coatings Me:a-C:H	Not assessed
Hydrogen-free DLC	Not assessed

The potential of engine valvetrain coatings to reduce friction were evaluated using existing performance data and information from a literature review. Analysis of the GX engine valvetrain indicated that, because it uses a roller-follower, the potential benefits of adding a low-friction coating like a DLC to the cam follower would only reduce total engine friction by approximately 0.5 percent. A further review of the total engine friction for the heavy-duty engine indicated that application of a DLC low-friction coating on the piston skirt could achieve a more significant reduction in engine friction. Over a 13-mode weighted average, analysis suggests that a reduction in fuel consumption of approximately 1.4 percent could be expected. The application of DLC to all six piston skirts would require substantial time and cost investments. As well, the durability of the DLC in a heavy-duty engine was thought to be unacceptably short, leading to benefits that would only be realized early in the life of the engine. As such, evaluation of this efficiency improvement strategy would require long-term durability testing to evaluate, which is beyond the scope of this program. As the expected benefits are small and the durability question could not be addressed, experimental testing was not conducted.

Exhaust Energy Recovery

One of the main sources of inefficiency in an internal combustion engine is the enthalpy in the high-temperature exhaust stream that is not converted to useful work. Exhaust energy recovery is an area of current research to recover some of that enthalpy and convert it to

useful work. A literature review and analysis was conducted to assess different strategies of exhaust energy recovery. The identified strategies were:

- Turbo compounding with a mechanical connection to the drive shaft
- Turbo compounding with an electrical connection to the drive shaft
- Direct mechanical energy recovery from the turbocharger
- Rankine cycle waste heat recovery
- Brayton cycle waste head recovery
- Thermo Electric Generator

For the identified strategies, suppliers—where a commercial product existed—and drive-cycle impact analysis based on efficiency gains were cited in the literature.

The fuel efficiency improvement, the cost, the complexity and the level of development for each of those strategies were the main evaluation criteria. These are summarized in Table 5.

Table 5: Comparison of energy recovery technologies

Technology	Efficiency Improvement from Literature Review (drive cycle)	Cost	System Complexity	Level of Development
Mechanical Turbo-compound	2-3%	Low	Low, but base engine modifications needed	Production applications for HD diesel
Electrical Turbo-compound	3-7%	Medium	Medium	In production for power gen. applications
Turbocharger Energy Extraction	2-3%	Low	Medium	Prototype (single supplier identified)
Rankine Cycle Energy Recovery	6-8%	High	High	Limited demonstration (diesel)
Brayton Cycle Energy Recovery	~2%	High	High	Limited demonstration (diesel)
Thermo-electric Generator	1%-3% current Up to 20% projected	Uncertain	Low	Low

The two most promising technologies identified, which are both current (and near-term) products that claim to offer drive cycle efficiency benefits of 3 to 5 percent for heavy-duty engines, are: (1) electrical turbo-compound and (2) direct energy extraction from a drive-connected turbocharger. Preliminary engine model (GT-Power) testing was conducted on both concepts. The modeling work was conducted on a validated Westport HD 15L engine model at two modes: 100 percent load and 25 percent load at 1490 RPM. The models indicated that both the electrical turbo-compound and the drive-connected turbocharger could offer 3 to 5

flow and EGR levels to avoid significant impact on emissions or performance. The results at peak torque (mode 8) are shown in Figure 21; a reduction of as much as 8 percent in fuel consumption could be achieved at this mode. Benefits are reduced at lower load conditions, but the model results revealed that a composite reduction in fuel consumption of 4 percent could be expected over the 13-mode drive cycle using an exhaust turbine with an optimized turbocharger, as shown in Table 6. Equivalence ratio and EGR level were maintained at each point, so the implications of this system on combustion efficiency and emissions are expected to be minimal.

Figure 21: Net system efficiency improvement (including engine and turbo-generator work) as a function of engine brake power with constant fueling at SET mode 8 (B100 – 100 percent load at 1490 RPM)

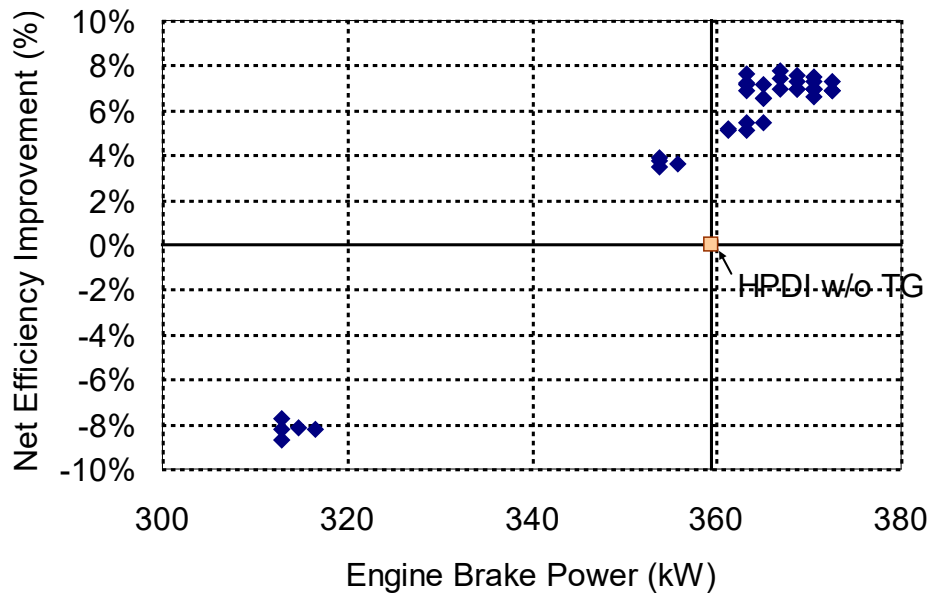


Table 6: Mode-by-mode Efficiency Improvements with Electrical Turbo-Compound

SET Mode	Speed	Load	Weighting Factor	Efficiency Improvement
1	Idle	0%	0.15	-5%
2	1220	100%	0.08	7%
3	1493	50%	0.1	1%
4	1493	75%	0.1	3%
5	1220	50%	0.05	1%
6	1220	75%	0.05	3%
7	1220	25%	0.05	0%
8	1493	100%	0.09	7%
9	1493	25%	0.1	0%
10	1750	100%	0.08	7%

SET Mode	Speed	Load	Weighting Factor	Efficiency Improvement
11	1750	25%	0.05	0%
12	1750	75%	0.05	3%
13	1750	50%	0.05	1%
Composite Efficiency Improvement				4%

Efficiency Improvement and Energy Recovery Conclusions

Various strategies to achieve improved efficiency without impacting the engine combustion system performance were evaluated analytically. These included changes in intake valve timing, adding low-friction coatings to key engine components, and exhaust energy recovery. These analyses revealed that:

1. Intake valve timing could improve efficiency by 1 to 3 percent but would have significant impact on the air handling system performance, influencing combustion by changing the in-cylinder EQR and EGR level.
2. Applying low-friction coatings to the valvetrain will achieve little friction reduction benefit as the base engine uses a low-friction roller-follower design. The low-friction coatings could provide as much as a 1.5 percent improvement in fuel economy if applied to the cylinder liner or piston skirt, but the longevity of such coatings under those difficult conditions is uncertain.
3. Various waste energy recovery strategies are identified in the literature and evaluated. Advanced techniques including thermo-electric generators, Rankine cycle, and Brayton-cycle based systems show promise but are relatively immature and complex systems. Mechanical turbo-compound was also evaluated, and while providing potential benefits imposes too large an impact on the base engine to be considered for an HPDI variant.
4. Exhaust energy recovery through electrical turbo-compounding was identified as a potentially suitable technology for an HPDI engine. Modeling results suggest that an efficiency improvement of 4 percent over the weighted SET cycle could be achieved with suitable hardware. If the turbocharger is optimized in conjunction with the turbo-compound system, these benefits could be achieved with no impact on the in-cylinder conditions.

CHAPTER 5:

Virtual Sensor for Combustion Robustness Control

One of the main challenges facing a natural gas engine is that the fuel composition is not necessarily uniform, which can significantly influence the combustion event. The main variations are in the percentage of heavier hydrocarbons (primarily ethane, C₂H₆, and propane, C₃H₈) and the concentration of inert species such as Nitrogen or CO₂. This variability increases when non-conventional fuels (such as waste-derived biogas) are added to the fuel supply. Although the late cycle direct injection of natural gas in an HPDI engine means that end-gas autoignition (knock) is not a significant concern, changes in energy density with composition can impact power production and cylinder pressure. The presence of higher hydrocarbons will lead to the engine generating more power, while inert species will lead to less power for a given injection command. To address these challenges, a new sensor and control strategy (a 'virtual sensor') was developed that identifies changes in combustion energy release and phasing due to variations in fuel composition and then compensates for these changes. This system must be based on low-cost sensors to be commercially practicable. The engine controller can then adapt the fueling commands to adjust the combustion process (including combustion timing and total energy release), avoiding potential engine damage and enabling maximum engine performance.

Available Virtual Sensing Technologies and Hardware Selection

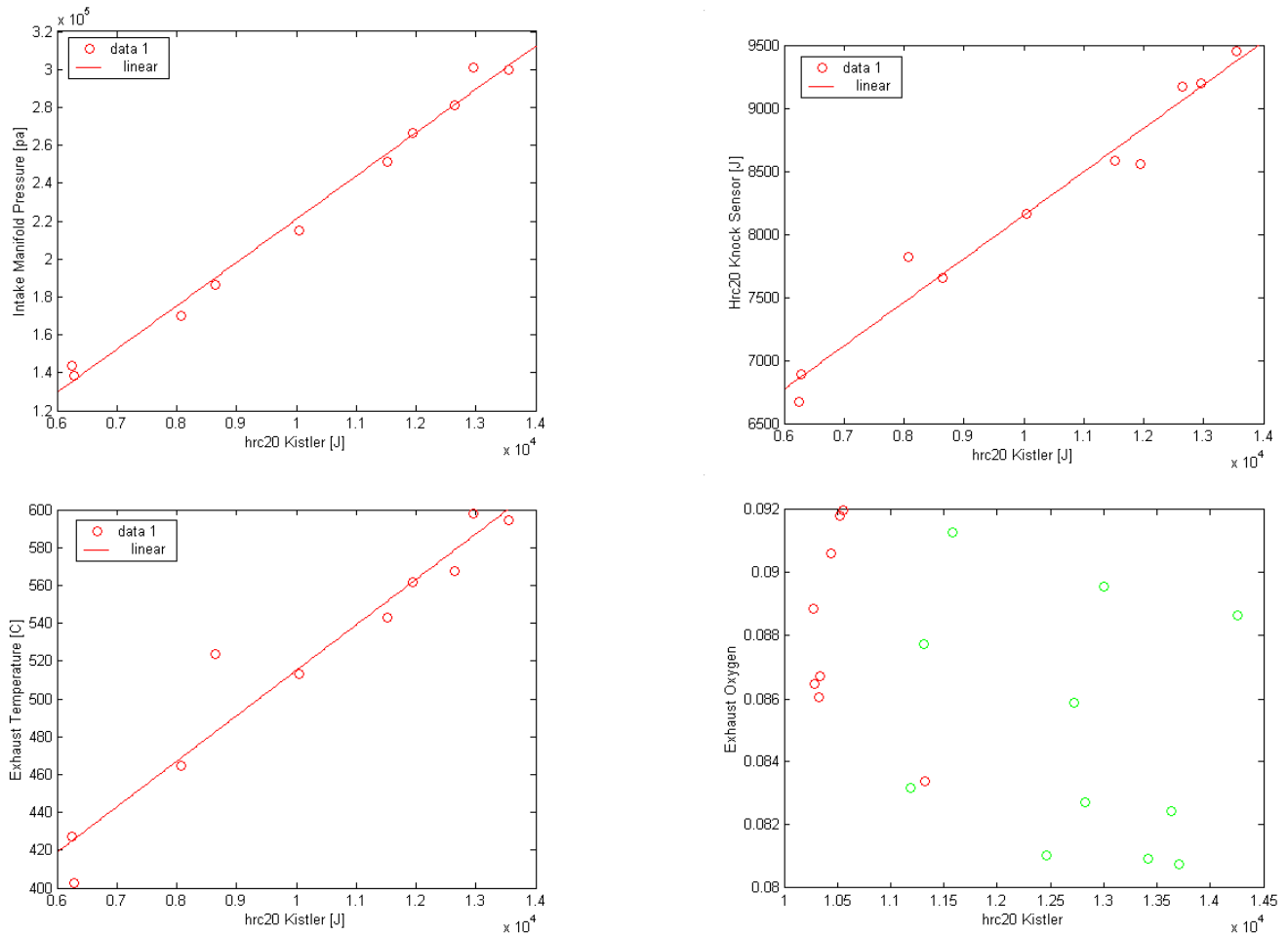
A range of sensors were evaluated for use in the virtual sensor, as shown in Table 7. These sensors were selected for their demonstrated durability and reliability, their expected sensitivity to changes in fuel composition, and their reasonable cost.

Table 7: Sensors Evaluated for Virtual Sensor

Sensor Type	Number Required	Durability	Incremental Cost (Total)	Remarks
Knock Sensors (on main bearing caps)	4	Excellent	Est. \$40-\$100	Can be used to estimate pressure trace for individual cylinder
Intake Manifold Pressure (P0)	1	Excellent	\$0 (already included)	Indicate energy in exhaust stream from change in boost pressure
Exhaust Temperature	1	Good	Est. \$30 + Signal Conditioner	Exhaust temperature proportional to energy from combustion
Exhaust Oxygen (Wide Band Lambda)	1	Good	Est. \$100-\$300	Direct measurement of exhaust oxygen content

The effects of variations in fuel composition on the HPDI research engine were identified using high-cost water-cooled in-cylinder pressure transducers not suitable for a production application. This in-cylinder pressure data are then used to calculate the energy release rate over the combustion event and the total energy release. The output from sensors that could be installed on a production engine, listed in Table 7, were compared against the integral of the energy release (from start-of-combustion to 20oCA ATDC). This parameter was selected as it is expected to provide a strong indication of changes in engine performance related to changes in fuel composition. The correlations for each of the sensor outputs to this value are shown in Figure 22.

Figure 22: Sensitivity of individual sensor measurement values to changes in net heat release calculated from cylinder pressure data. Shown are: intake manifold pressure (top-left); calibrated knock sensor output (top-right); exhaust temperature (lower-left); exhaust oxygen concentration (lower right).



Of the sensors tested, the intake manifold pressure had the strongest correlation with the energy release rate, as shown in Figure 22. Similarly, the knock sensor based data also correlated well. For this work, the output from the four knock sensors was collected with a separate analysis computer; these signals were then used to reconstruct the cylinder pressure trace. The reconstructed pressure trace was then used to estimate the start-of-combustion

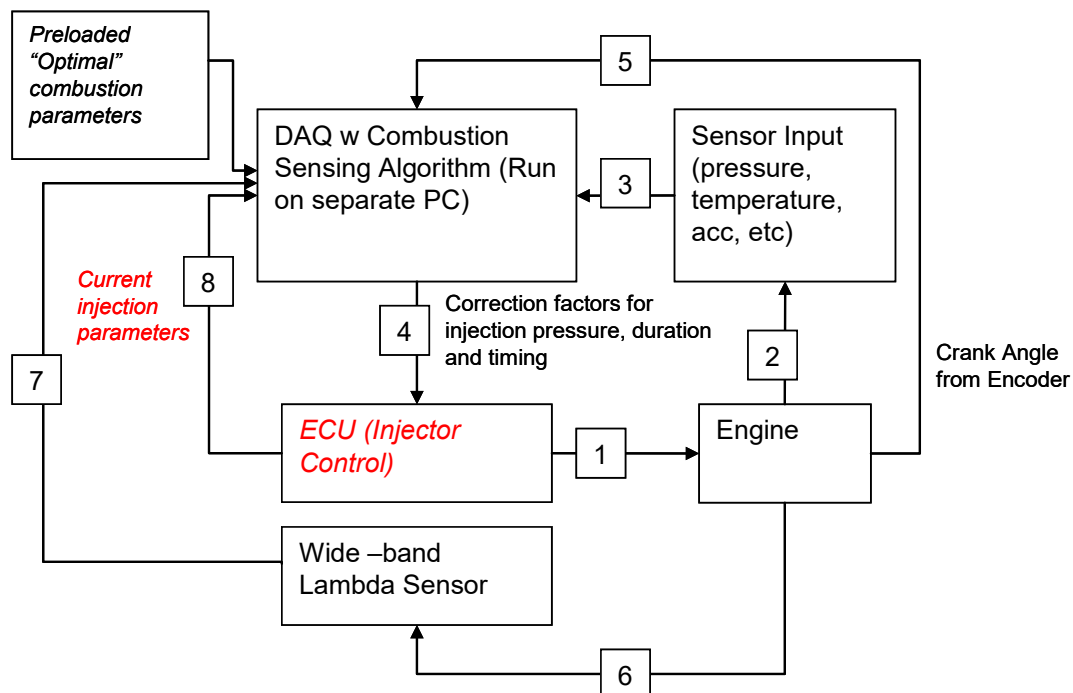
phasing and the heat release after the end of the main combustion phase. The latter parameter is shown in Figure 22 relative to the equivalent measurement from the in-cylinder pressure transducers. The exhaust temperature also showed a good correlation with net energy release. Conversely, the exhaust oxygen concentration, as measured using a Universal Exhaust Gas Oxygen sensor, does not resolve changes in net combustion energy release. The results, shown in the lower-right plot in Figure 22, reveal that the Universal Exhaust Gas Oxygen sensor is insensitive to the differences attributed to variations in fuel composition.

The results of the analysis reveal that the best sensors for detecting changes in the heat release rate (HRR) are the intake manifold pressure combined with the knock sensor output. While the knock sensor poses control and data processing challenges, it provides the benefit of estimating both energy release and combustion phasing. When combined with the intake manifold pressure, the output from the two sensors can be used to identify the impacts on combustion phasing and energy release due to changes in fuel composition. As a result, these two sensors were selected for integration into the virtual sensor.

Virtual Sensor Architecture and Controls Integration

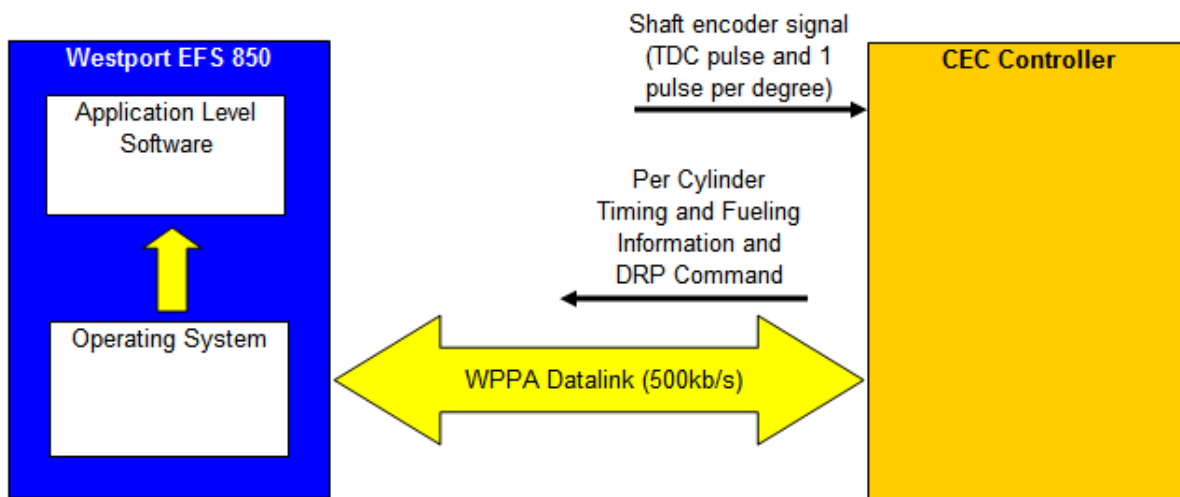
The sensing and control implementation of the virtual sensor includes both high speed sampling from the knock sensor and algorithms to reconstruct the pressure trace. The required information flow is shown in Figure 23. For the project, the sensor input was fed into a stand-alone computer used to evaluate the sensor input and compare it to previously stored conditions for a reference fuel at the same throttle conditions. If deviations above a preset threshold are identified, the computer then sends a command modifying either the injector pulse-width or injection timing to the engine ECU. Long-term, the sensor and control functions would be integrated into the existing engine controller.

Figure 23: Schematic of information flow for virtual sensor



The existing fuel system control architecture was modified to allow switching fueling control from the ECU to the personal computer-based virtual controller via a CAN interface. The required communication and processing speed was determined to be approximately 50,000 bits per second for the high-speed data, and a detailed CAN message structure was devised. The functional architecture is shown in Figure 24. Communication is based on a 32 bit identifier followed by an 8 byte data transfer, with all messages between the Consumer Electronics Control controller and the ECU following a fixed hexadecimal format. The new command logic allows the Consumer Electronics Control controller to control the timing and duration of up to two gas and two pilot injections per cylinder per cycle, and it allows variation in command parameters between cylinders during the same cycle.

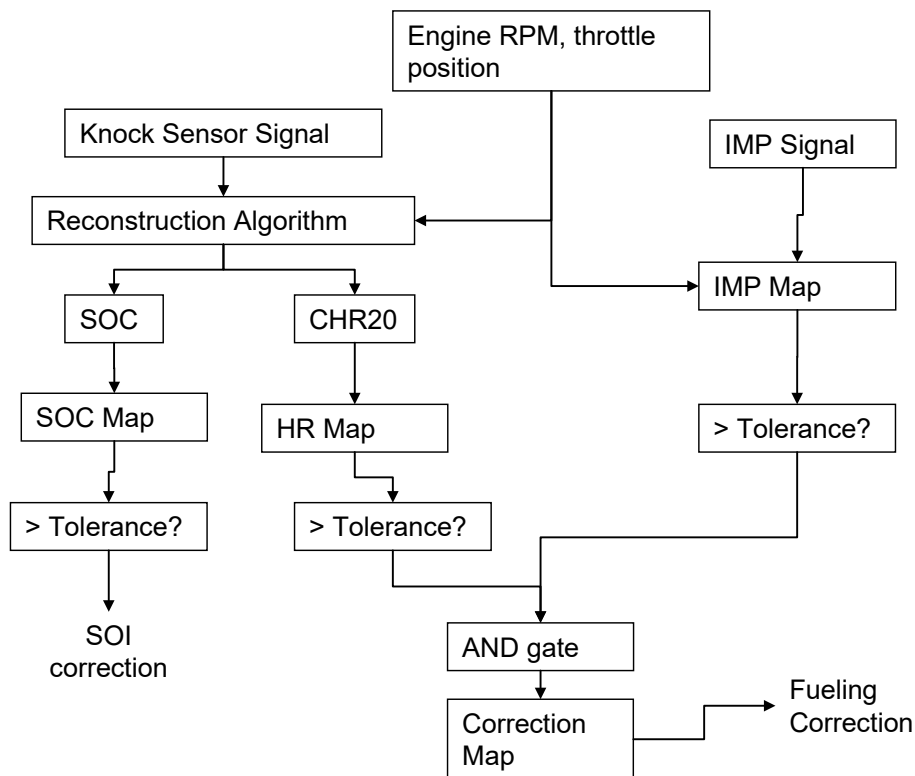
Figure 24: Functional architecture for prototype-A control system



Design of Virtual-Sensor Based Combustion Control

The overall strategy to achieve combustion robustness control using the virtual-sensor based controller is outlined in the flow chart shown in Figure 25. In summary, the reconstructed cylinder pressure is used to estimate the start-of-combustion phasing and the total heat release at 20oCA ATDC. These two values, along with the intake manifold pressure, are individually compared to baseline engine operation maps for those parameters at the given speed and load (engine RPM and throttle position). If the calculated values diverge by more than 3 percent, a correction is applied. If the start-of-combustion is observed to be outside the expected window, the injection phasing is adjusted. If the total energy release and the intake manifold pressure are both different from the expected values, then the injection pulse width is adjusted. The fueling and SOI corrections are then passed from the virtual-sensor based controller to the main engine ECU.

Figure 25: Virtual sensor control algorithm flow chart. SOC, HR, and CHR stand for start-of-combustion, heat release, and cumulative heat release, respectively.



The control system was validated in the test cell at different engine speeds and different loads to verify the accuracy of control messages sent from the PC controller. These tests show that the busload increases by 27 percent between the base and new control systems but remains within the acceptable range.

Fuel Composition Compensation with Virtual-Sensor Based Controller

The intent of the virtual-sensor based controller is to adapt the fueling and combustion process to variations in fuel composition. This was demonstrated on the prototype-A engine by comparing a baseline, high quality, fuel (methane number [MN] 90), with two lower-quality fuels, with MN65 and MN54. In these cases, the engine was operated over the 13-mode steady-state test points on the baseline fuel, with the standard engine controller fueling commands. The same fueling commands were then repeated for each mode on each of the two lower-quality fuels. Finally, the same points were repeated again with the two lower-quality fuels, but with the virtual-sensor based controller correcting the fueling timing and pulse-width. An example of the in-cylinder conditions for the baseline fuel, the MN65 fuel with baseline fueling commands, and the MN65 fuel with the corrections from the virtual sensor, is shown in Figure 26. The transition to a lower MN fuel results in more energy release (shown by the wider HRR), higher engine power, and higher cylinder pressures (due to increased exhaust energy leading to increased boost as well as more energy released from the combustion). The virtual sensor corrects for these effects, resulting in a HRR and cylinder

pressure that are indistinguishable from the MN90 fuel case. Equivalent results are seen at the other modes with both the MN65 and the MN54 fuels. The ability of the virtual-sensor based controller to maintain the engine torque at its desired value is shown for all 12 non-idle modes with MN54 fuel in Figure 27.

Figure 26: Demonstration of virtual sensors correction of fueling quantity to maintain target power. Cylinder pressure (left) and HRR (right) for standard (MN87), base fueling with low MN fuel (MN65) and the virtual-sensor corrected fueling (MN65).

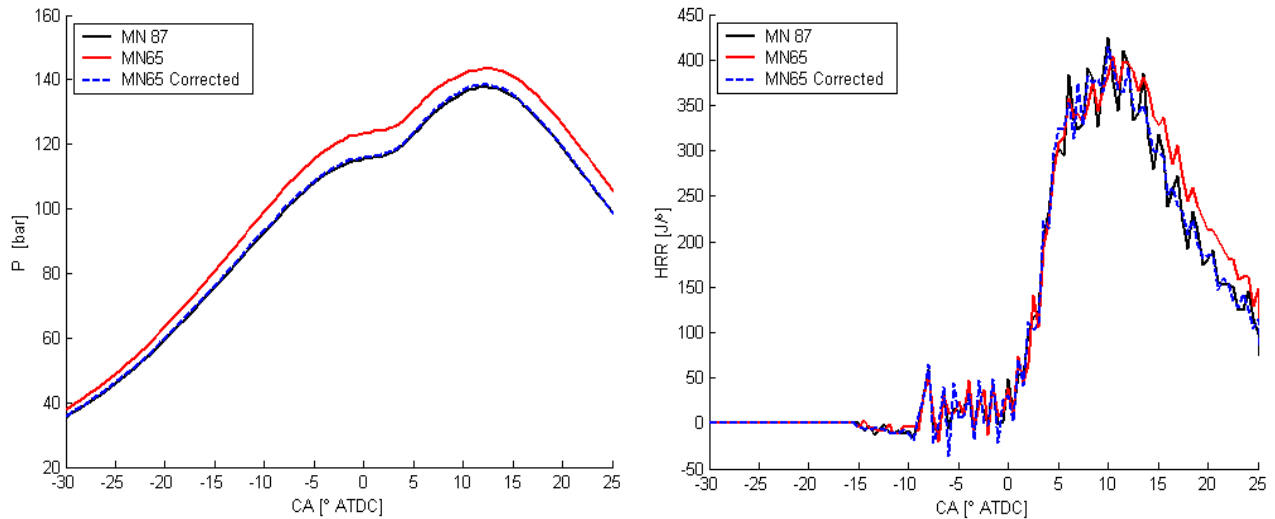
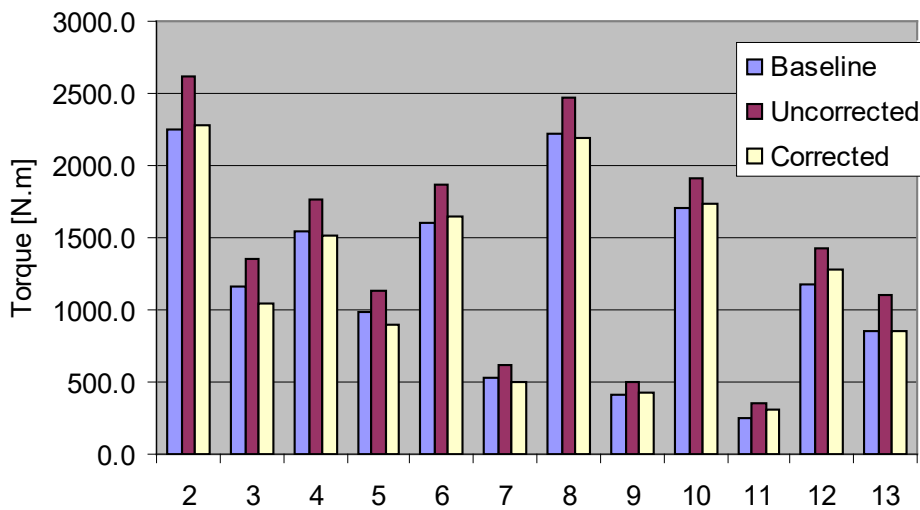


Figure 27: Torque at each of the 12 SET modes (excluding idle) for the baseline (MN87), uncorrected (MN54 with baseline injection commands), and corrected (MN54 with the virtual-sensor based injection correction) conditions.



Virtual Sensor Combustion Compensation Conclusions

The ability of the HPDI engine to operate on a wider range of natural gas compositions than other natural gas engine technologies is one of HPDI's key advantages. However, significant variations in fuel composition could reduce engine performance. As a result, a new sensor-controller system was developed that could identify variations in engine performance resulting from fuel composition changes and then correct the injection event. The key findings from this work are:

1. Increases in propane and ethane content in the fuel increase engine torque and peak cylinder pressure. These effects can be identified from the in-cylinder pressure by integrating the total energy release up to 20°CA after top-dead-centre.
2. The best low-cost sensors for identifying the change in engine performance due to fuel composition variations is through a combination of knock sensors mounted on the main bearing end caps and by monitoring the intake manifold pressure. Exhaust temperature and exhaust oxygen content are found to be less representative and hence are not used in the final virtual sensor.
3. The virtual sensor reconstructed the pressure trace based only on the output from the knock sensors and the intake manifold pressure. From these results, the virtual sensor can identify the combustion phasing and total energy release. Comparing these values against stored values for a reference fuel allows the virtual sensor to identify when a significant change in fuel composition occurs.
4. The output from the virtual sensor with low-quality fuel is used to adjust the fuel injection commands to return the engine torque and combustion phasing to the same levels as for the standard fuel.

CHAPTER 6:

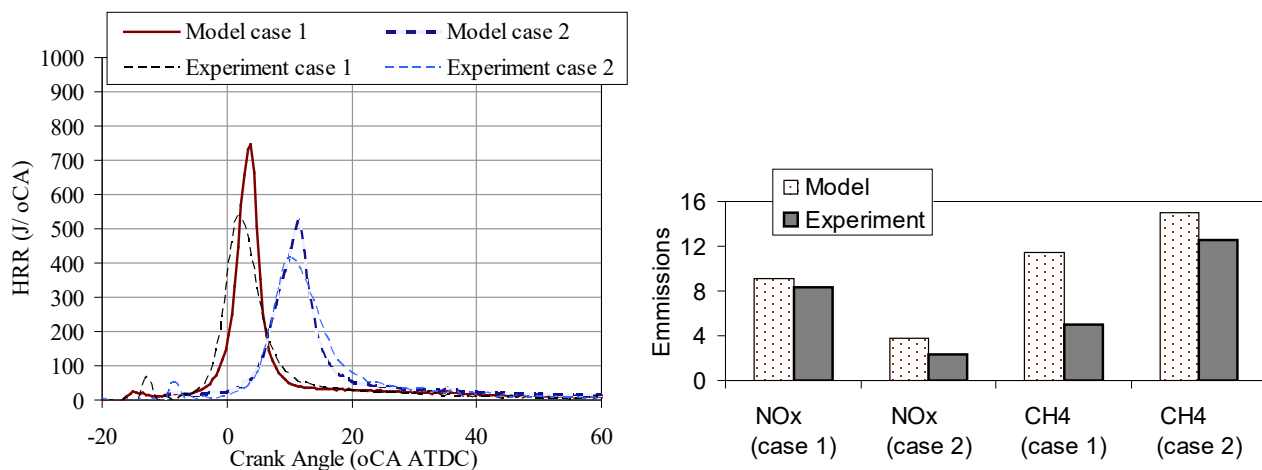
Engine Combustion Enhancement

One of the key objectives of this project was to evaluate combustion enhancements to the HPDI combustion process to achieve increased efficiency and/or reduced emissions. This was done using computational fluid dynamics (CFD) simulation of the combustion process and experimental testing on the prototype-A engine. The CFD simulation was used both to guide engine hardware investigations and to provide further insight into the combustion event.

CFD Model

An existing in-house combustion CFD model known as a Generic Open Foam Low Dimension (GOLD) manifold used in previous work at Westport was selected to simulate in-cylinder engine combustion with detailed chemistry. A set of Matlab programs were written to generate tables for probability density functions, which are required for implementing the flamelet model. A trajectory-generated low dimensional manifold (TGLDM) based flamelet turbulent combustion model was implemented in the current CFD program through a set of Fortran programs. The model passed initial stability test and a beta version was released for subsequent calibration and validation work. A new TGLDM library based on GRI-Mech2.11 was generated for reaction rate calculation for natural gas combustion. The model was then successfully validated against available engine data. A sample of the comparisons used for validation are shown in Figure 28.

Figure 28: CFD validation results, heat-release rates (left), and emissions (right) for two generic HPDI combustion conditions



During this project, a sub-grid diffusion model was also added to the GOLD combustion CFD package. The model deals with exchange of mass between the quenching sub-layer and mainstream flow field. The simulation results from GOLD were compared with experimental results for selected engine operating conditions. The conditions cover a wide range of load and speed. The agreement between the model and simulation results is satisfactory. The Hiroyasu

PM model was also implemented in GOLD. The Hiroyasu model is a two-step phenomenological model widely used in predicting soot formation and oxidation in diesel engines. The results from the Hiroyasu model were compared to experimental results and the reaction rate constants were adjusted to better match the measurement from natural gas engines.

CFD Simulation of Advanced Combustion Strategies

CFD simulations were carried out to study PM formation and oxidation in HPDI engines under various combustions modes. The study was focused on effects of piston bowl shape, injection parameters, and advanced combustion strategies.

Piston Bowl Shape

CFD simulations of the piston bowl shape were conducted. As part of this work, several bowl geometry variants were identified, that included modification of the piston bowl depth ('pip' height), the degree of re-entrantness of the bowl, and the presence of a separating lip on the bowl wall. The end result is a direct comparison between the prototype-A engine piston and a new piston with a vertical wall and no lip. Cross-sectional views of the two simulated combustion chambers are shown in Figure 29, along with the concentrations of acetylene (a key soot precursor) and the mixture fraction. The effects of the modified geometry on the emissions are shown in Figure 30. The results demonstrate that the base piston is particularly well suited to HPDI combustion, and that modifications from the base piston design tend to result in significant compromises with little net benefit. In summary, the CFD simulations indicate that the piston bowl from the prototype-A engine could be retained for the final engine hardware configuration.

Figure 29: Acetylene concentration and mixture fraction in combustion chamber with base piston geometry (top) and new piston design (bottom)

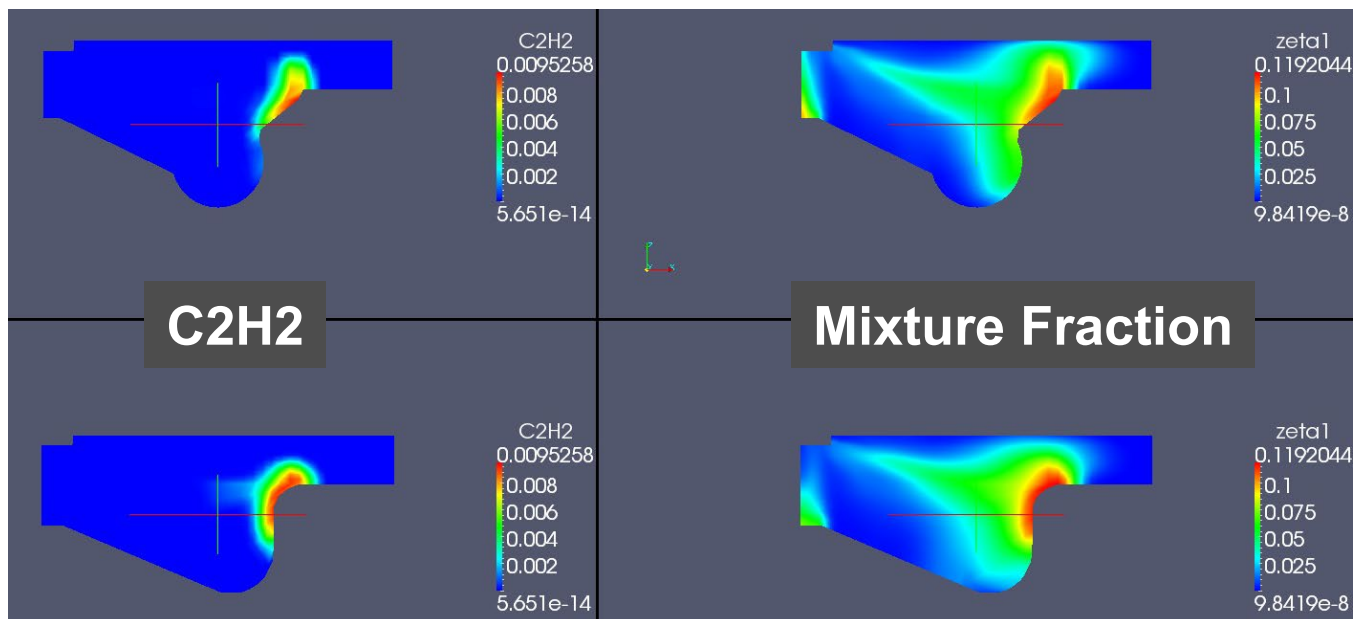
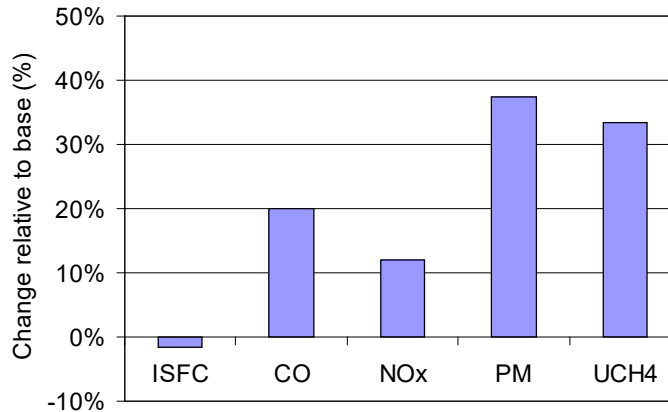


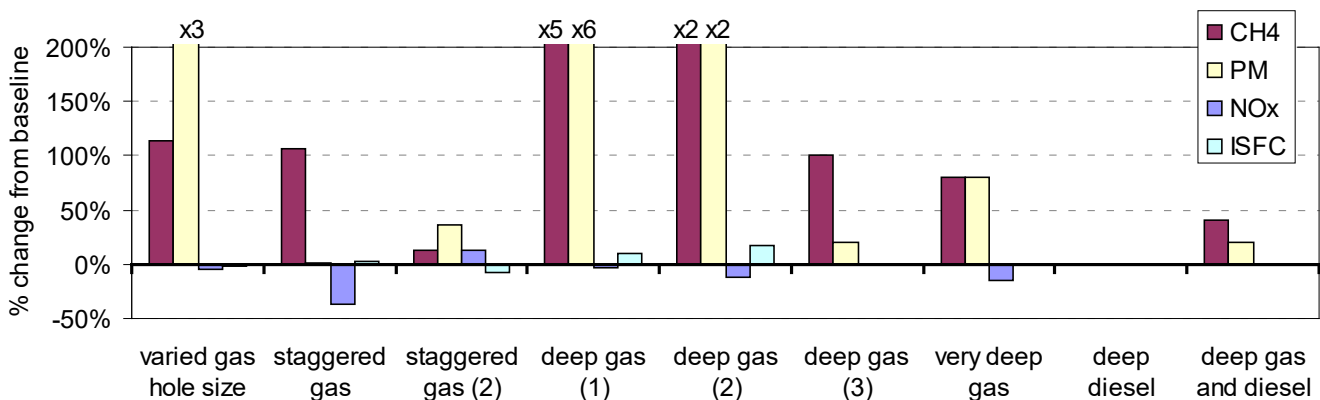
Figure 30: Change in CFD-based predicted emissions at high load from base piston to new piston design



Injector Parameters Modeling Analysis

CFD simulations were then performed using GOLD model to investigate effects of injector tip geometry and injection pressure on PM and other regulated emissions from HPDI combustion. Simulations were focused on high load conditions where fuel consumption and emission levels for most pollutants are highest. Various injection strategies including gas spray hole configurations were evaluated. The concepts evaluated include varying the angle relative to the cylinder head fire deck at which the gas is injected. Changes in nozzle size, which have been evaluated previously for HPDI, were revisited and an optimal sizing selected for comparison with the baseline case. The angle of the diesel injection was also evaluated, both with and without a variation in the gas jet angle. A selection of the results from these CFD studies is shown in Figure 31. The results of the modeling indicate that only a deep pilot with fixed gas angle led to either improvements or no change in all assessed emissions; however, none of the benefits identified are significant. As a result, the baseline nozzle configuration is recommended as the preferred configuration from the CFD analysis.

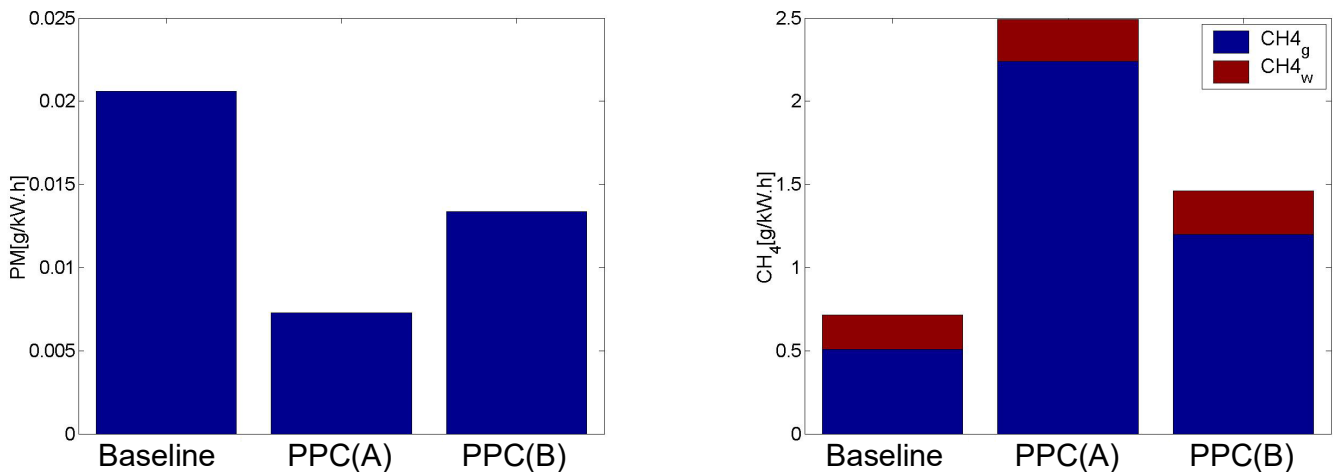
Figure 31: Effect of nozzle geometries on predicted PM, unburned fuel, NOx, and indicated specific fuel consumption (ISFC), compared to baseline. All at SET mode 8 (full load, 1500 RPM), with EGR.



Partially-Premixed Combustion

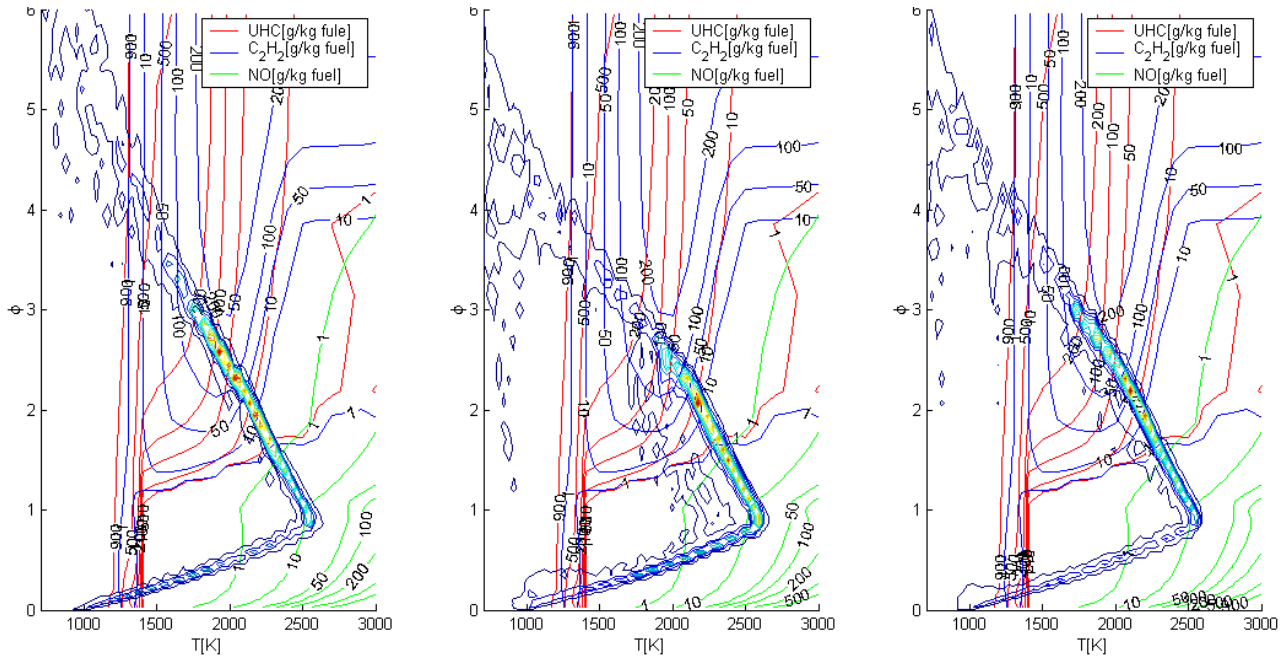
The CFD modeling tool was used to evaluate partially-premixed combustion strategies generated through early direct injection of the natural gas. The modeling was conducted at a fixed operating condition (equivalent to B100 in the experimental testing at 1500 RPM 100 percent load). In general, the model demonstrated similar results to the engine tests – with both partially premixing combustion strategies ('PPC(A)' and 'PPC(B)') generating lower PM emissions but higher unburned fuel emissions, as shown in Figure 32.

Figure 32: CFD predictions of engine-out PM and CH₄ for baseline and two partially-premixed combustion strategies (PPC(A)' and 'PPC(B)')



One of the key benefits of the CFD modeling is that the in-cylinder conditions can be evaluated in a more detailed manner than the experimental results can provide (which are limited to engine-out emissions and global in-cylinder conditions: pressure and heat-release rate). Examples of these results for the partially premixed combustion are shown in Figure 33, in the form of EQR – temperature (phi-T) plots. These phi-T plots provide a visual interpretation of the local conditions at all points in the combustion chamber at any point in time. In this case, the 'mixture fraction' concentration is shown at a point 10oCA after top-dead-centre of the compression stroke (right in the middle of the combustion event). These results show that the partial premixing reduces the concentration of burned and unburned gases in the regions that are most likely to form PM (as represented by regions of high Acetylene [C₂H₂] formation on the phi-T plots). This reinforces the understanding generated during the experimental testing and highlights the analytical value of the CFD testing.

Figure 33: Phi-T plots for baseline and two partially-premixed combustion strategies, showing mixture fraction concentration at a fixed timing (10oCA ATDC). Left: baseline; center: PPC(A); right: PPC(B). The plots show the relative concentration of the unburned and burned gases relative to the regions where significant concentrations of NO, acetylene, and unburned hydrocarbons are formed.



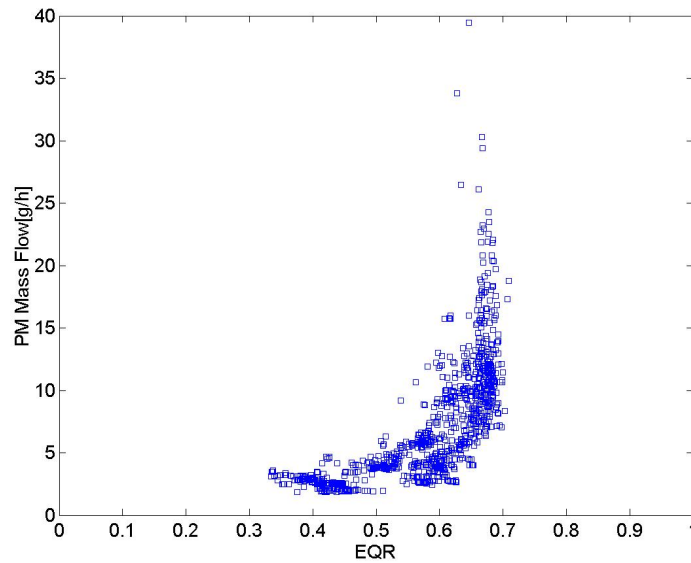
Experimental Engine Testing of Improved HPDI Combustion Strategies

The testing focused on all the adjustable aspects of the HPDI combustion process. The overall objectives of the work were to maintain low emissions while improving power and/or efficiency, or alternatively to reduce engine-out emissions while maintaining power and efficiency. The latter would enable lower-cost aftertreatment while maintaining tailpipe emissions below regulated levels. The key strategies investigated include engine operating parameter variations (such as injection pressure ratio and timing, EGR rate, and engine temperatures), and changes to the engine hardware (including injector sizing, valve timing, compression ratio, and swirl level).

Engine Operating Parameter Variations

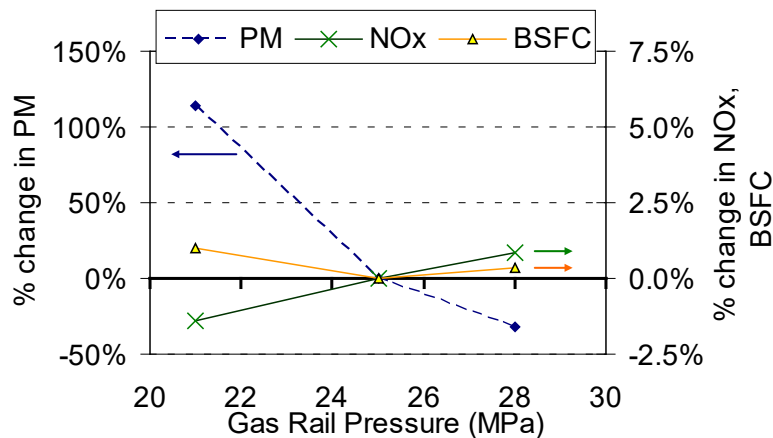
The operating parameters of the prototype-A engine were evaluated over selected modes of the SET cycle. The aspects investigated are: EGR, injection pressure ratio, injection timing, diesel pilot quantity, delay between pilot and natural gas injection, intake manifold temperature, and engine coolant temperature. The results were also evaluated from a global viewpoint to evaluate the effects of fundamental parameters, such as the EQR on emissions. For all the tests conducted, it is possible to identify some general trends; among these is a strong dependence of PM emissions on the global EQR. This is shown in Figure 34.

Figure 34: Effects of EQR on engine-out PM for all tests conducted using the prototype-A engine and standard fuel quality



Increasing the gas injection pressure relative to the cylinder pressure significantly reduces the particulate matter emissions, as shown in Figure 35 for a specific mode (B75). This mode was the focus of research for increased injection pressure studies as the baseline calibration at high load uses the highest available injection pressure, while the reduction in PM achievable at lower loads is offset by significant increases in unburned fuel emissions due to over-mixing of the gas jet. At this mode, the effects of injection pressure on NO_x emissions and BSFC are negligible. Similar results were identified at other speeds.

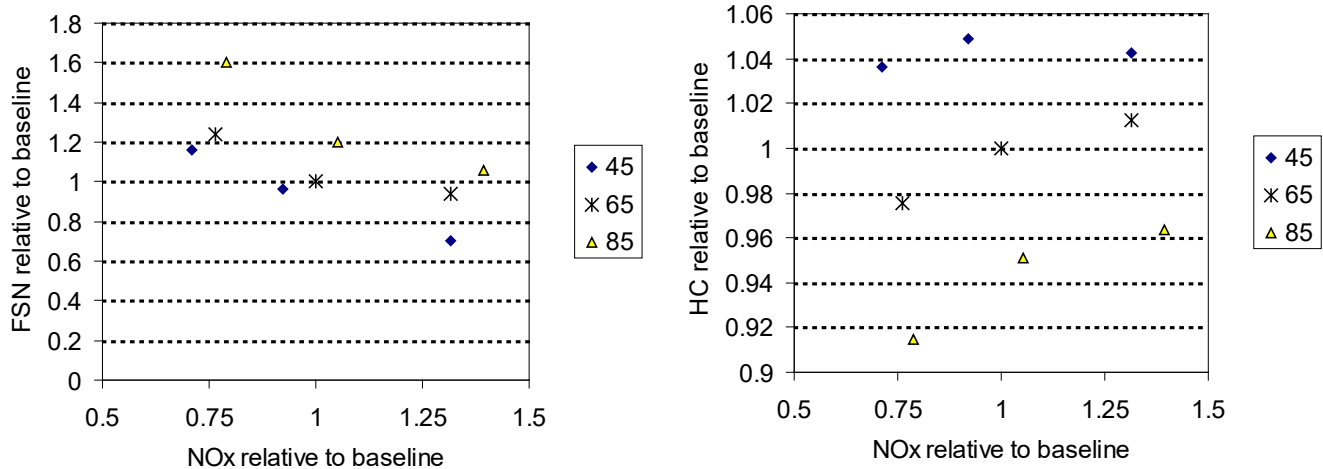
Figure 35: Effect of injection pressure on PM mass, BSFC, and NO_x emissions at mid-speed, 75 percent load operating condition (B75)



The effect of charge air temperature on engine-out emissions was also studied to further understand the potential of optimizing the air exchange system to minimize emissions. Base HPDI timing sweeps with varied IMT were carried out at SET modes 4 and 8 (B75 and B100). Increasing charge air temperature generally causes a simultaneous increase in PM and NO_x

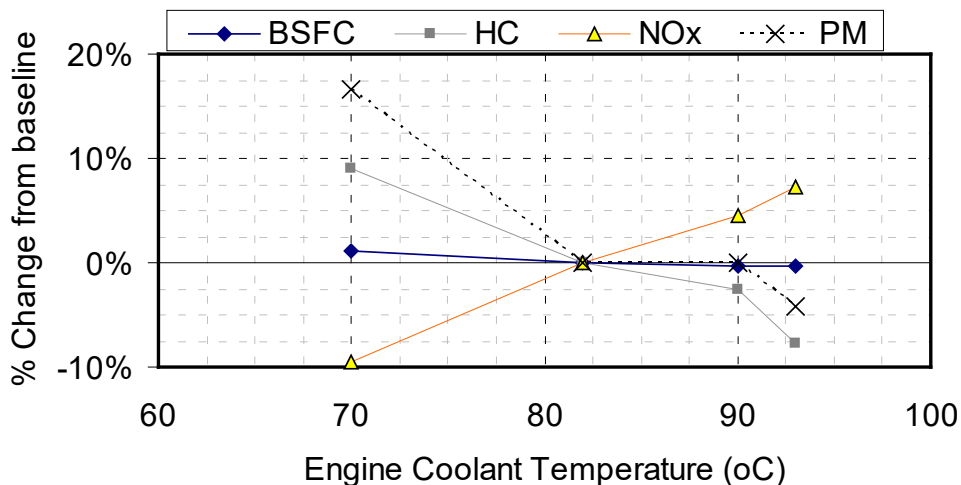
(as shown in the FSN-NOx trade-off in Figure 36) as well as increasing BSFC. Only HC emission improvements were demonstrated, as shown with the HC-NOx trade-off in Figure 36.

Figure 36: Effects of IMT on FSN-NOx and HC-NOx trade-offs. Multi-cylinder engine operating at steady state at mode 4 (B75: 1493 RPM, 75 percent load)



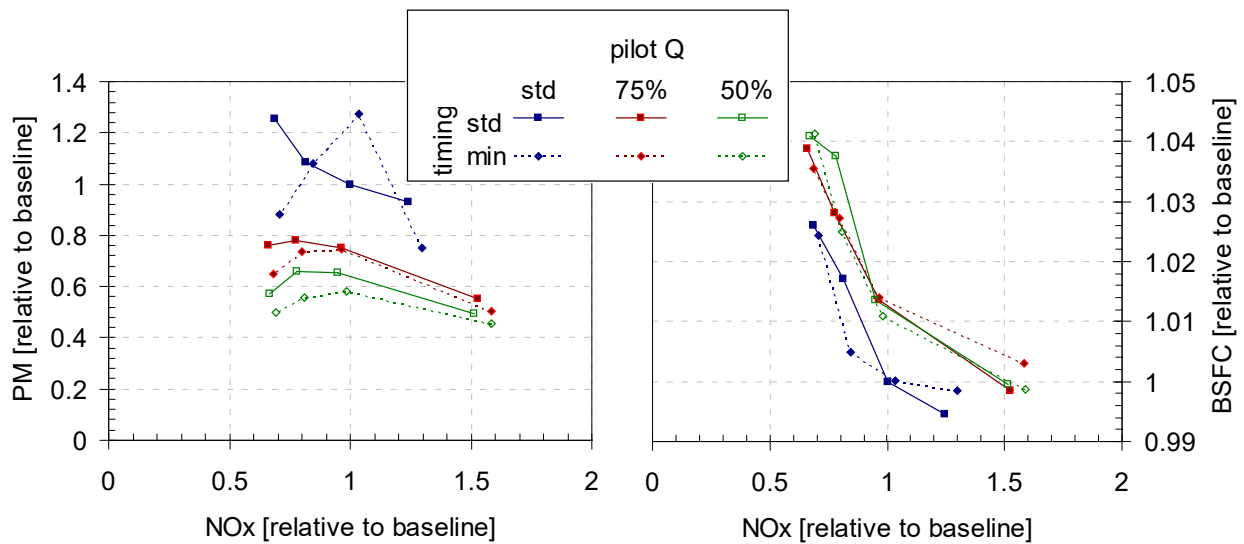
The effect of engine coolant temperature on performance and emissions was also investigated over the SET cycle at 158°F (70°C), 180°F (82°C) (base) and 199°F (93°C) (control system limited). The motivation behind this test is to quantify the resulting engine friction and combustion heat loss reduction with higher engine temperature. These results are shown in Figure 37. A composite efficiency gain of less than 1 percent was measured at the 199°F (93°C) condition relative to baseline 180°F (82°C). The hotter operation reduces HC emissions by approximately 7 percent but increases NOx by 7 percent. Smoke measurements also decrease at higher coolant temperatures as a result of lower EQR. Conversely, reducing coolant temperature leads to approximately 1 percent higher BSFC, 16 percent higher PM, and 10 percent higher HC, but 10 percent lower NOx.

Figure 37: Effects of coolant temperature on composite BSFC, PM, NOx, and HC over the SET cycle



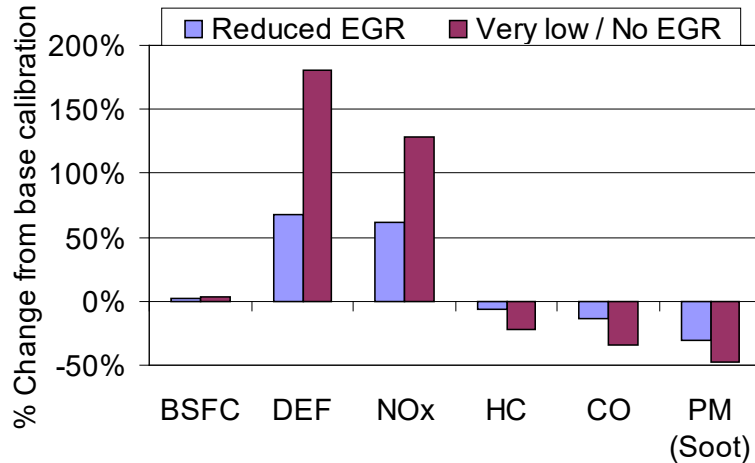
The effect of pilot fueling quantity on performance and emissions was investigated. The purpose of this testing was to determine the potential for DPF size reduction or elimination with reduced engine-out PM. Trade-offs of engine-out emissions and performance with reduced pilot reveal composite FSN reductions of up to 50 percent while maintaining similar to baseline levels NOx and BSFC. However, a hydrocarbon emissions penalty of about 25 percent is observed. These results are shown in Figure 38, where the trade-offs between PM and NOx and BSFC and NOx are shown for the three pilot quantities. The figures also show the effect of reducing the delay between the diesel pilot and main gas injections as a method to reduce PM under most conditions, especially with reduced pilot, while maintaining constant BSFC and NOx emissions.

Figure 38: Combined effects of pilot fueling quantity (pilot Q) and separation delay (timing) on PM-NOx and BSFC-NOx tradeoffs, at baseline and reduced pilot quantities and standard and minimum pilot-gas delay



The potential for fuel economy and PM improvements due to allowing higher engine-out NOx was also studied. EGR and SOI sweeps were carried out over the SET modes to analyze trade-offs at each mode. The results were summarized for two conditions: a reduced EGR where engine-out NOx is allowed to increase by approximately 50 percent, and a minimum EGR case with optimized timing solely to maximize efficiency. Optimum composite results indicate potential for 2 to 3 percent BSFC improvements with engine-out NOx increasing up to about 3 grams per brake horsepower-hour. When urea (diesel emissions fluid [DEF]) consumption is factored in, the fuel consumption plus DEF consumption improvement is about 1 percent. Significant FSN reductions were also obtained as well as improved HC emissions and reduced CO. The relative changes in engine-out emissions, total fuel consumption, and DEF consumption are shown in Figure 39.

Figure 39: Composite emissions results; emissions are engine-out



Compression Ratio and Swirl Effects

The potential of lower compression ratio (CR) pistons and increased in-cylinder charge motion to reduce NOx and PM emissions was also evaluated on-engine over a composite cycle. To maximize the experimental similarity and to remove sources of variability, the testing was conducted on a SCRE. To achieve the desired swirl levels, a pair of shrouds was added to the intake ports to modify the flow through the ports and hence affect the in-cylinder charge motion. These are shown in Figure 40. As the figure shows, the swirl plates significantly obstruct the flow through the intake port. Based on the results from the simulation studies, the most promising modified piston design involves a reduction in CR. A comparison of the baseline piston and the new piston are shown in Figure 41.

Figure 40: Image of cylinder head fire deck (viewed from below [inside the combustion chamber]) showing swirl plates installed in intake ports

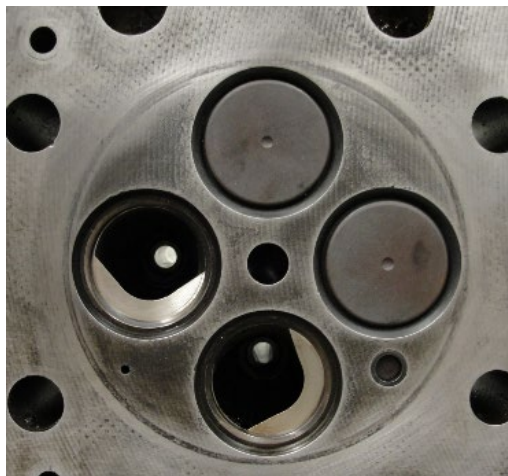
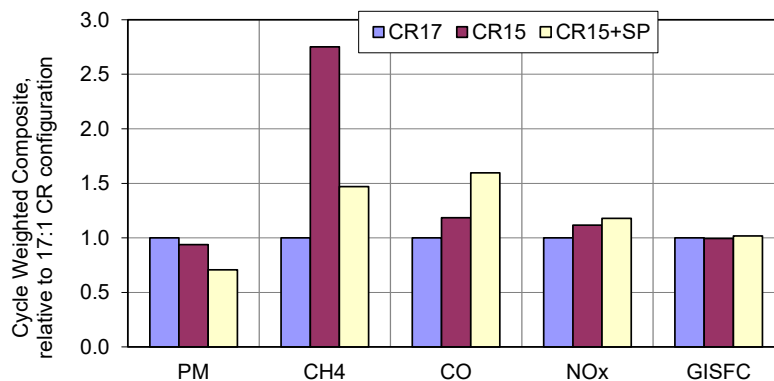


Figure 41: Images of baseline piston (left) and modified piston (right)



The results indicate that lower CR substantially reduces PM under some conditions but tended to increase NO_x (Figure 42). The results are found to be highly sensitive to engine operating condition, such that an emission comparison over a full composite cycle shows small PM and fuel consumption (gross indicated specific fuel consumption) benefits. A further analysis was conducted on the SCRE, with the low CR piston combined with increased charge motion through the addition of swirl plates. A further reduction in PM is observed with increased swirl, although NO_x and fuel consumption both increase compared to the standard swirl.

Figure 42: Full single-cylinder engine cycle composite (engine-out) emission results comparing emissions with base (17:1) compression ratio with 15:1 CR standard intake ports and 15:1 with swirl plates (SP) installed in the intake to increase swirl

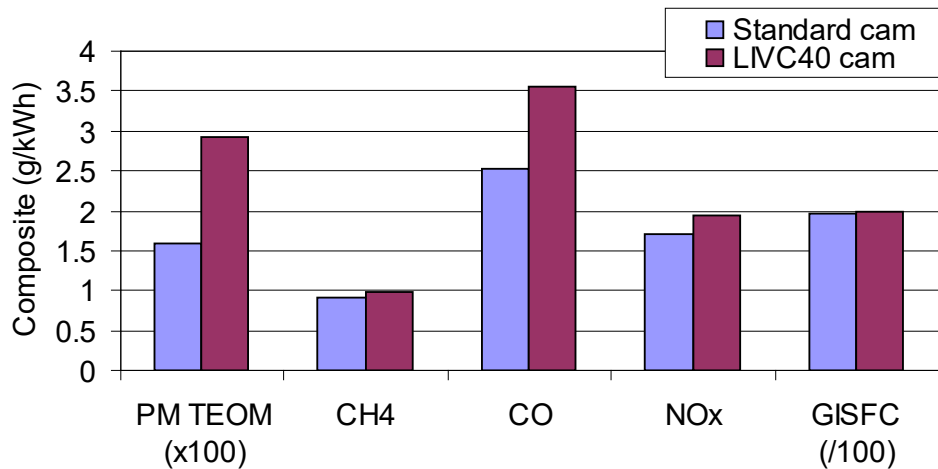


Intake Valve Closing Timing

One area of interest for optimization is the phasing of the IVC, as could be achieved either with a different fixed-geometry camshaft or through a variable-valve actuation system. Initial modeling (discussed earlier in this report) indicated some potential efficiency benefits from a re-optimization of the IVC timing. A study of the effects of IVC on combustion and emissions was conducted on the SCRE, as this engine was equipped with a camshaft that could provide a variety of different intake valve lift profiles. Developing such a flexible system for the multi-cylinder engine is considered to be prohibitively expensive unless sufficient benefits could be identified using the SCRE. A late-intake valve closing (LIVC) cam timing, 40 crank angle

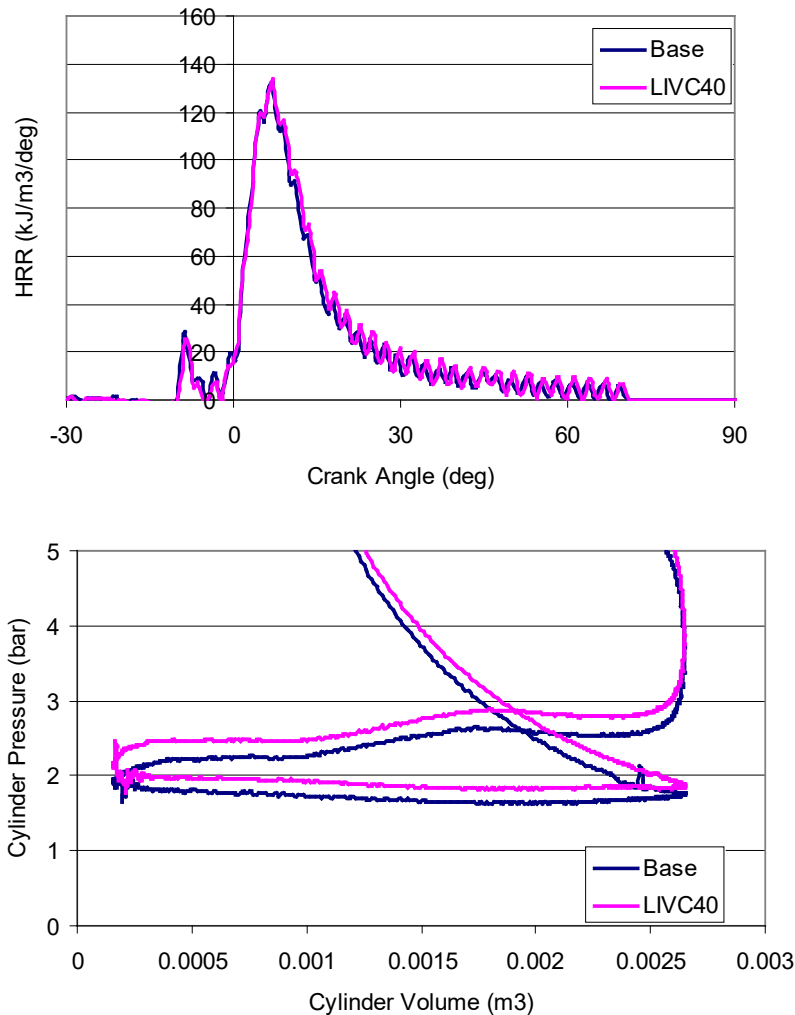
degrees after the standard cam timing (LIVC40), was selected for analysis as modeling suggested it could effectively reduce charge mass at low load without excessively restricting air flow at high load. A 9-mode test, similar to the SET mode tests conducted on the multi-cylinder engine, was conducted with this intake valve timing and compared to the base cam timing. All other parameters (fueling quantity and timing, air flow rate, EGR level, global EQR) were fixed for the two intake valve lifts. As the SCRE had a different control system, the operating conditions were not directly equivalent to the baseline-A engine; however, equivalent trends are expected for the two engines. The effects on emissions and efficiency over the 9-mode composite are shown in Figure 43. PM and CO are substantially increased while NOx also increases. There was no significant effect on CH₄ emissions, or fuel consumption from the evaluated system.

Figure 43: Effect of LIVC on single-cylinder engine emissions over the SCRE 9-mode test cycle. Emissions are composite over the full test range.



The principal effect of LIVC was on the air exchange system performance. As the SCRE was equipped with a flexible air compressor that could maintain a fixed air flow-rate, the testing could be conducted so that the air flow rate was constant between the standard and LIVC40 cases. However, to do this, the boost pressure in the LIVC40 case was increased to offset the air pumped out of the cylinder while the intake valves were open during the start of the compression stroke. These results are shown in Figure 44, where an essentially equivalent HRR is seen for the two combustion events, but both intake and exhaust pressures are higher in the pumping event for the LIVC40 case. This imposes a greater challenge for the turbocharged multi-cylinder engine, where the boost pressure would need to be increased at a fixed mass flow-rate to maintain the same charge mass.

Figure 44: Heat release rate and cylinder pressure during pumping for standard and LIVC40 cam phasings. SCRE data taken at 1500 RPM, 50 percent load.



High Flow Injectors

One of the key objectives of the project was to evaluate higher power ratings for the HPDI engine. One way to achieve this is to increase the injector natural gas flow area, to deliver higher fuel flow without increasing the injection duration. A set of injectors with larger gas nozzle hole sizes and greater gas needle lift were compared to the baseline J36 injectors; the results are shown in Figure 45 for the three full-load points on the SET cycle. The performance and emission trade-offs were also quantified at the torque curve for the three speed points. The relative changes in emissions compared to the baseline are shown in Figure 46. The results show that the CO and PM increases, primarily due to the higher EQR that results from the turbocharger providing a smaller increase in air flow relative to the increase in fueling through the injector. This is particularly noticeable at high speed, where the turbine is operating near its maximum air flow rate. The increases in both CO and PM are within the ranges that are controlled by the EATS, and hence tailpipe emissions do not exceed the regulated levels. It should be noted that these results were achieved with only a crude optimization of the fuel and air handling commands, and hence improved performance would

be expected with a more thorough optimization. This is evaluated as part of the prototype-B engine hardware development.

Figure 45: Torque at high load with high-flow injectors compared to baseline injector capabilities

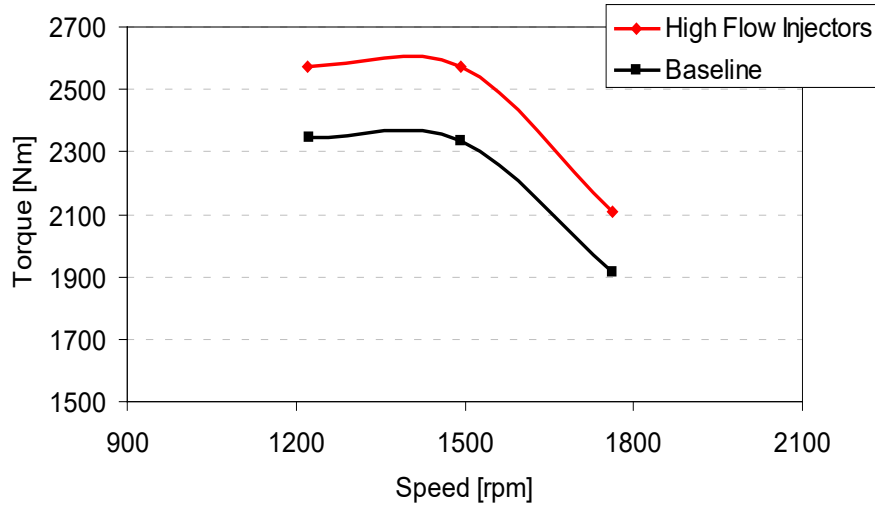
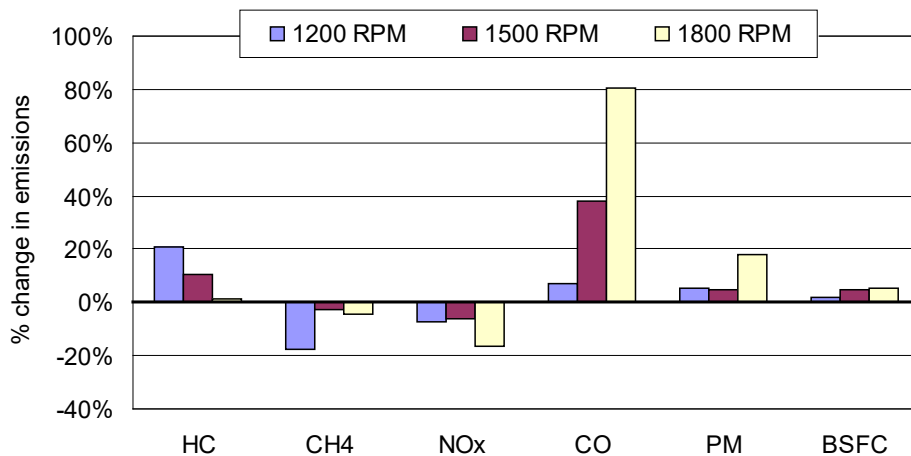


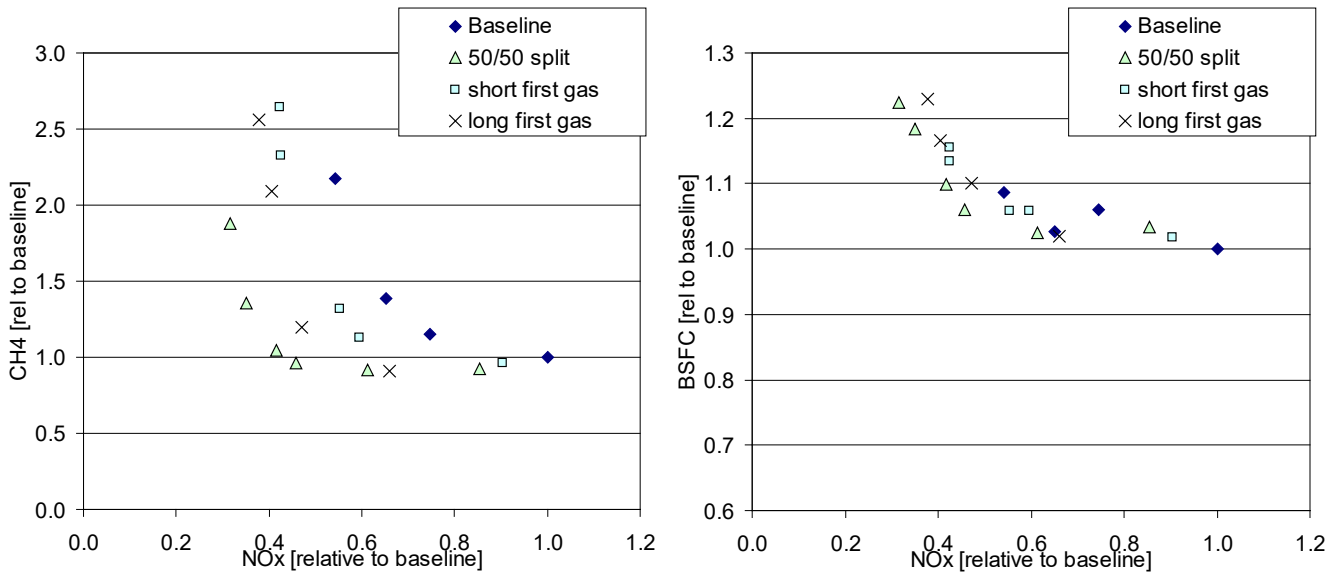
Figure 46: Relative change in power-specific emissions and fuel consumption at the torque curve for the high-torque calibration versus the baseline torque settings



Split Injection/Multiple Injections

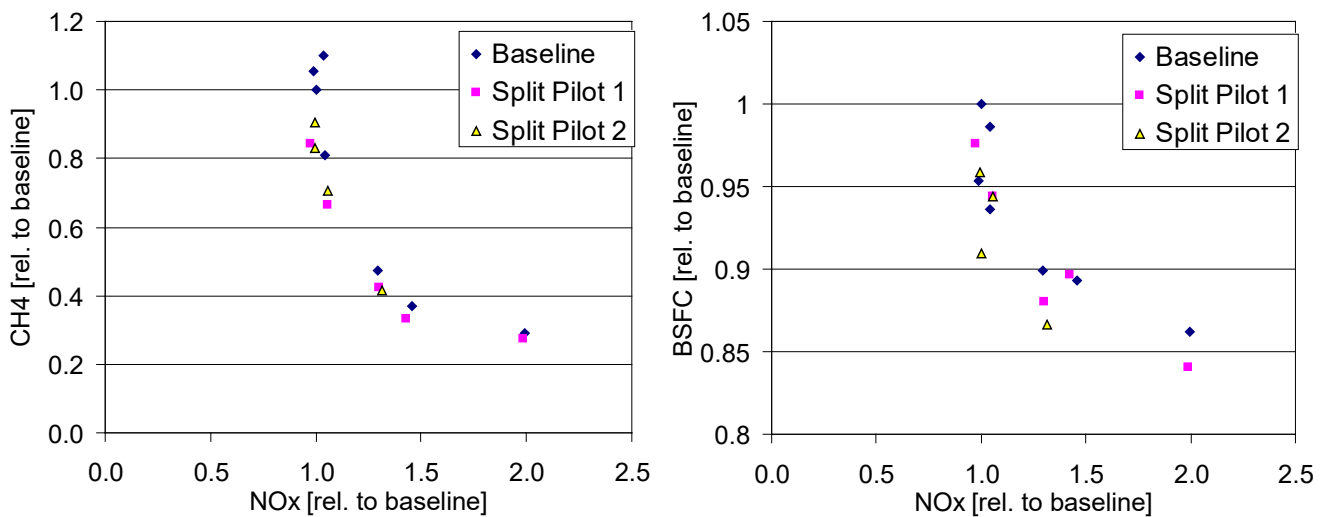
One technique used in the diesel engine industry to optimize the combustion event is multiple injections. As the HPDI combustion process behaves similarly to the diesel combustion event, it is not unreasonable to expect that multiple injections could be used to enhance HPDI combustion, in particular to reduce unburned fuel emissions. Results at a single low-speed, low-load mode (A25) are shown in Figure 47 for both CH₄-NO_x and BSFC-NO_x trade-offs. At this mode, the split injection cases resulted in substantially lower CH₄ for a given NO_x level, with little net impact on diesel consumption.

Figure 47: Effects of split gas injection on CH₄ and BSFC, relative to NO_x, at 1200 RPM, 25 percent load



Another option evaluated for enhanced HPDI performance, in particular at low load, was using two diesel pilot injections rather than the conventional single pilot. This was evaluated at various low-load modes with the intent of improving the ignition process and hence reducing unburned fuel emissions and increasing efficiency. Results are shown in Figure 48, which reveals that split pilot injection has no significant effect on unburned methane emissions. The main drawback (not shown) is that the pilot contribution is essentially doubled, as the injector pulse width is typically near its minimum for even a single injection case.

Figure 48: Split pilot injection effects on CH₄-NO_x and BSFC-NO_x trade-offs. Split pilots 1 and 2 refer to two different pilot separation timings. Results shown for 1200 RPM, 25 percent load.



Experimental Evaluation of Advanced Combustion Modes

The work reported above focused on improvements to the HPDI combustion process. However, the fundamental structure of the combustion remains unchanged, with a diesel pilot injection preceding the gas injection. The natural gas then burns in a predominantly non-premixed fashion, similar to a conventional diesel engine. Potential power, emission, and efficiency benefits could be gained from using the flexibility of the HPDI injector to premix some of the diesel or gas prior to ignition, leading to partially-premixed combustion or other similar advanced strategies.

Partially-premixed Combustion

One aspect of the experimental work was to shift the combustion towards a more premixed mode by advancing the gas injection relative to the diesel. This demonstrated the potential of partially-premixed combustion (PPC) from an efficiency and emission viewpoint. These results are shown in Figure 49 for PM and NO_x as a function of EGR, and in Figure 50 for BSFC as a function of EGR. The results reveal that the PPC concept results in much lower PM for a given EGR level. NO_x emissions at a given EGR level are higher, so to match NO_x emissions without significantly impacting BSFC, the EGR level would have to be increased with PPC. These results suggest that the optimum PPC strategy uses EGR levels higher than the baseline HPDI, maintaining both NO_x and BSFC at essentially the same level as the base case while reducing PM by 30 to 50 percent. Other options for reducing NO_x, such as delaying the combustion, achieve similar results but result in a more substantial fuel consumption penalty.

Figure 49: Effects of PPC on PM and NO_x emissions as a function of EGR

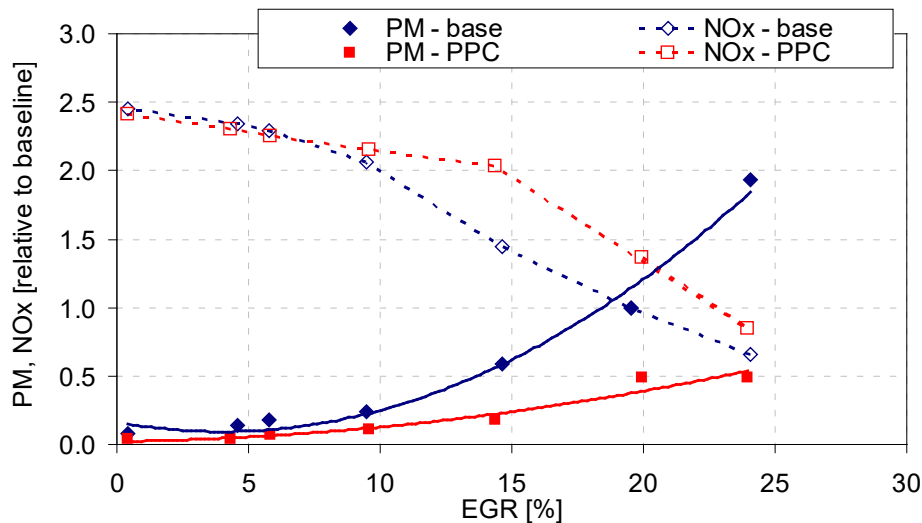
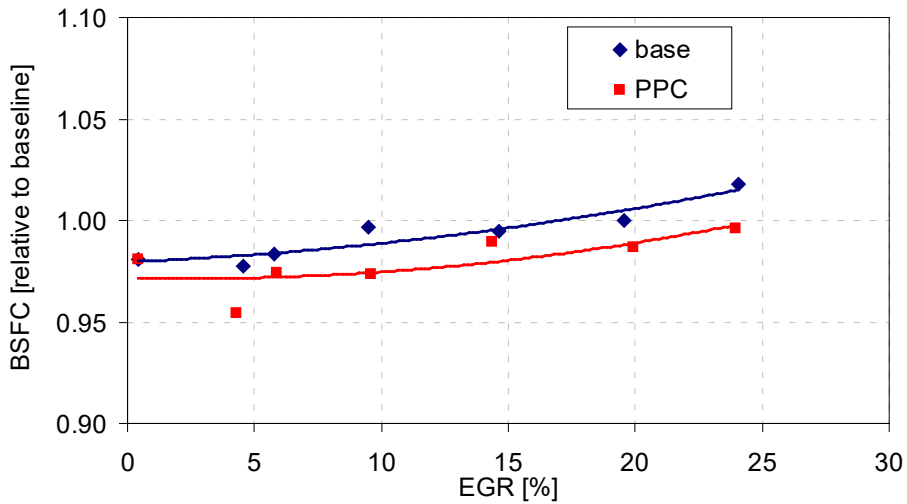
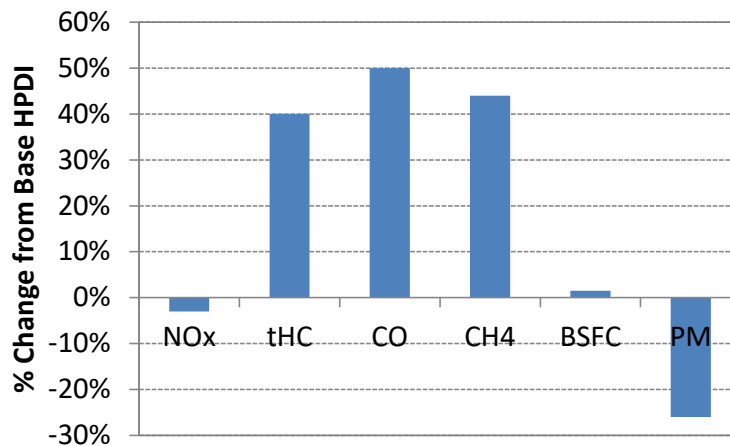


Figure 50: Effects of PPC on BSFC as a function of EGR



A SET cycle composite evaluation was conducted using the PPC combustion strategy identified above; the composite results are shown in Figure 51. This reveals that the use of PPC at high load modes could reduce engine-out PM by more than 25 percent without a negative impact on NOx or fuel consumption. Tailpipe emissions meeting the U.S. EPA 2010 standards are maintained. Unburned fuel emissions increase, but the absolute values remain relatively low (compared to fully premixed combustion systems).

Figure 51: Composite emissions for PPC over 13 mode cycle



Homogeneous Charge Compression Ignition

The research program also investigated more advanced combustion strategies. One of these is a mixed-mode homogeneous charge compression ignition (HCCI) and homogeneous charge direct injection (HCDI) combustion strategy. In HCCI, all of both diesel and natural gas fuels are injected well before the piston reaches top-dead-centre. The mixture then auto-ignites, providing a theoretically high-efficiency, low-emission combustion mode that is limited by knock to relatively low loads. To achieve higher loads, a second injection of gas is injected after top-dead-centre, towards the end of the HCCI combustion event; this is referred to as

HCDI, as it is an amalgamation of conventional HCCI and HPDI combustion strategies. HCDI results in a non-premixed combustion event that allows the engine to achieve higher power levels without knock. Emissions are controlled by varying the HCCI combustion event and the timing of the second gas injection. As with HCCI programs reported by other researchers, the HCCI part of the HCDI process is highly dependent on the engine conditions. To evaluate this, a test matrix investigated key parameters such as pilot quantity and timing, early and late gas quantity and timing, IMT, and EGR. The results are shown relative to baseline HPDI (both with and without EGR) in Figure 52 and Figure 53 for HCCI at low load and HCDI at mid-load. As the figures show, the FSN-NOx trade-off indicates that HCDI could achieve relatively low NOx emissions without EGR (nearly the same as base HPDI with EGR). The FSN is relatively low under the non-EGR conditions, unless a very early diesel injection is used in which case wall impingement of the diesel leads to a sudden increase in PM. The main barriers to the HCDI strategy are a significant efficiency penalty (shown in Figure 52) and a substantial increase in emissions of unburned methane (not shown), due to the increased premixing of natural gas with the charge air. The HCCI strategy (results shown in Figure 53) also shows high unburned fuel and lower efficiency compared to the baseline HPDI case; in this case fuel consumption is more than 10 percent above the baseline HPDI.

Figure 52: FSN-NOx and BSFC-NOx trade-offs comparing HCDI and HPDI strategies at 1500 RPM, mid-load conditions

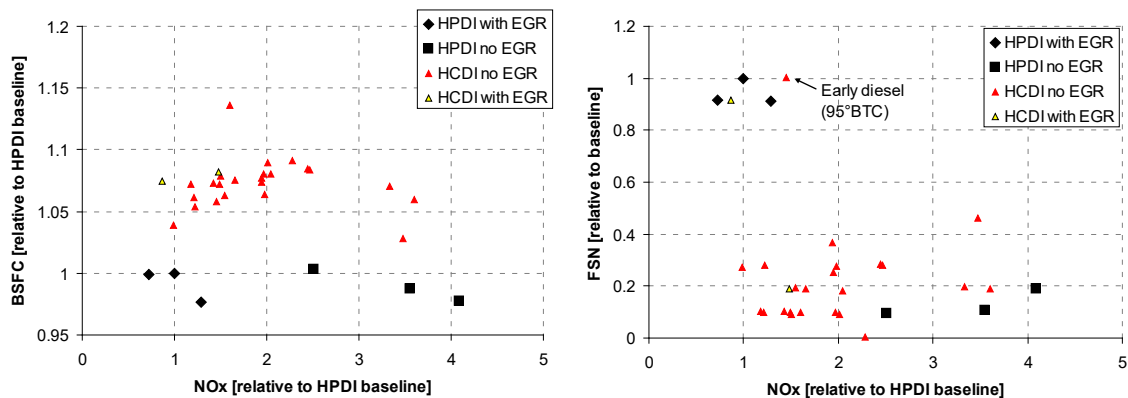
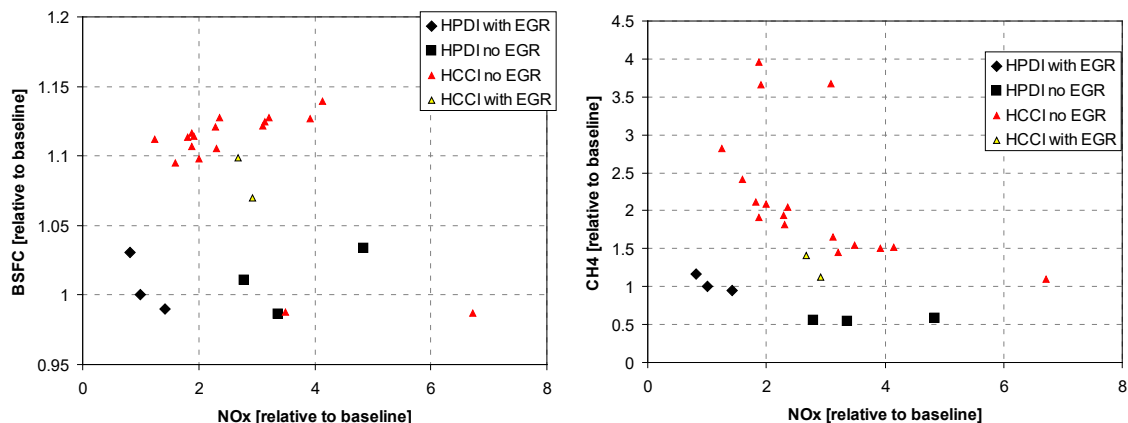


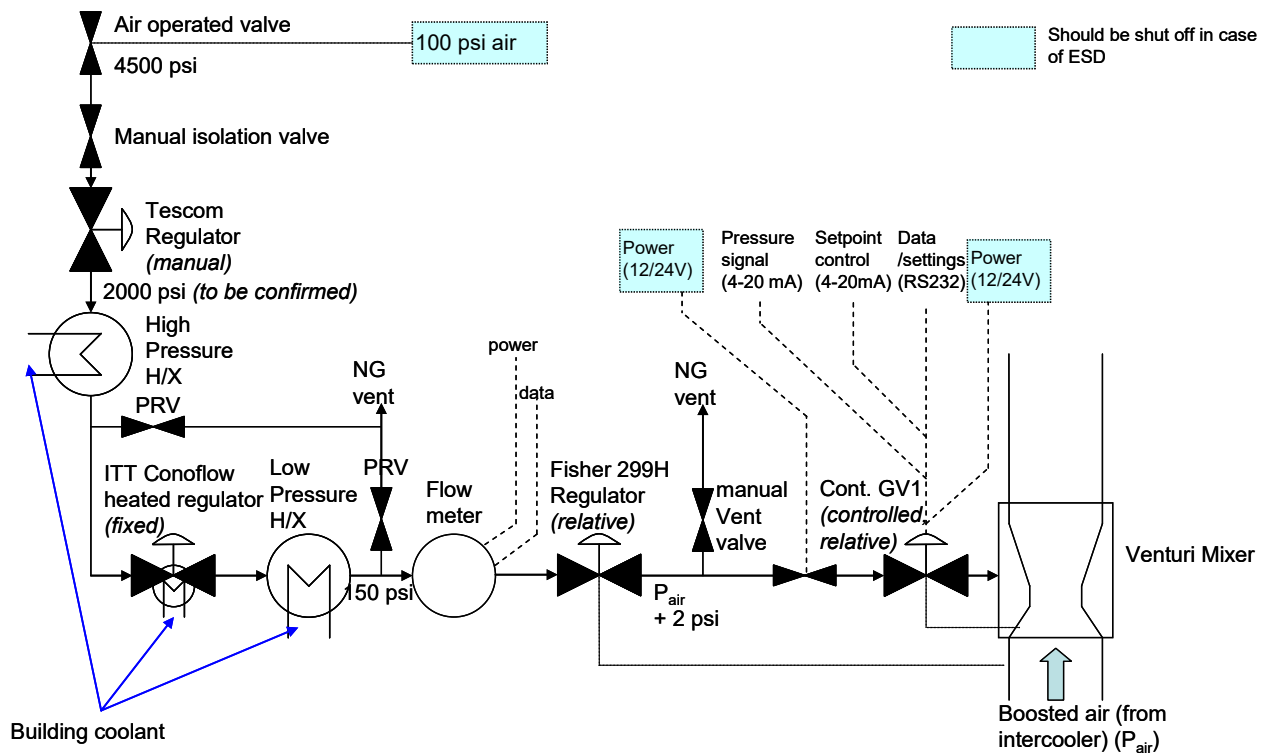
Figure 53: CH₄-NOx and BSFC-NOx trade-offs, comparing HCCI and HPDI strategies at 1500 RPM, low-load conditions



Fumigated (Premixed) Combustion

The preceding work demonstrates the potential benefits of premixing the natural gas with the charge air for reduced emissions through an early direct injection of natural gas using the HPDI injectors. While this process increases the charge motion, it has the drawback of potentially incomplete mixing. This is exacerbated by control system limitations that prevent very early injections (during the intake stroke) so it was not possible to establish the effects of full premixing; the charge remained partially stratified at even the earliest timings. To investigate this further, a fumigation system was constructed to mix the natural gas with the air charge in the intake manifold, as shown in Figure 54. The core of the system is the Continental Controls Corporation flow control valve (model GV-1) and gas-air venturi mixer (VM-350). The system is designed to give complete test-cell flexibility, with adjustable gas pressures and flows and pressure, temperature, and flow measurement.

Figure 54: Fumigation system schematic, including control connections



Premixing the gas results in a substantial reduction in PM (as shown by the FSN in Figure 55). However, the maximum torque in this combustion mode is limited to approximately 75 percent load by engine knock. Testing was conducted with and without EGR to evaluate NO_x reduction as well as knock avoidance; while the EGR successfully reduces NO_x, it does not increase the achievable torque before detecting an unacceptable level of knock. Furthermore, exhaust gas temperatures increase with fumigation (Figure 56), which limits the ability to retard the timing as a technique to avoid knock. As such, the application of fumigation to the prototype-A engine is limited by hardware. Further optimization was conducted on the prototype-B engine to overcome some of these limitations, as will be discussed later in this report.

Figure 55: FSN versus torque comparing fumigated combustion to HPDI at 1493 RPM

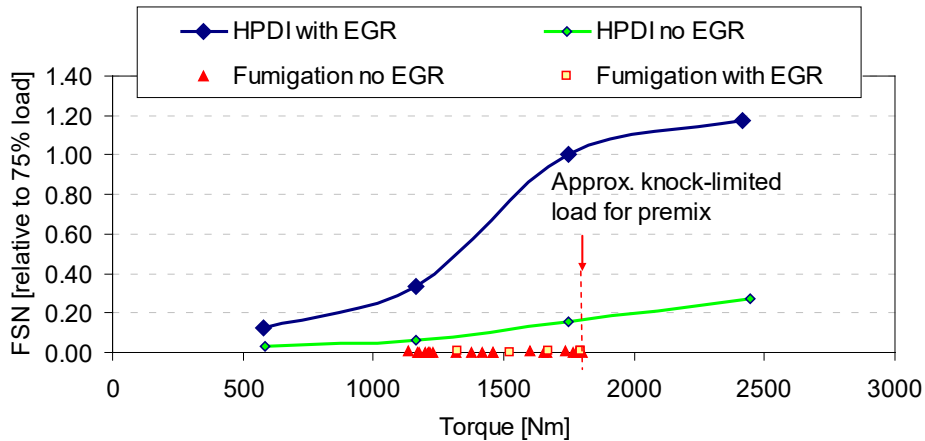
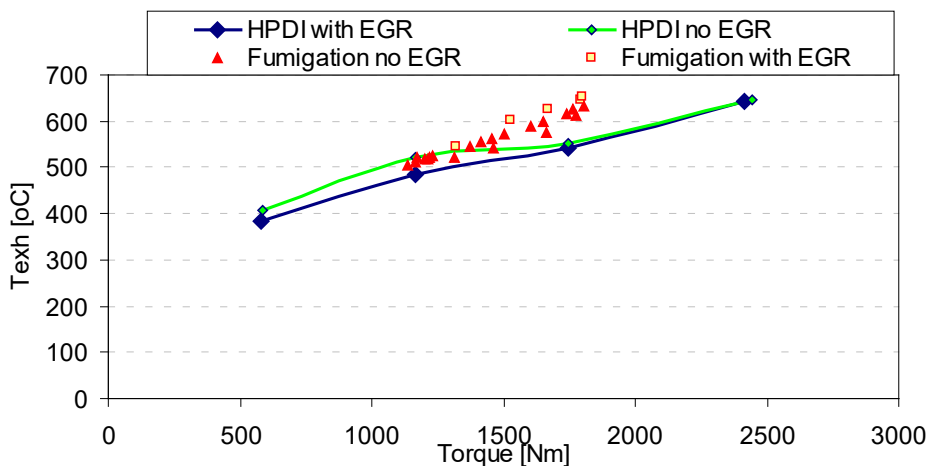


Figure 56: Exhaust gas temperature versus torque for fumigated and HPDI combustion



Combustion Enhancement Summary

Research was conducted on enhancing combustion to maximize efficiency while reducing emissions. The influences investigated focus on the injection process: including pilot quantity and timing, rail pressure, and split injections. The greatest benefits are found in reduced pilot quantity at high load for reduced engine-out PM, while multiple gas injections are found to provide some CH₄ benefits at lower load. Other engine operating parameters, including EGR level, coolant temperature, and intake manifold temperature, were also investigated. Maintaining EGR level near the reference value is found to be critical for NO_x control, but further increases in EGR did not enable the injection phasing to be adjusted to improve efficiency without negatively affecting PM emissions. Increased coolant temperature provides only a marginal improvement in BSFC while increasing NO_x, and increased intake manifold temperature reduces unburned methane emissions at the expense of increased PM. The results from these studies provide improved understanding of the influences of the various combustion parameters on engine performance, emissions, and efficiency. The key strategies

for subsequent stages of this work were to optimize the EGR, combustion phasing, and pilot quantity for best efficiency and low PM while maintaining NO_x at levels where the EATS conversion efficiency could ensure levels below the emission standards.

Engine hardware changes were also investigated. The effects of swirl ratio and compression ratio were tested on a single cylinder version of the GX engine; swirl was found to provide no consistent benefit while lower CR provided a small improvement in efficiency over a 9-mode composite cycle. Delaying the intake valve closing timing was also evaluated, and found to have no fuel consumption benefit while increasing emissions of all species. The results from this work indicate that a lower CR piston with the base engine swirl ratio and intake valve timing would provide the optimum combustion system, especially for higher-load operation expected to be more limited by peak-cylinder pressure.

Finally, advanced partially- and fully-premixed combustion strategies were evaluated. Engine knock limits the maximum achievable power under fully-premixed conditions using both conventional pilot combustion timing and early timing to create an HCCI-like combustion event. Peak cylinder pressure limits also restrict the combustion event, as does the turbine inlet temperature. Emissions of unburned methane were also significantly increased for all premixed combustion strategies. Reducing the engine's compression ratio could help to overcome some of these engine hardware limitations.

CHAPTER 7:

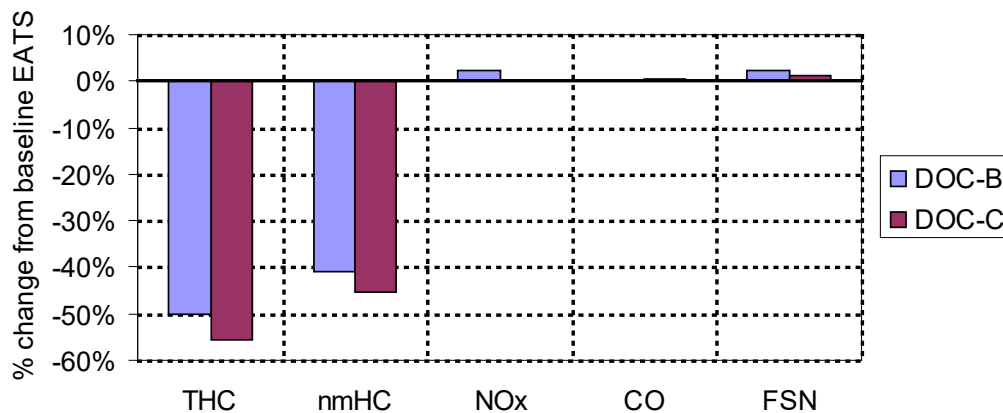
Aftertreatment Optimization

Reduction of engine-out emissions, as evaluated in the previous sections, is beneficial in terms of reducing the requirements on the EATS. However, the ultimate objective is to reduce tailpipe emissions while minimizing fuel consumption and maximizing engine power with the lowest-cost aftertreatment system. As such, the optimization of the EATS is directly related to the overall combustion system enhancements. The cost-reduction potential in the EATS was discussed earlier in this report and is not reproduced here. However, the performance of the prototype DOCs and the metallic DOC/DPF systems are evaluated here and compared to the base EATS.

DOC Performance

The first round of testing of prototype EATS hardware focused on enhanced DOCs. Two ceramic DOC's with reduced platinum group metal loading (34 percent lower than baseline, one of which was zoned), as discussed earlier in this report, were compared to the baseline DOC performance. The enhanced DOC prototypes were installed in place of the base DOC with the rest of the base EATS components in place. The SET cycle was used to quantify the performance. While both prototypes had approximately half the conversion efficiency for nmHC emissions of the base EATS, tailpipe levels remained below the regulated standards. PM measured via FSN at the tailpipe showed no significant change relative to the baseline. For both prototype DOCs, as well as for the base EATS, CO emissions post-catalyst were negligible. The results for all the measured emissions are summarized in Figure 57; the small change in NOx and FSN conversion reported in the figure is attributable to experimental variability.

Figure 57: Comparison of emissions conversion efficiency across EATS with two prototype DOCs relative to baseline EATS performance (negative value indicates reduced conversion efficiency)



Metallic DOC/DPF

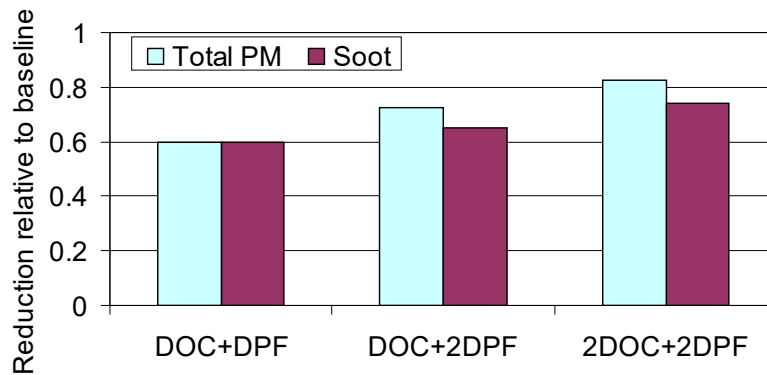
As a further upgrade over the existing system, a metallic partial flow DOC/DPF system was also evaluated. The functioning of the partial flow DPF is such that it is not a 'plug flow' so not all the gas passes through the walls of the filter, as in a conventional DPF. Gaps ('scoops') in the wall encourage some cross-flow, which results in particle deposition. As it is not a plug-flow system, it should never plug, and should always be able to regenerate passively. As such it provides both an efficiency boost and a cost savings over the base system, as was discussed in more detail in Table 3. The system installed on the test engine is shown in Figure 58. The system was also specified to have an overall smaller volume (44 percent smaller than the base GX system) with the intent of reducing both cost and engine backpressure.

Figure 58: Prototype DOC/DPF system installed on test cell engine



The performance of the new system was evaluated at SET modes with a post-DPF gravimetric measurement of PM, which was then compared to baseline measurements. The reduced volume system was found to be about half as effective as the baseline system in general, as shown in Figure 59. Further testing was conducted using two metallic DPFs installed in series, aimed at determining if additional DPF volume would be beneficial in reducing PM. A final set of tests were conducted with two metallic DOCs (to provide higher NO₂ concentrations to encourage DPF performance) followed by two metallic DPFs. The results are all shown in the figure below. Total PM and black carbon emissions are reduced more with the increased volumes, but the reductions remain below the levels achieved by the base EATS. However, the demonstrated reductions with the new DOC/DPF should be sufficient to meet current emission standards, especially if some of the techniques discussed earlier in this report are applied to reduce engine-out emissions.

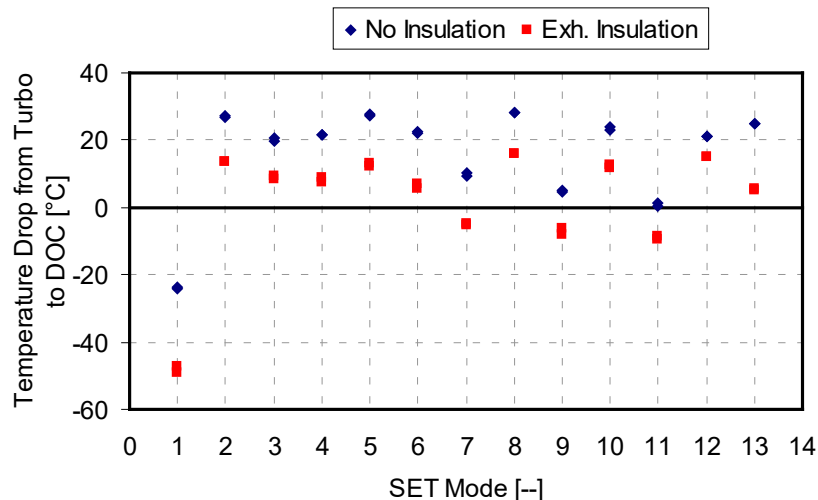
Figure 59: Metallic DPF results, including single or double-brick systems for both DOC and DPF



Exhaust Thermal Management:

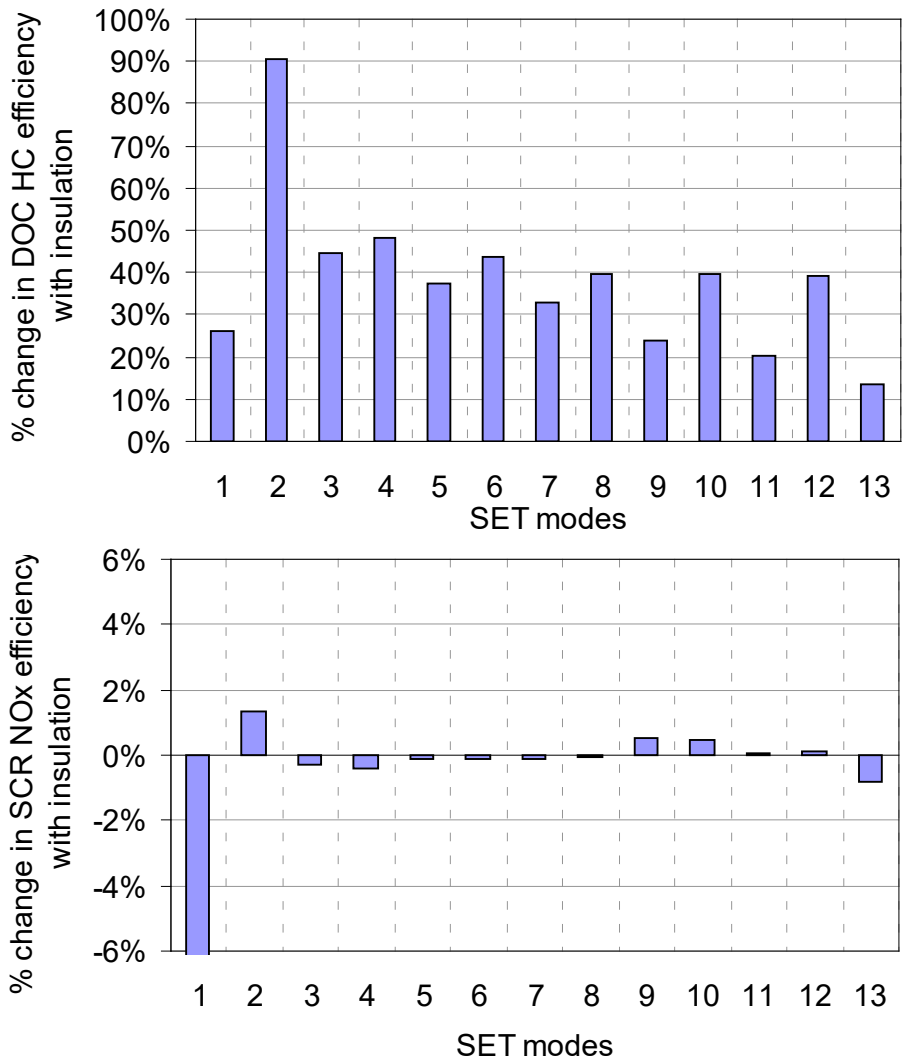
Thermal management of the exhaust stream is an area of particular interest as increasing the exhaust temperature can help enhance the performance of the DOC and selective catalytic reduction system for NO_x control as well as increasing auto-regeneration of the DPF, thereby reducing the need for fuel-consuming active regenerations. To investigate this, the exhaust system (from the turbocharger to the inlet of the DOC, and between the DPF and the SCR) for the prototype-A engine was insulated with the base EATS in place. The effect on the temperature drop between the turbocharger and the DOC inlet, where the insulation was expected to have the greatest effect, is shown in Figure 60. As the results show, at all modes the insulation reduced the temperature drop by approximately 50°F (10°C). At the low-load modes (idle: mode 1; and 25 percent load: modes 7, 9, and 11) the addition of insulation actually results in an increase in the temperature at the DOC inlet compared to the turbocharger outlet. This is primarily the insulation keeping the exhaust system temperature higher, enabling a transfer of heat from the insulated walls to the gas at these low exhaust temperature modes.

Figure 60: Temperature drop between turbocharger outlet and DOC inlet over all 13 SET modes, with and without insulation on the exhaust system



The increase in DOC-inlet temperature would be expected to increase the emissions reduction potential of both the DOC and the SCR. The DOC was more effective at reducing HC emissions, as shown in Figure 61; the composite average reduction increased by nearly 40 percent, with individual modes (mode 2 in particular) having an increase of nearly 90 percent. The SCR did not show the same sensitivity; at most modes, the performance was essentially the same with and without insulation. As a result, the addition of insulation to the exhaust does not appear to offer a strong benefit in terms of improving the NOx reduction potential of the SCR, and its main benefit remains an improvement in nmHC emissions reduction.

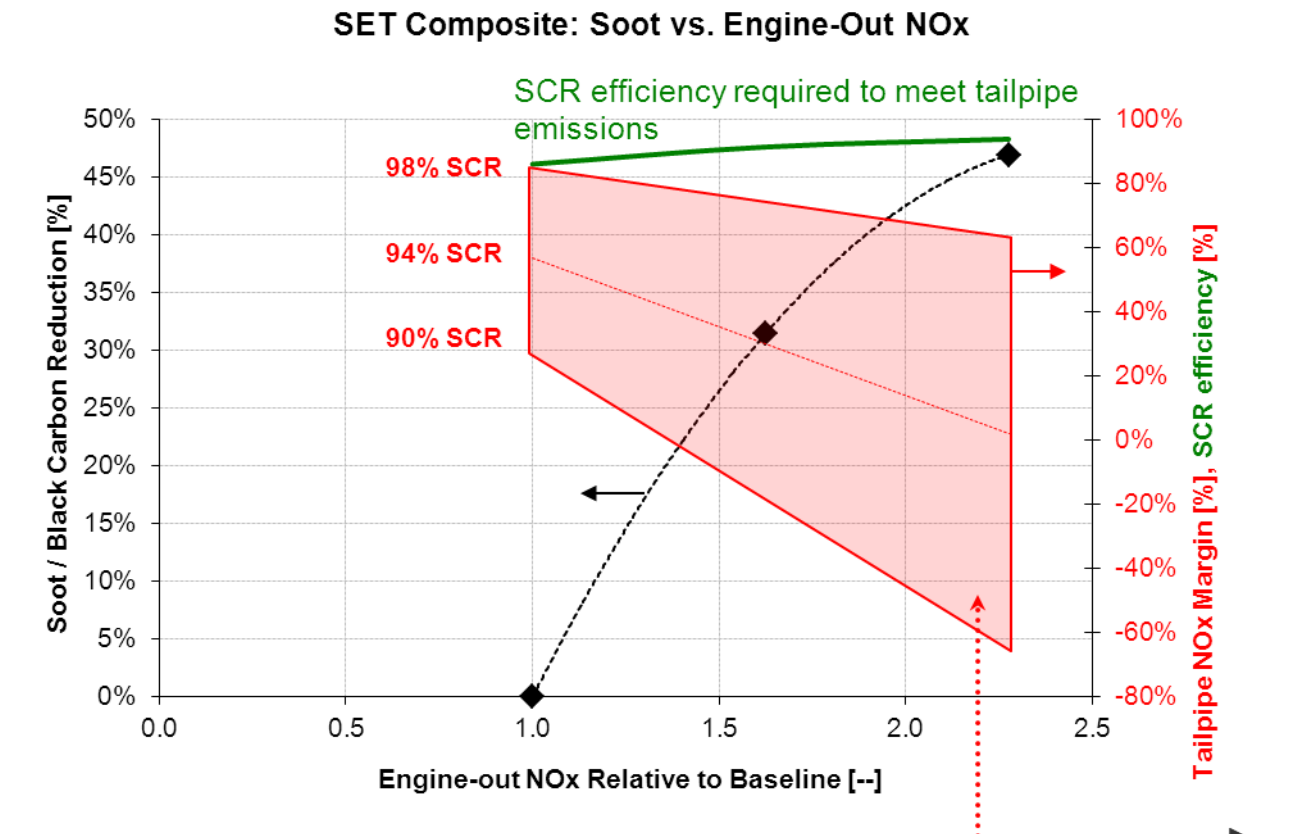
Figure 61: Changes in DOC and SCR emission conversion efficiencies with the addition of insulation. DOC results refer to reduction in total HC across the DOC, SCR refers to reduction in total NOx across the SCR. For the SCR, DEF injection was equal with and without insulation.



Joint EATS Optimization in Conjunction with Engine Optimization

The prototype DOC/DPF systems were jointly evaluated with the NOx aftertreatment system under varying engine EGR levels and combustion strategies to evaluate the options for the optimization of the overall system. This was evaluated over the full composite cycle, with a particular emphasis on improving NOx conversion efficiency to enable a higher engine efficiency and to lower engine-out PM. The latter is important as it could enable the use of a lower-cost DPF system such as the metallic-substrate DOC/DPF evaluated in this work. The benefits of optimizing SCR efficiency are shown in Figure 62, in terms of reduced black carbon emissions. An increase in engine-out NOx of approximately 50 percent would reduce black carbon by 30 percent. The analysis indicates that an SCR conversion efficiency of slightly more than 90 percent would be needed to meet tailpipe emissions standards. Similarly, a doubling of engine-out NOx would require an SCR efficiency approaching 95 percent on the composite cycle but would enable a reduction in engine-out black carbon of more than 40 percent. These PM reductions would enable a substantial reduction in the size, cost, and complexity of the DPF. The SCR efficiencies required to achieve this (in the 93 to 95 percent range) are within the range expected for latest-generation SCRs without requiring excessive increases in DEF consumption.

Figure 62: PM reduction versus NOx compared to the required SCR efficiency to maintain tailpipe NOx emissions, and regime where extra margin on tailpipe NOx would be available



CHAPTER 8:

Final Engine Configuration and Calibration

The overall research and development program focused on the development of a new, lower cost, higher performance HPDI engine. These objectives were evaluated through a series of individual tasks, as summarized in the preceding sections. The final task of the engine experimental program was to apply the findings from the previous studies to develop a final prototype engine (prototype-B) and develop a calibration that met the objectives of higher torque with improved efficiency while meeting the tailpipe emission targets.

Final Engine Architecture

The results from the previous development activities led to a final engine hardware configuration optimized to meet the objectives of the project. The final, prototype-B, engine used the following new hardware configuration:

- High-flow injectors for 10 percent extra torque
- Piston design with lower compression ratio (15.3:1)
- DOC with reduced precious metal loading
- Virtual sensor for engine protection and fuel composition robustness
- Exhaust system insulation to enhance aftertreatment performance

Modified valve timing and the new (J236) injectors were also considered for inclusion in the prototype-B engine. However, as neither demonstrated a performance or cost reduction benefit, they were excluded from the final system architecture. The fumigation system was also evaluated as part of the prototype-B engine specifications, with the expectation that the reduced compression ratio would enhance premixed combustion performance.

Fumigation System with Prototype-B Engine

The fumigation system was evaluated on-engine as part of the prototype-B refinement process, in conjunction with the new low CR piston bowls. The results with the stock piston bowl were presented earlier in this report and are not reproduced here. The main barrier identified in the initial work was high cylinder pressures attributed to endgas autoignition (knock) in the premixed charge at engine torques exceeding 1750 N.m (1,291 foot pounds). The reduced CR pistons of the prototype-B engine were expected to reduce the onset of engine knock and thereby enable fumigated operation at higher loads.

With the lower compression ratio pistons, testing revealed that fumigation could be operated knock-free up to a torque as high as 2200 N.m. However, this limit was highly sensitive to charge conditions and even varied with ambient conditions; the highest repeatable torque was closer to 2000 N.m (1,475 foot pounds). The engine-out PM remained very low (FSN near 0), as shown in Figure 63 with fumigation, both with and without EGR; this is equivalent to the findings from the prototype-A case discussed earlier in this report. The effects on BSFC are shown in Figure 64; at this compression ratio, most of the fumigated points showed BSFC

substantially above the HPDI case. Combining this reduced efficiency with a maximum fumigation torque significantly below the torque target for the prototype-B engine indicates that fumigation is not a viable solution to achieve the project objectives. As a result, the fumigation system was not used in the final prototype-B configuration.

Figure 63: FSN as a function of engine torque for prototype-B HPDI and fumigated combustion strategies. FSN normalized by the FSN at 75 percent load for the HPDI with EGR case.

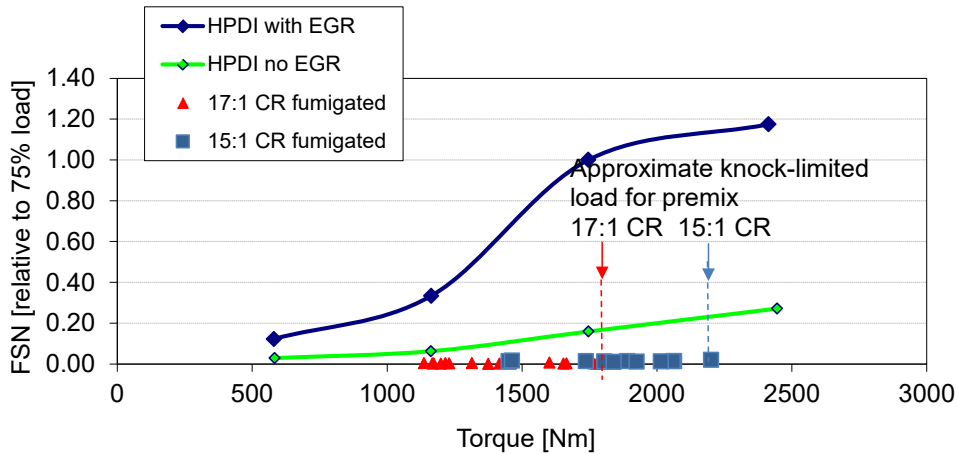
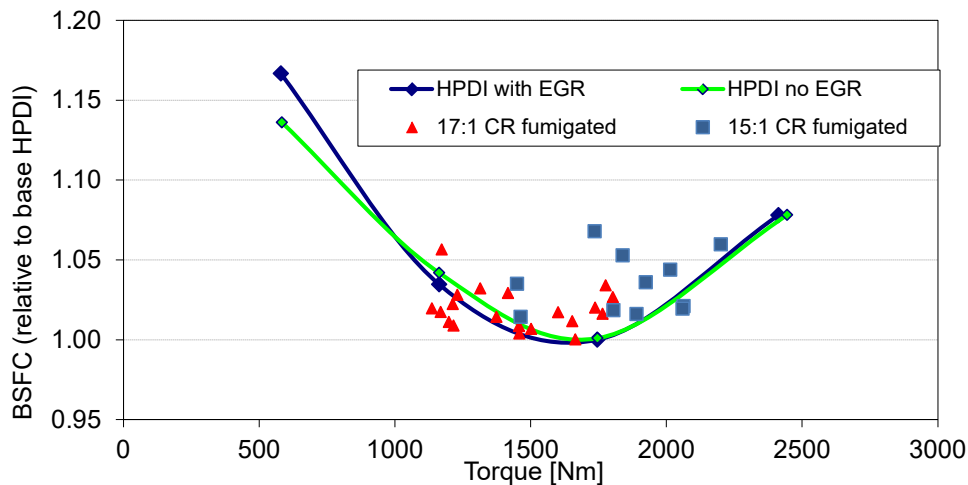


Figure 64: BSFC as a function of engine torque for prototype-B HPDI and fumigated combustion strategies. BSFC normalized by the BSFC at 75 percent load for the HPDI with EGR case.



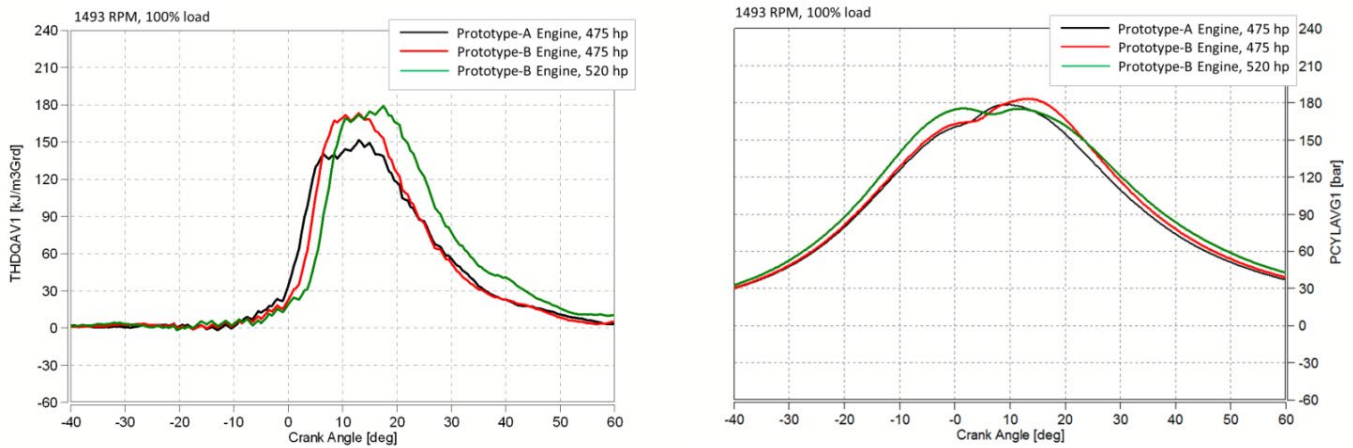
High-load Prototype-B Engine Performance

The ability of the prototype-A engine to achieve the target power density was reported earlier in this report. One of the main factors limiting the performance of the engine at the increased power rating was high cylinder pressures. This impacts the engine efficiency in three ways. First, avoiding the peak cylinder pressure (PCP) requires further delaying the injection event and subsequent combustion at high load, leading to higher cylinder pressures. Secondly, it

reduces the pressure ratio across the injector nozzle (between the cylinder charge and the fuel in the nozzle sac), reducing the gas flow rate and hence extending the injection and combustion durations. Thirdly, the higher cylinder pressures result in higher combustion temperatures leading to higher NOx production; this requires a larger quantity of DEF (or urea) to reduce NOx emissions through the SCR. As a result, a modified piston design with a 15.3:1 CR, as discussed earlier in this report, was used in the prototype-B engine.

The reduced compression ratio pistons resulted in lower PCPs and enabled more optimized combustion phasing. The higher flow injectors combined with the reduced CR resulted in a more rapid heat-release for a given load compared to the prototype-A engine, as shown in Figure 65. These two factors also enabled an increase in torque of 10 percent with only a slight delay in combustion phasing to avoid the PCP limit.

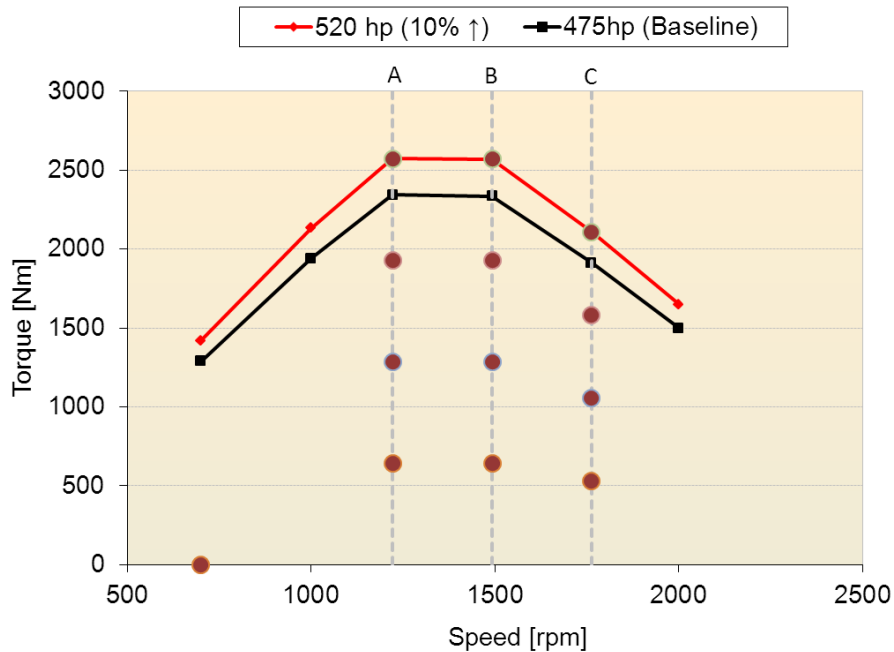
Figure 65: Heat-release rate and cylinder pressure at peak torque, 1493 RPM, for prototype-A and prototype-B engines. Prototype-B shown for both base (475 hp) and 520 hp ratings.



Calibration Points for Prototype-B Engine

The results from the evaluations identified above were used in the development of a final calibration. The full engine torque curve is shown in Figure 66, along with the individual modes used in the calibration process. For reference, the original (475 horsepower [hp]) torque curve is also shown in the figure. As discussed earlier in this report, the individual modes are four loads (25, 50, 75, and 100 percent of full load) at three speeds (A, B, or C); the 13th mode is idle. As the torque and power curves are simply linearly shifted up by 10 percent across the board, the predefined A, B, and C speeds remain the same for the 520 hp rating as for the 475 hp prototype-A engine.

Figure 66: Engine torque curve and calibration points for 520 hp prototype-B engine. The prototype-A (475 hp) engine torque curve is also shown for comparison.



Mode-by-mode Optimization with Prototype-B Engine

The optimization at the individual modes identified in Figure 66 was conducted with the objective of meeting tailpipe NO_x emissions while minimizing fuel consumption and avoiding mechanical engine limits, including PCP and turbine inlet temperature. Excessive emissions of CO, nmHC, and PM were also avoided, although the aftertreatment system’s effectiveness for these three species was very good such that engine-out emissions would need to increase substantially from the prototype-A engine level to cause significant concerns for tailpipe emissions.

As an example, the various points evaluated for the optimization at a single mode (B100, 1493 RPM at 2550 N.m torque) are shown in Figure 67 for emissions and Figure 68 for engine hardware parameters. In these plots, the emissions are normalized by the value at the point selected as ‘optimal’ for the final calibration (shown by the red square in the figures). As such, the final calibration point is the ‘1,1’ point in all four of the trade-off plots shown in Figure 67. For the engine parameters shown in Figure 68, the values are normalized by the engine hardware limit; the point selected as the optimum calibration at this mode is shown by the red square. The parameters varied for these points included injection timing, diesel pilot quantity, EGR level, and air-handling parameters. At this mode, the engine was running close to the PCP and turbine inlet temperature limits. As a result, the achievable variations in the different parameters were relatively small.

Figure 67: Optimization trade-offs at B100 (1493 RPM, 100 percent load) for calibration of prototype-B engine. All values normalized by the optimum point selected for the final calibration, shown by the red square.

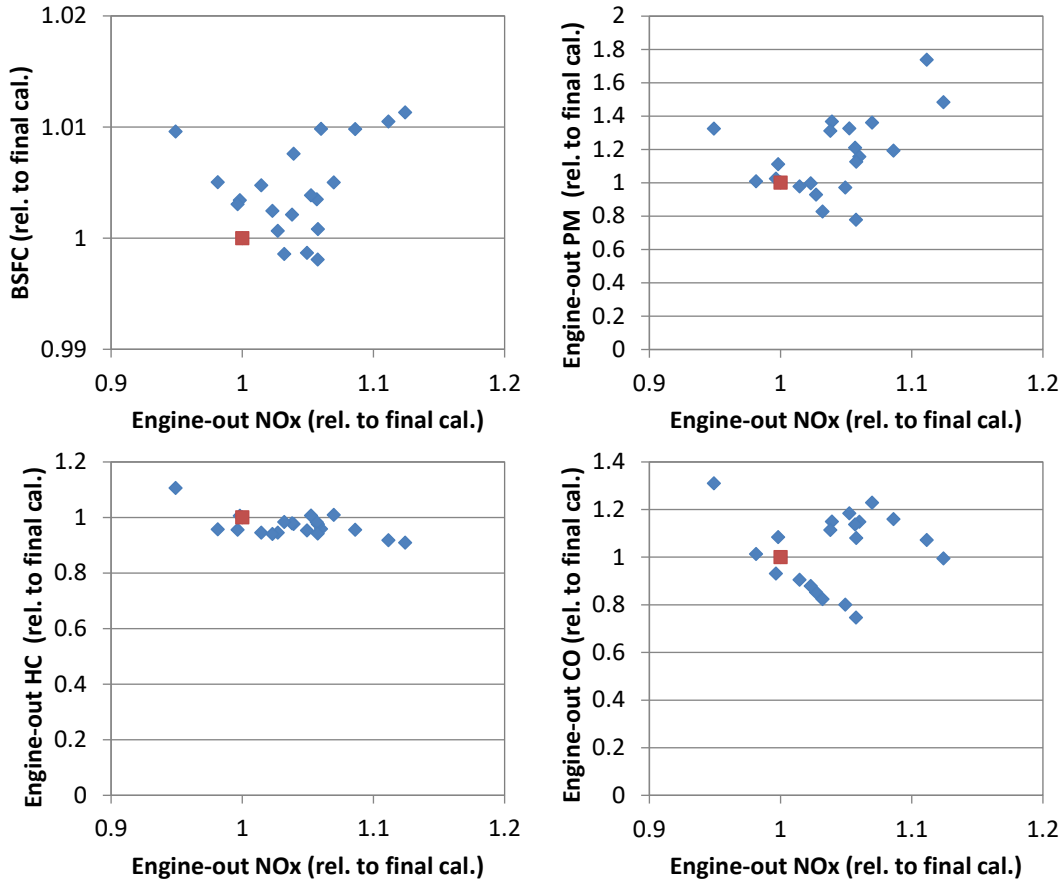
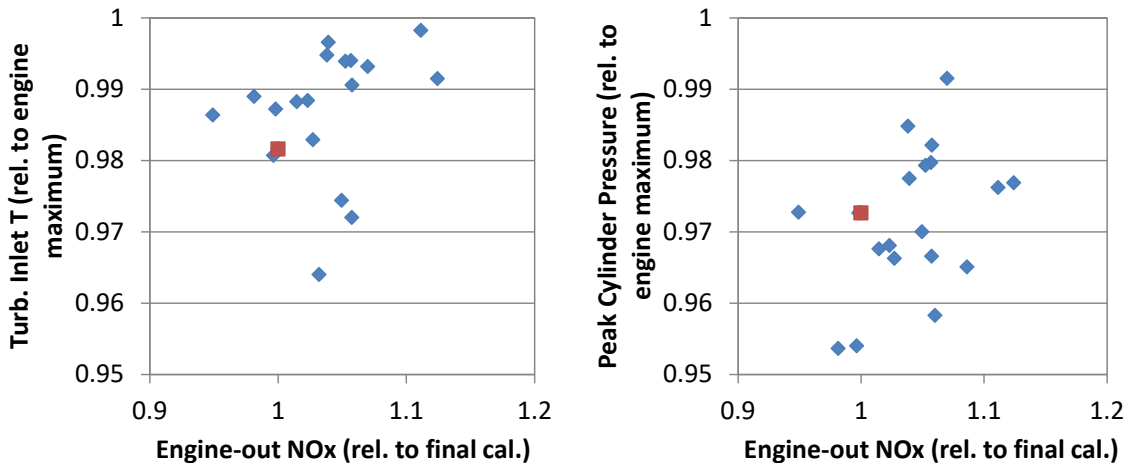


Figure 68: Turbine inlet temperature and peak cylinder pressure versus engine-out NOx for the final calibration at B100 (1493 RPM, 100 percent load) for the prototype-B engine. Turbine inlet temperature and PCP normalized by engine limit. NOx normalized by the optimum point selected for the final calibration, shown by the red square.



From the modes evaluated, the 'best' point was chosen on the basis of the lowest BSFC with acceptable NOx. PCP and turbine inlet temperature were a few percent below the engine maximums, which gives some margin for cylinder-to-cylinder and engine-to-engine variability. PM was lower than many of the other points, but the DPF efficiency was such that selecting the lowest possible PM emissions was not a primary consideration. Similarly, other operating parameter combinations would have had lower CO and HC emissions than in the selected point; however these reductions would have come at the expense of increased NOx and lower efficiency. Given the high effectiveness of the DOC at oxidizing these species, increases in engine-out levels are acceptable without causing tailpipe emissions to approach the regulated levels.

Similar processes were conducted at the other modes. At lower loads, a wider range of parameters were evaluated as there was more latitude for optimization without exceeding the PCP and turbine inlet temperature limits. The results at C50 (1780 RPM and 50 percent load) are shown in Figure 69 for BSFC and engine-out HC emissions, while the various points relative to the engine hardware limits are shown in Figure 70. As the figures show, when freed from the engine hardware restrictions, the optimum efficiency point could be selected. If NOx emissions were deemed too high at this mode, it would be possible to achieve significant reductions in engine-out NOx (approximately 20 percent) at the expense of a 1 percent increase in fuel consumption. However, as the tailpipe NOx at this mode was considered acceptable, the target focused on optimum efficiency. HC emissions, which were predominantly methane, were a secondary objective of the optimization. Figure 69 shows that these were also relatively low at the selected point for this mode.

Figure 69: Optimization trade-offs at C50 (1770 RPM, 50 percent load) for final calibration of prototype-B engine. All values normalized by the optimum point selected for the final calibration, shown by the red square.

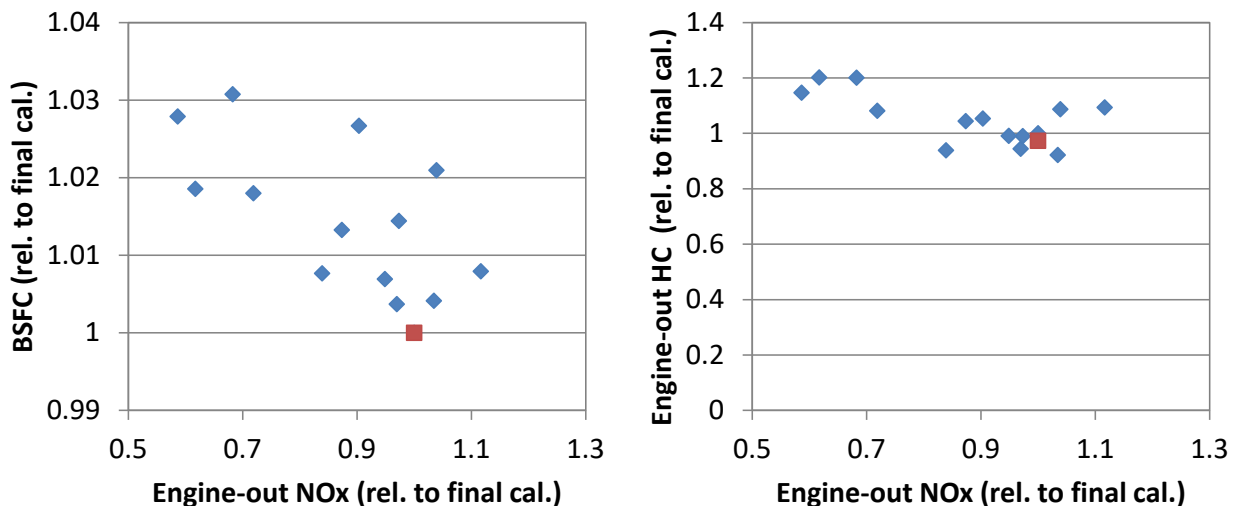
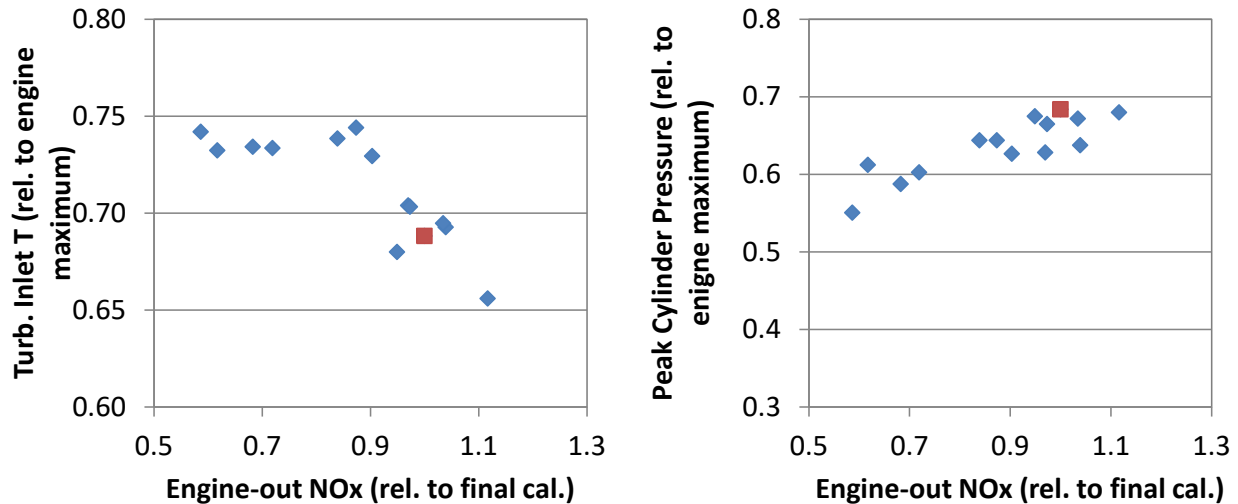


Figure 70: Turbine inlet temperature and peak cylinder pressure versus engine-out NOx for the final calibration at C50 (1770 RPM, 50 percent load) for the prototype-B engine. Turbine inlet temperature and PCP normalized by engine limit. NOx normalized by the optimum point selected for the final calibration, shown by the red square.



Final Calibration Development

The final calibration was formed by combining the optimizations at the individual modes, as shown in the two examples above. The parameters varied including the air handling parameters (EGR and VGT position), injection timing, injection pressure, pilot quantity, and pilot-gas separation.

In general, EGR levels were highest at low loads and lowest at high loads, ranging from 12 percent to 26 percent (excluding idle). Similarly, the diesel pilot quantity was lowest at high loads (approximately 5 milligrams per injection), increasing to higher values at lower loads to provide a stronger ignition source and to help in controlling hydrocarbon emissions. Pilot-gas separation was adjusted at higher loads to maintain a similar delay between start-of-combustion of the diesel pilot and the main natural gas injection. The overall calibration was defined on the basis of these parameters, which were then applied to the prototype-B engine to develop the final whole-map calibration.

Performance and Emissions Verification of Prototype-B Engine

Final verification of the prototype-B engine hardware and calibration was conducted using two fuels: standard natural gas that is generally representative of LNG (MN90) and a high-hydrocarbon fuel representative of weathered LNG (MN54). The MN54 fuel was evaluated to demonstrate the capability of the virtual sensor to protect the engine from damage and maintain performance. The MN90 fuel was used for the principal verification of the combustion system and calibration and for demonstration of emissions below the regulated limits.

Verification of Fuel Composition Protection from Virtual Sensor

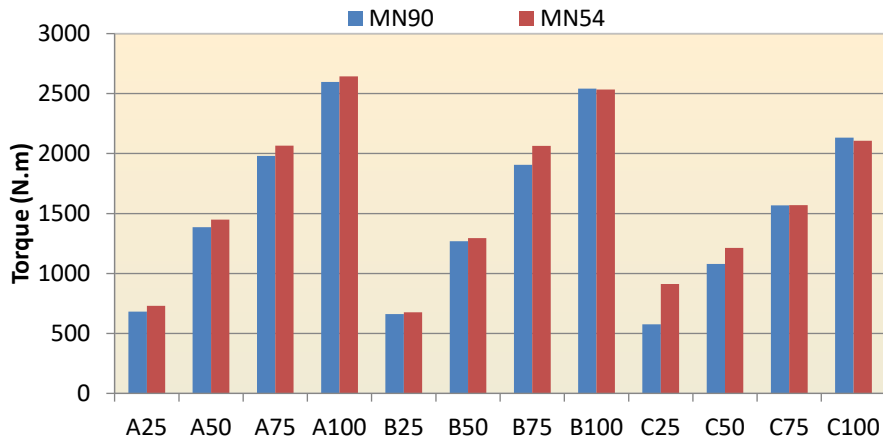
The operating principle and demonstration of the virtual sensor and associated controller were described earlier in this report on the prototype-A engine at the 475 hp rating. The impacts of poor quality gas would cause even greater risk to the engine at the higher power rating. Therefore, it was important to demonstrate the engine-protection capabilities of the system for the prototype-B engine at the 520 hp rating. To that end, the prototype-B engine was operated over the full 13 mode SET cycle on both regular (approximately MN90) and low quality (approximately MN54) fuel. The specific composition of the two fuels tested is provided in Table 8.

Table 8: Mass-based Gaseous Fuel Composition for Virtual Sensor Verification

Species	MN90 Line Gas	MN54
Methane (CH ₄)	92.0%	41.5%
Ethane (C ₂ H ₆)	4.2%	38.5%
Propane (C ₃ H ₈)	1.3%	18.4%
Butane (C ₄ H ₁₀)	0.6%	0.4%
Pentane (C ₅ H ₁₂)	0.2%	0.1%
Hexane (C ₆ H ₁₄)	0.0%	0.0%
Heptane (C ₇ H ₁₈)	0.0%	0.0%
Octane (C ₈ H ₁₈)	0.0%	0.0%
Nitrogen (N ₂)	0.9%	0.5%
Carbon Dioxide (CO ₂)	0.9%	0.6%

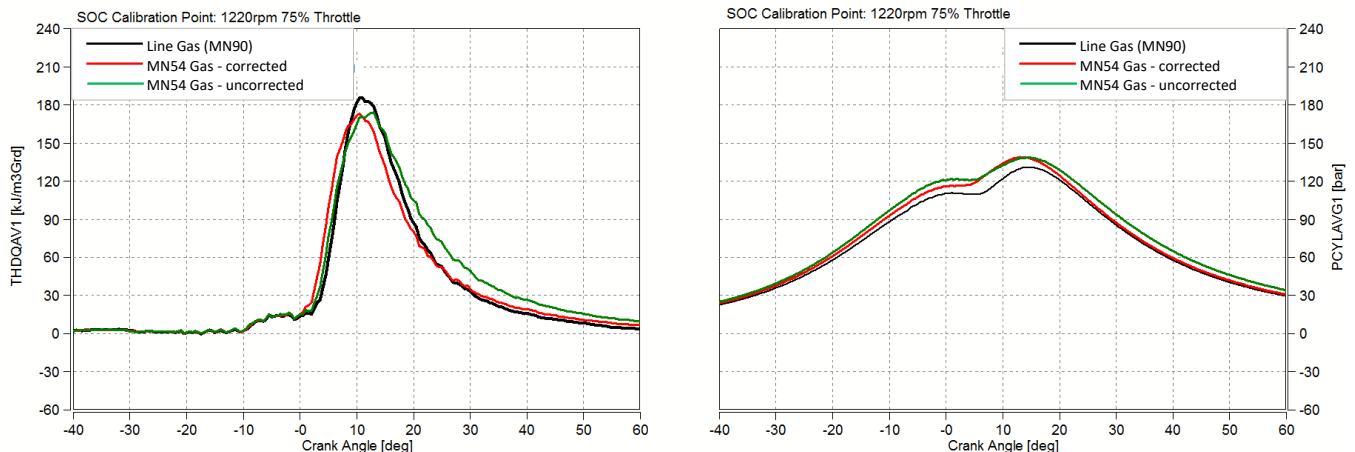
At each mode, the virtual-sensor based controller was used to adapt the fueling commands to maintain engine power while avoiding engine hardware limits (rate of pressure rise, PCP, exhaust gas temperature) that would have been approached or exceeded if the virtual sensor had not been employed. For the testing, first a full composite cycle was run on the MN90 fuel; the cycle was then repeated with the low-quality gas. Upon detection of the change in fuel quality, the virtual sensor based control system adjusted the natural gas injection quantity and timing to maintain engine torque and combustion timing. To demonstrate the applicability of the control system, the torques are shown for each mode for the base MN90 and the low-quality MN54 fuels in Figure 71. As the figure shows, the torque is essentially the same for the two fuels when using the virtual sensor based controller to correct the fueling.

Figure 71: Mode-by-mode torque for MN90 and MN54 fuels using the virtual sensor



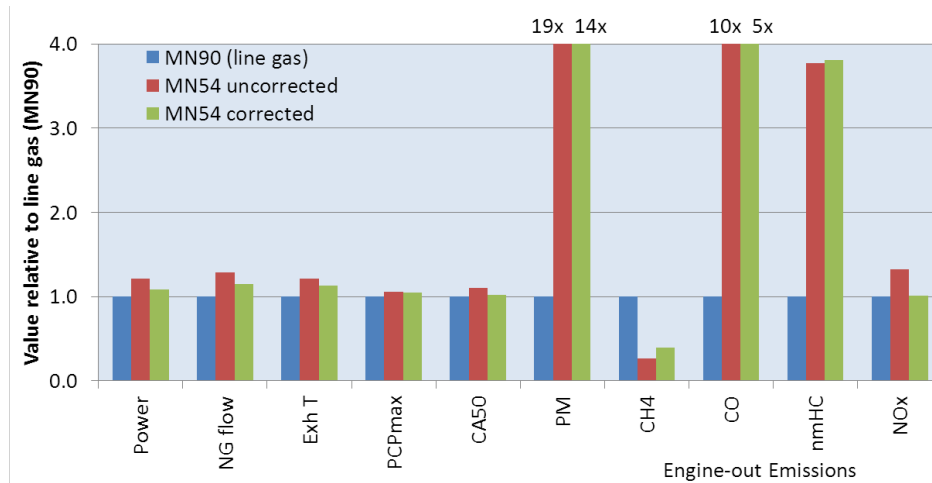
For reference, the effectiveness of the virtual sensor based control system for controlling combustion can be shown by comparing the engine performance under corrected and uncorrected conditions. Using mode A75 as an example (1200 RPM, 75 percent load), Figure 72 compares the in-cylinder pressure and HRR for the reference fuel (MN90) with the pressures and HRR for MN54 with both the base (uncorrected) timing and with the injection timings corrected by the virtual-sensor based controller. As the HRR shows, with the MN54 fuel, the combustion duration is increased substantially, leading to higher torque. The virtual sensor brings the combustion duration back to be essentially the same as the base fuel. The in-cylinder pressure is also reduced by the correction, especially during the compression process indicating reduced charge mass. These results demonstrate the effectiveness of the virtual-sensor based controller at maintaining the engine performance. A similar comparison was not conducted at any of the 100 percent load points as this would have led to excessive engine torque and potential engine damage.

Figure 72: Pressure trace and heat release rate for reference fuel (MN90), MN54 fuel with base injection timings, and MN54 fuel with corrected injection timings set with the virtual-sensor based controller. Prototype B engine with 520 hp calibration, 75 percent load, 1220 RPM (A75).



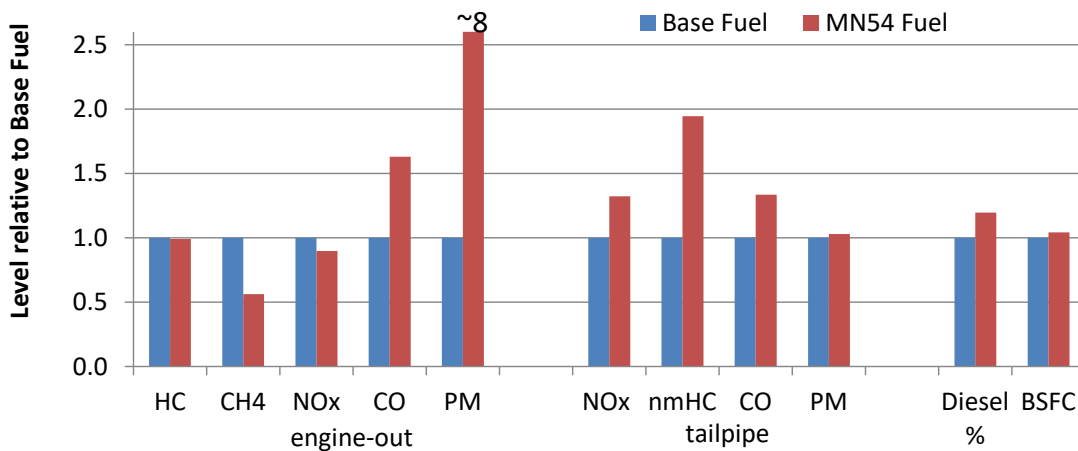
The effects of the lower MN fuel on key engine-out emissions and engine hardware parameters are shown in Figure 73 at the 75 percent load case at 1220 RPM. As the figure shows, the virtual sensor based controller reduces the exhaust temperature and PCP; although the values remain above those of the baseline calibration, they are within the safety margin for the engine at all modes. The combustion phasing, demonstrated by the CA50, is brought back to essentially the same level as for the MN90 gas. It also brings NOx emissions back to the same levels, indicating that the SCR will be able to control the tailpipe emissions at each mode. However, engine-out PM, CO, and nmHC substantially increase while CH₄ greatly reduces. These effects are all a direct result of the increased concentrations of ethane and propane in the MN54 fuel, as shown in Table 8.

Figure 73: Key engine-out emissions and hardware parameters for reference fuel (MN90), MN54 fuel with base injection timings, and MN54 fuel with corrected injection timings set with the virtual-sensor based controller. Prototype B engine with 520 hp calibration, 75 percent load, 1220 RPM (A75).



The main intention of the virtual-sensor based control system is to protect the engine from providing excessive torque. An added benefit of the virtual sensor is to minimize the impact of large variations in fuel quality on tailpipe emissions. To evaluate this, the composite engine-out and tailpipe emissions for the MN54 fuel with the virtual sensor based controller are compared over the 13-mode cycle with equivalent points on the standard fuel (MN90). Results over the full cycle are shown in Figure 74. Engine out NOx and methane emissions are significantly reduced, while CO increases. PM increases substantially due to the presence of ethane and propane in the MN54 fuel. However, tailpipe FSN measurements indicate that tailpipe PM is indistinguishable between the two fuels, demonstrating the effectiveness of the DPF at removing PM from the exhaust stream.

Figure 74: Effect of low-quality (MN54) fuel on composite emissions for the prototype-B 520 hp engine. Emissions are shown relative to the standard (MN90) fuel.



Tailpipe NO_x, nmHC, and CO do increase relative to the standard fuel. However, the levels of all three remain below the U.S. EPA 2010 regulated standards, even though this fuel is substantially worse than the fuels generally used for calibration. Fuel consumption also increases, due to the lower gravimetric energy density of the MN54 fuel (volumetric energy content increases due to the higher density of the ethane and propane, but the gravimetric energy density is lower). Diesel consumption is also slightly increased with the virtual sensor-based control compared to the standard engine control system.

Overall, the results show that the virtual sensor not only protects the engine from operating under potentially damaging conditions but is also able to maintain tailpipe emissions within the U.S. EPA 2010 standards without significantly degrading fuel economy. The long-term implications for the engine and aftertreatment system of operating on such a poor-quality fuel were not evaluated, but as a protection strategy the virtual-sensor based controller has been demonstrated to be highly effective.

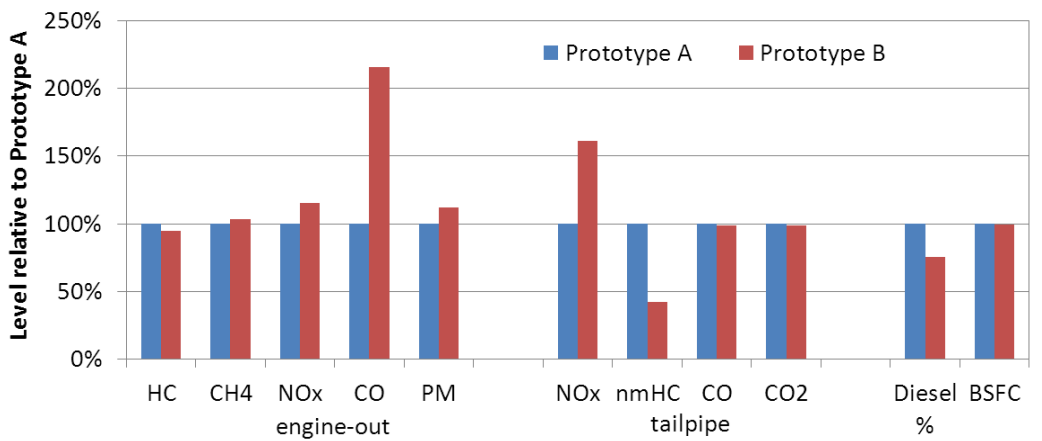
Verification of Final Engine Hardware and Calibration

Interactions among the key parameters on the prototype-B hardware were presented earlier in this report. In summary, the key parameters for optimization are the EGR level, SOI timing, pilot quantity, relative delay between the pilot and gas injections, the fuel injection pressure, and the charge temperature and pressure (as controlled by the air handling system).

The net engine-out emissions and tailpipe emissions for the prototype-B engine are shown in Figure 75 for the composite 13 mode cycle with the 520 hp level shown in Figure 66. These results are relative to the baseline prototype-A engine over the original (475 hp) cycle. The results demonstrate that tailpipe emissions of nmHC and CO are at or below the levels for the prototype-A engine, whose tailpipe emissions were below the U.S. EPA 2010 requirement levels; the prototype-B engine is therefore also compliant on these emissions. Tailpipe NO_x emissions are actually higher than the base prototype-A engine, but they remain approximately 40 percent below the U.S. EPA 2010 regulated levels. Tailpipe particulate

emissions were measured with the AVL smoke meter; levels below 0.002 FSN were recorded, which is consistent with the emission levels from the prototype-A engine. Gravimetric filter analysis has shown that these FSN levels are substantially below the 0.01 grams per brake horsepower-hour regulated standard.

Figure 75: 13-mode cycle composite engine-out and tailpipe emissions and fuel consumption for prototype-B engine for 520 hp, relative to the prototype-A engine for 475 hp



Fuel consumption is also shown in Figure 75; a small reduction in fuel consumption (approximately 0.5%) is observed for the prototype-B engine. This is achieved despite its significantly higher power. Brake-specific CO₂ emissions are also reduced by approximately 1 percent from the 475 hp prototype-A to the 520 hp prototype-B engine; this is attributed to the improved efficiency and a reduction in the diesel contribution to the total energy. This reduction in pilot fuel is approximately 25 percent over the cycle compared to the prototype-A engine.

Prototype-B Emissions and Fuel Consumption

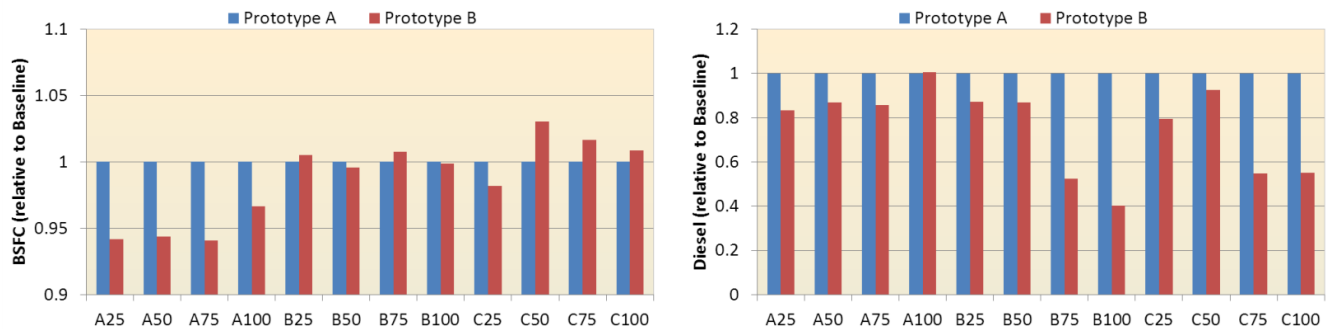
The composite engine-out emissions over the 13-mode cycle are also shown in Figure 75. The most obvious difference between the prototype-A and prototype-B engines is that CO is increased substantially. There is also a smaller increase in engine-out PM, while NO_x, CH₄, and THCs are reduced. In Figure 75, PM emissions are based on gravimetric filter measurements.

In general, CO increases at high load, which is a result of the higher EQR at these conditions with the 520 hp rating. However, the DOC successfully minimizes these emissions. Further optimization of the air handling system, including investigating the potential of a higher-flow turbocharger to better match the higher engine power, would be expected to reduce the engine-out CO levels. Similarly, it is likely that air-handling limitations lead to the observed 10 percent increase in engine-out PM. Further refinement of the calibration could improve these engine-out values, but tailpipe measurements show that the PM levels remain at virtually undetectable levels after the DPF, and hence further effort was not devoted to reducing engine-out PM at the expense of other emissions or efficiency.

For NOx emissions, there is a small increase in engine-out NOx to optimize for efficiency; however, tailpipe NOx emissions remain well below regulated levels. It should be noted that the large increase in NOx apparent in Figure 75 is primarily a result of low tailpipe emissions from the prototype-A engine, based on good performance of the SCR. This good performance enabled an increase in engine-out NOx at each mode. The approximately net 10 percent increase in engine-out NOx is offset by improved heat retention in the exhaust system at low loads to result in no significant change in required DEF consumption while maintaining tailpipe NOx levels. Meanwhile, the higher engine-out NOx results in an improvement in fuel consumption despite the prototype-B engine’s higher power rating and lower compression ratio.

The mode-by-mode BSFC and diesel pilot contribution are shown Figure 76 for the 520 hp prototype-B engine, relative to the baseline engine. On a mode-specific basis, fuel consumption is significantly reduced at low (‘A’, 1220 RPM) speed, but increased slightly at high (‘C’, 1770 RPM) speed. For a lower-speed duty cycle, the efficiency improvement is significantly higher than the approximately 0.5 percent reported for the composite 13 mode steady-state cycle.

Figure 76: Total fuel consumption and diesel contribution at individual modes, for the 520 hp prototype-B engine relative to the 475 hp prototype-A engine. All individual modes except idle shown.



Diesel fuel consumption is also a significant consideration for an HPDI engine, as diesel fuel is generally more expensive than natural gas, it has higher carbon content so generates more CO₂ per unit energy, and it requires separate storage. As a result, the 25-percent reduction in diesel consumption shown in Figure 75 is a useful result. As shown in Figure 76, this reduction is biased towards the higher load modes at mid- and high-speeds.

Final Engine Calibration Summary

The prototype-B engine was successfully calibrated at 520 hp. The margin for key parameters relative to the U.S. EPA 2010 standards for the steady-state modes with standard fuel are shown in Table 9. CO is included as it is a regulated emission, although tailpipe emissions are extremely low compared to the standards, and are near the limits for the measurement equipment. PM is also included, based on tailpipe PM mass derived from FSN measurements. When this is compared with expected DPF PM removal efficiency and gravimetric engine-out PM measurements, the differences are within the uncertainty of the measurement methods.

The 520 hp prototype-B engine also reduces total fuel consumption by 0.5 percent and diesel consumption by 25 percent compared to the 475 hp prototype-A engine.

Table 9: Margin for regulated emissions for prototype-B engine and standard fuels at 520 hp

	NOx	nmHC	PM	CO
Percent margin from U.S. EPA 2010 regulation target	41%	78%	~73%	100%

CHAPTER 9:

Final Cost Reduction Evaluation

The main objectives of this project were to reduce the cost of an HPDI engine while improving fuel efficiency, increasing power, and improving protection against poor-quality gaseous fuels. This involved the design and implementation of new engine components, improvement of existing systems, and re-calibration of the improved engine system. The final results of the calibration, shown earlier in this report, demonstrate that tailpipe emissions standards are easily met for the new engine on the base fuel at 520 hp, while providing safe engine operation on fuels down to MN54 with emissions below the regulated levels. The system also employs lower-cost aftertreatment and reduced cost fuel system components. The net benefits in terms of reduced engine system and operating costs are quantified in the following sections.

Engine Cost Savings

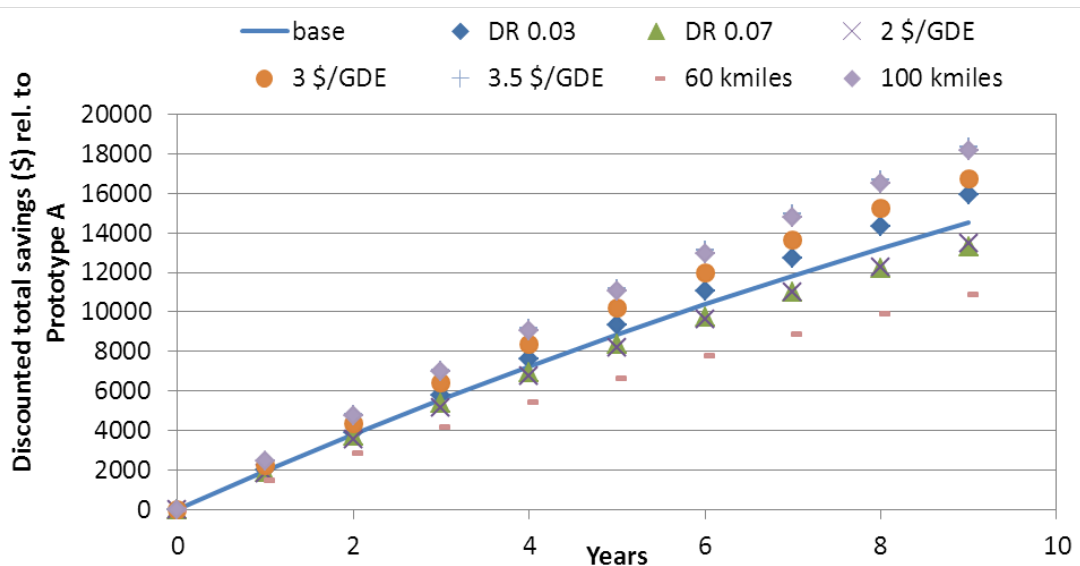
As discussed earlier in this report, Westport devoted significant effort to reducing overall system cost via design changes to simplify the manufacturing and assembly of the HPDI injector. A system-wide cost reduction effort was also undertaken, targeting savings through design and process improvements, as well as supplier changes where necessary. This effort was highly successful, achieving cost reductions of approximately 75 percent in each of the injector, fuel rail pressure control, and additional engine component modules. The system cost reductions, relative to a baseline value from 2009, are shown in Figure 7. For the prototype-B engine, the cost savings from the injectors and the other engine components achieve a reduction of approximately 30 percent in total fuel system costs.

The aftertreatment cost reduction was assessed earlier in this report. The prototype-B engine made use of a DOC with 33 percent less precious metal than the base DOC. This is expected to provide a cost savings of approximately 10 percent for the integrated DOC/DPF, which represents about half the cost of the aftertreatment system. Therefore, the new DOC is expected to reduce the aftertreatment system cost by approximately 5 percent, depending both on production volumes and on precious-metal costs.

Fuel Consumption Cost Savings

An economic analysis compares the financial savings from the reduced fuel consumption of the prototype-B engine to the prototype-A engine. This analysis evaluates the fuel cost reduction achieved through the improved efficiency of the prototype B engine with exhaust energy recovery. The combination of analysis and experimental results indicate a total efficiency improvement of 4.5 percent and a reduction in diesel consumption of 25 percent compared to the prototype-A engine. A summary of the analysis results, in terms of cost savings relative to a prototype-A engine, is shown in Figure 77.

Figure 77: Discounted savings from prototype-B improved efficiency relative to prototype-A. Base condition values: discount rate (DR) 0.05; natural gas fuel cost: 2.32 \$/gallon diesel equivalent; annual mileage: 80,000; diesel fuel cost: 4.12 \$/gallon.



The analysis used a net-present-value method, where the future financial savings from fuel cost reduction are discounted. The analysis assumes a constant discount rate over the period of analysis and that the costs of the fuel are constant. This method thereby indirectly accounts for inflation by assuming that the discount rate is supplemental to inflation (the analysis uses current-year dollars). Baseline values for the key parameters used in the analysis are:

- Discount rate: 5%
- Natural gas fuel cost: 2.32 \$/gallon diesel equivalent
- Diesel fuel cost: 4.12 \$/gallon²
- Annual mileage: 80,000 miles

The analysis includes a sensitivity study to evaluate the influences of changes in mileage, fuel costs, and discount rate. As would be expected, lower fuel prices, higher discount rates, and lower mileage result in reduced fuel cost savings benefits compared to the prototype-A engine.

On these values, the two year payback relative to the prototype-A engine is approximately \$4,000 (range: \$2,900 to \$4,800). This indicates the added cost that would be acceptable for the prototype-B engine versus prototype-A to achieve the efficiency benefits offered by the engine. As 90 percent of those efficiency benefits are a result of the exhaust-energy recovery turbine, this indicates a reasonable per-unit cost to the customer for that system would be around \$3,000 to \$4,000 for a 1.5 to 2 year payback period. Longer acceptable payback periods would, obviously, allow a higher up-front cost.

It should be noted that this analysis does not include a consideration of the higher power rating of the prototype-B engine versus the prototype-A. The 10 percent higher power should

² Values taken from the U.S. Department of Energy "Clean Cities Alternative Fuel Price Report," dated April 2012. Available at http://www.afdc.energy.gov/uploads/publication/afpr_apr_12.pdf

support a 10 percent payload increase, increasing the potential revenue per mile driven and a corresponding increase in income to the vehicle owner. However, a detailed analysis of these benefits, and the corresponding impact of increased payload on engine fuel consumption, was beyond the scope of the current project. It should be noted that the reduced base cost of the prototype-B engine compared to the prototype-A was also not considered in the payback analysis, which simply assesses the fuel consumption cost/benefit aspect. Finally, this analysis does not include any consideration of the relative payback for either prototype-A or prototype-B engines compared to a conventional diesel engine or earlier versions of the Westport HPDI engine.

CHAPTER 10:

Final Conclusions

At the completion of the project, the new prototype-B engine was commissioned and fully calibrated. The main changes from the original Westport HD 15 L engine were:

- New high-flow injectors for 10 percent extra torque
- New piston design with lower compression ratio (15.3:1)
- New DOC with reduced precious metal loading
- New virtual sensor for engine protection and fuel composition robustness
- New exhaust insulation to enhance aftertreatment performance

The calibration of the prototype-B engine was developed to achieve the program targets on the new hardware by varying EGR level, pilot quantity, injection parameters, and combustion phasing and air handling system parameters. This calibration was conducted over the entire 13-mode steady-state SET cycle that covers the key areas of the engine operating map.

Compared to the original engine, the prototype-B engine was demonstrated to:

1. Achieve a peak power of 520 hp with a 10 percent increase in torque across the evaluated engine torque curve
2. Emit tailpipe concentrations of NO_x, nmHC, PM, and CO substantially below U.S. EPA 2010 emission standards at the 520 hp rating
3. Consume slightly less fuel (approximately 0.5 percent) relative to the baseline prototype-A engine at 520 hp
4. Operate on fuels as low as MN54 while maintaining engine power up to 520 hp without exceeding any engine hardware limits
5. Reduce diesel consumption by 20 percent

Engine system modeling also indicates that efficiency improvements could be achieved either through coating addition to the piston skirts or through the addition of an exhaust energy turbine. These are estimated to offer potential fuel consumption reductions of approximately 1.5 percent and 4 percent, respectively. When combined with the fuel consumption improvement reported above, it is expected that an efficiency improvement of 5 percent could be achieved over the base engine. Further experimental work would be required to demonstrate these benefits. Tailpipe CO₂ emissions reductions would be reduced by an amount equivalent to the reduction in fuel consumption.

Hardware improvements, including reduced platinum group metal loading on the DOC, lower-cost manufacturing for the injectors and FCM, and other fuel system cost reductions led to a 30-percent reduction in fuel system costs and a 5-percent reduction in aftertreatment system costs. The addition of the exhaust energy turbine would be an incremental cost; however, costs for series production units were not provided by any of the contacted manufacturers. An analysis of the fuel consumption cost reductions achieved through the addition of this

component to the prototype-B engine suggests that, for a 1.5 to 2 year payback value, the cost would have to be less than \$3,000 to \$4,000.

The results demonstrate that the prototype-B engine is a significant improvement over the current engine product, with lower cost, higher power, and more robustness to changes in fuel quality. Engine emissions and efficiency have been shown to be maintained or improved. As such, all the principal targets of this research program have been met.

CHAPTER 11:

Technology Transfer and Production Readiness Plans

Technology Transfer Plan

This section covers the transfer of technology from the Technology Development Group used as part of the technologies and feature improvements to the “HD increased Ratings and Improved Fuel Efficiency” production project. This project draws from a wide number of Westport’s internal technology improvement, advanced engineering as well as supply chain and market development efforts; these are additional to the technical advances achieved as part of the current California Energy Commission (CEC)-funded project. The HD improvement production project is currently in progress, so while the initial technology transfer from the CEC-funded project has occurred, the remaining steps of the project are planned but not yet executed. Therefore, much of the discussion here covers the plans for the remainder of the production project.

A review of the CEC-funded project results initiated the transfer of technology from the Technology Development group to the Westport HD Business unit; this led to recommendations for possible production implementation. The progress of the technology development was evaluated with respect to the Product Plan for the existing Westport HD 15L product currently being sold through Kenworth and Peterbilt. The individual technologies were grouped into either Short Term or Long Term for the HD 15L Product Plan based on the production readiness of the technology. This was assessed on the technology’s ability to meet customer expectations of reliability, durability, cost, and performance while aligning with U.S. EPA and California Air Resources Board regulations including emissions, fuel economy, and diagnostics.

For the overall technology transfer project, the sponsor was the President of the Westport HD Business unit. With the project sponsor in place, a Project Charter was created to provide definitions of: market description, customer needs, and market opportunities; proposed product delivery strategy; and strategic importance. A Core Team was created to lead the work in the different areas, consisting of group leads from the various departments including Sales/Marketing, Engineering, Manufacturing, and Production. In addition to the Core Team, a Management Review Group was identified to serve as the evaluators of the work led by the Core Team. The Management Review Group consisted of senior leadership from the various departments involved with the project. With this project framework established, discussions were held with the identified Core Team, and this technical team was tasked with creating an outline of the project scope, resource, and support requirements and the schedule and milestones.

After evaluating the voice of the customer and the results of ongoing work at Westport, including the current CEC-funded project, higher torque/power rating was selected as one of the improvement features to be offered in the next product iteration. The results from the current project have demonstrated that it is possible to achieve a 10 percent higher power

rating (up to 520 hp) while continuing to meet the U.S. EPA 2010 emission targets over a steady-state test cycle. The next phase of the work will involve developing a proper engine calibration for an even higher power rating (up to 550 hp) while continuing to meet U.S. EPA 2010 certification requirements over both steady state and transient operation. This phase of the work will be conducted by the Westport HD team as part of the next cycle of product development at Westport.

The process described above is applied to each technology to be evaluated, including the technologies generated in the CEC-funded project. Each is subject to final review and approval through a management review process. This includes an evaluation of the technical results to date and comparison to the project plan, to determine if the predicted outcome is still expected and that it continues to support the overall business plan. This review is conducted by the project lead with the support of the Core Team and consists of evidence to support the business plan. The Management Review Group evaluates this evidence and then decides whether to approve further development work through to the next review point.

Production Readiness Plan

The next steps after establishing the Technology Transfer plans is to define the Production Readiness plans for the various technologies of interest. This starts with the technology's fit relative to the System Requirements. The system requirements for the final product were primarily collected outside of the CEC-funded project as the Voice of the Customer (VOC) as part of on-going market and product evaluations. These were used to update the business case used to define the initial objectives for the CEC-funded project.

The VOC is captured continuously through interactions with existing and prospective customers at Truck Shows or Ride & Drive events and through discussions with truck OEMs. Many roles at Westport acquire customer feedback such as the Field Service, Sales Managers, Market Development personnel, and OEM Relation Manager. The information is fed back to the Product Manager to correlate with Product Change Requests and further technology development. Additional market trends and indirect VOC information gained from industry conferences, trade journals, and other publications are also captured and compared with the direct VOC. The VOC results form the basis of the scope of Product Improvement Plans and are grouped as either short term or long term improvements. The results from the CEC-funded project pertain primarily to short term (next 1 to 2 years) improvements.

The process followed in converting a newly developed technology for application to an existing final product is:

1. The revised product and customer requirements are translated into engineering language in the form of a revised Technical Request. For example, one of the significant changes to the overall System Technical Profile was to include the specific measurable target of 550 horsepower per 1,850 foot pounds top engine rating.
2. A safety review of the revised product overall design is then conducted through a revision of the previously completed System Design Failure Modes and Effects Analysis. This revision focuses on the changes to the system technical profile.

3. While the design changes are made to drawings and calibrations, testing is needed to verify these changes will meet the predicted outcome and the product characteristics listed in the Technical Request. Using the existing System Design Verification, a revision is made based on the above Design Failure Modes and Effects Analysis and Technical Request revisions.
4. The Production Design Team, in strong consultation with Advance Engineering, assesses the design alternatives and selects the final system architecture based on expectations for performance, reliability, manufacturability, serviceability, and cost. This architecture leads to a preliminary system bill of material and a product cost estimate and assessment of system reliability. Again, since this project is a product improvement, the changes to the existing system cost and reliability are evaluated.
5. The Design Development activities are planned and carried out including the analytical assessment and physical testing as part of the design verification activities. All product issues are captured and addressed through an Issues Resolution process. A Field Trial plan is created for "real world" verification activities.
6. Field Trials are initiated based on this revised product. With Field Trials underway, the Customer Care activities include the definition of service tools, training material, and spare parts identification. A project review is held to evaluate Process Development status along with updated product design status.

All remaining activities are then completed in order to get ready for production and commercial launch. At each stage the individual results and the overall production plan are reevaluated in a management review process.

GLOSSARY AND LIST OF ACRONYMS

Term	Definition
ATDC	after top-dead-centre
BMEP	Break Mean Effective Pressure
BSFC	brake specific fuel consumption
CEC	California Energy Commission
CFD	computational fluid dynamics
CH ₄	methane
CO	carbon monoxide
CO ₂	carbon dioxide
CR	compression ratio
DEF	diesel emissions fluid
DLC	diamond-like carbon
DOC	diesel oxidation catalyst
DPF	diesel particulate filter
EATS	exhaust aftertreatment system
ECU	engine control unit
EGR	exhaust gas recirculation
EQR	equivalence ratio
ESC	European Steady-state Cycle
FCM	Fuel Conditioning Module
FSN	filter smoke number
GCM	gas control module
GHG	greenhouse gas
GOLD	Generic Open Foam Low Dimension
HC	hydrocarbon
HCCI	homogeneous charge compression ignition
HCDI	homogeneous charge direct injection
HPDI	high-pressure direct injection
HRR	heat release rate
hp	horsepower
IMT	intake manifold temperature
IVC	intake valve closing

Term	Definition
L	liter
LIVC	late-intake valve closing
LNG	liquefied natural gas
mm	millimeter
MN	methane number
MPa	megapascals
N.m	Newton-metres
nmHC	non-methane hydrocarbon
NOx	nitrogen oxides
O ₂	oxygen
PCP	peak cylinder pressure
PM	particulate matter
PPC	partially-premixed combustion
RD&D	research, development, and demonstration
RPM	revolutions per minute
SCR	selective catalytic reducer
SCRE	single-cylinder research engine
SET	supplemental emissions test
SOI	start-of-injection
TGLDM	trajectory-generated low dimensional manifold
THC	total hydrocarbon
U.S. EPA	United States Environmental Protection Agency
VAVE	Value Analysis/Value Engineering
VGT	variable geometry turbochargers
Westport	Westport Fuel Systems Inc.

References

U.S. Department of Energy. 2012. "[Clean Cities Alternative Fuel Price Report](http://www.afdc.energy.gov/uploads/publication/afpr_apr_12.pdf)." April. Available at http://www.afdc.energy.gov/uploads/publication/afpr_apr_12.pdf.